Bioreactor system for cardiovascular tissue engineering

Dissertation

der Mathematisch-Naturwissenschaftlichen Fakultät

der Eberhard Karls Universität Tübingen

zur Erlangung des Grades eines

Doktors der Naturwissenschaften

(Dr. rer. nat.)

vorgelegt von

Nian Shen, M. Sc.

aus Henan/China

Tübingen

2017

Tag der mündlichen Qualifikation:	19.07.2018
Dekan:	Prof. Dr. Wolfgang Rosenstiel
1. Berichterstatter:	Prof. Dr. Katja Schenke-Layland
2. Berichterstatter:	Prof. Dr. Garry Duffy

Table of content

Abstract

A successful cardiovascular tissue engineering construct should consist of functional cardiac cells and cardiac extracellular matrix (ECM) that can provide structural and biochemical support. Embryonic stem cells derived cardiomyocytes (ESC-CMs) represent one promising source; however, differentiated ESC-CMs often possess an immature phenotype compared to adult CMs. Fibroblasts have been commonly used as an alternative cell source for in vitro generation of cardiac ECM, nevertheless, the formation of one of the most important structures in the cardiac ECM, elastic fibers, remains a challenge. Mechanical forces, such as pulsatile shear stress and regular contraction, are crucial for heart development and growth. Therefore, it was hypothesized that the application of physiologically relevant mechanical stimuli to ESC-CMs using bioreactor systems can potentially induce ESC-CM maturation and elastogenesis by fibroblasts. A flow/stretch bioreactor system was designed, validated and utilized to apply pulsatile flow and cyclic strain to murine and human ESC-CMs. The dynamic stimulation of ESC-CMs over extended culture time resulted in an increased expression of cardiac-associated proteins and ion channel-related genes, as well as an improved Ca^{2+} handling property, compared to static controls. In addition, using Raman spectroscopy, it was shown that dynamically cultured ESC-CMs display a comparable Raman fingerprint to primary isolated CMs. This data highlights the potency of combined pulsatile flow, cyclic strain and extended culture in the maturation process of murine and human ESC-CMs. Subsequently, another custom fluid flow bioreactor system was used to promote elastogenesis in human fibroblasts. Fibroblasts seeded in hybrid electrospun scaffolds showed an increase in the elastin and elastin-associated proteins, followed by elastin fiber deposition after 6-days of culture under pulsatile shear stress conditions, compared to static controls. Furthermore, to visualize the activity of cells in a non-invasive fashion, a flow bioreactor was designed and validated to be compatible with high-resolution imaging systems. This newly designed bioreactor offers significant advantages compared to traditional bioreactor systems, where the culture needs to be sacrificed at regular intervals to analyze samples using invasive methods. The possible applications of the designed bioreactor include in vitro ESC differentiation, ECM synthesis and cell-scaffold interactions.

Zusammenfassung

Eine Herausforderung im kardiovaskulären Tissue-Engineering ist es, definiert funktionelle PSC-abgeleitete Kardiomyozyten (engl. embryonic stem cell derived cardiomyocytes (ESC-CMs)) zu generieren, sowie eine extrazelluläre Matrix zu etablieren (engl. extracellular matrix (ECM)), die elastische Fasern enthält. Bioreaktorsysteme, welche eine mechanische Stimulation erlauben und dadurch physiologische Eigenschaften nacharmen können, bieten eine potenzielle Lösungsstrategie.

In der vorliegenden Arbeit wurde ein Flow-/Strech- (Fluss-/Dehn) Bioreaktor entworfen, um die Reifung von ESC-CMs anzuregen. Eine Kombination aus pulsierendem Durchfluss und zyklischer Dehnung, sowie eine verlängerte Zellkultur erwiesen sich als ausschlaggebend für den Reifungsprozess. Dynamisch kultivierte ESC-CMs wiesen eine erhöhte Expression von herzspezifischen Proteinen und Ionenkanälen auf, sowie eine funktionelle Verbesserung im Vergleich zu statisch kultivieren Zellen. Der Raman Fingerabdruck der dynamisch kultivierten ESC-CMs war vergleichbar mit dem primär isolierter CMs.

Um die Bildung von ECM zu stimulieren wurde ein eigens Flow-Bioreaktorsystem entwickelt, welcher die die Elastinsynthese in Fibroblasten begünstigte. Nach 6 Tagen Zellkultur war die Elastin-Expression in dermalen Fibroblasten erhöht gegenüber der statischen Kultur. Elastinablagerungen auf den Scaffolds und mit dem Elastogenese Prozess-assoziierten Proteine wurden im System nachgewiesen.

Darüber hinaus wurde ein weiteres Bioreaktorsystem entworfen, welches kompatibel mit einem hochauflösenden bildgebenden Modul ist. Dieses System bietet die Möglichkeit zur Analyse von Echtzeit-Aufnahmen von Zell- und Gewebekulturen. Das Bioreaktorsystem erzeugt einen reproduzierbaren laminaren Fluss, ist biokompatibel und einfach in der Handhabung.

Die Ergebnisse der vorliegenden Arbeit zeigen, dass Bioreaktorsysteme ein vielversprechendes Instrument sind, um die Reifung von ESC-CMs in vitro zu erreichen und die ECM Synthese inklusive der Bildung von elastischen Fasern zu stimulieren. Bioreaktorsysteme sind demnach ein wichtiges Instrument, um funktionelle kardiovaskulären Gewebe in vitro zu erzeugen.

Abbreviations

2D	two-dimensional
3D	three-dimensional
BMP	bone morphogenetic protein
CAD	computer-aided design
CMs	cardiomyocytes
CVDs	cardiovascular diseases
ECM	extracellular matrix
EGF	epidermal growth factor
EMILIN1	elastin microfibril interface located protein I
ERK	extracellular signal-regulated kinase
ESCs	embryonic stem cells
FAK	focal adhesion kinase
FDA	Food and Drug Administration
FDA/PI	fluorescein diacetate/propidium lodide
FLIM	fluorescence lifetime imaging microscopy
hESC-CMs	human embryonic stem cell derived cardiomyocytes
hPSC	human pluripotent stem cells
hPSC-CMs	human pluripotent stem cells derived cardiomyocytes
HA	hyaluronic acid
HUVECs	human umbilical vein endothelial cells
IF	immunofluorescence
JAK/STAT oftranscription	Janus kinase/signal transducers and activators
iPSCs	induced pluripotent stem cells
isl1	homeobox gene islet-1

LOX	lysyl oxidase
MAPK	mitogen-activated protein kinase
mESC-CMs	murine embryonic stem cell derived cardiomyocytes
MI	myocardial infarction
mL/min	ml per minute
MSCs	mesenchymal stem cells
PCL	poly-epsilon-caprolactone
PDGF	platelet-derived growth factor
PDMS	poly(dimethylsiloxane)
PEEK	Polyether ether ketone
PEGdma	poly(ethylene glycol) dimethacrylate
PGA	polyglycolic acid
PGS	poly(glycerol sebacate)
PI3K	phosphatidylinositol-4,5-bisphosphate 3-kinase
PLA	poly(l-lactide)
PSCs	pluripotent stem cells
ROCK	Rho-associated protein kinase
SMC	smooth muscle cells
VEGF	vascular endothelial growth factor
β-MHC	β-myosin heavy chain

List of figures

List of publications

Accepted papers

1. **Shen N,** Knopf A, Westendorf C, Kraushaar U, Riedl J, Bauer H, ..., Schenke-Layland K, et al. *Steps towards maturation of embryonic stem cell-derived cardiomyocytes using defined mechanical stimulations.* Stem Cell Reports. 9 (1):122-135. 2017.
2. **Shen N,** Hinderer S, Schenke-Layland K, *Scaffold and biomechanical transductive approaches to elastic tissue engineering,* in A. Ramamurthi and C. Kothapalli (Eds), Elastic fiber matrices: biomimetic approaches to regeneration and repair. Taylor & Francis Group, 2016.
3. Eoh J, **Shen N,** Burke JA, Hinderer S, Xia ZY, Schenke-Layland K, and Gerecht S. *Enhanced elastin synthesis and maturation in human vascular smooth muscle tissue derived from induced-pluripotent stem cells.* Acta Biomaterialia. 52: 49-56, 2017.
4. Hinderer S, **Shen N,** Ringuette LJ, Hansmann J, Reinhardt DP, Brucker SY, Davis EC, Schenke-Layland K. *In vitro elastogenesis – Instructing human vascular smooth muscle cells to generate an elastic* fiber-containing extracellular matrix scaffold. Biomedical Materials 10(3): 034102, 2015.
5. Brauchle E, Knopf A, Bauer H, **Shen N,** Linder S, Monaghan MG, Ellwanger K, Layland SL, Brucker SY, Nsair A and Schenke-Layland K. *Novel non-invasive identification of chamber specific cardiomyocytes in differentiating pluripotent stem cells.* Stem Cell Reports. 6(2): 188-199, 2016.
6. Hinderer S, Seifert J, Votteler M, **Shen N,** Rheinlaender J, Schäffer TE, Schenke-Layland K, *Engineering of a bio-functionalized hybrid off-the-shelf heart valve.* Biomaterials. 35(7):2130-9, 2013.
7. Brougham CM, Levingstone TJ, **Shen N**, Cooney G, Jockenhoevel S, Flanagan TC, O'Brien FJ. *Freeze-drying as a novel biofabrication method for achieving a controlled microarchitecture within large, complex natural biomaterial scaffolds.* Advanced Healthcare Materials. 2017. doi: 10.1002/adhm.201700598.
8. **Shen N,** Riedl J, Carvajal Berrio DA, Davis Z, Monaghan MG, Layland SL, Hinderer S, Schenke-Layland K, *A flow bioreactor compatible with real-time*

marker free fluorescence lifetime imaging microscope. Accepted by Biomedical Materials. 2017.

Submitted papers

9. Ryan A., Kearney CJ, **Shen N**, Khan U, Kelly AG, Probst C, Brauchle E, Biccai S, Carciarena CD, Kerrigan SW, Kelly DJ, Schenke-Layland K, Coleman JC, O'Brien FJ, *Electroconductive biohybrid collagen and pristine graphene composite biomaterials with enhanced biological activity*. Submitted.

Contributions

Nr.	**Accepted for publication yes/no**	**Number of all authors**	Position of the candidate in list of authors	Scientific ideas of Candidate (%)	Data generation by candidate (%)	Analysis and interpretation by candidate (%)	Paper writing by candidate (%)
1	yes	14	1	15	70	85	60
2	yes	3	1	10	90	90	60
3	yes	7	2	20	0	10	5
4	yes	8	2	10	70	10	10
5	yes	11	4	0	20	5	0
6	yes	7	4	0	5	0	0
7	yes	7	3	10	20	0	0
8	yes	8	1	30	15	55	40
9	no	14	3	0	15	5	0

1 Introduction

1.1 Cardiovascular tissue engineering and its challenges

Cardiovascular diseases (CVDs), such as acute myocardial infarction (MI), stroke, hypertension, and heart valve diseases, are the leading causes of mortality and morbidity globally [1, 2]. The World Health Organization of the United Nations (WHO) estimates that CVDs are responsible for over 17.5 million deaths each year, which is twice as many deaths as all cancers combined [1, 2]. The conventional surgical treatment has been used to treat patients for decades. Nevertheless, for some types of the heart surgeries, such as total heart transplantation and valve replacement, surgical intervention is restricted by human heart availability, acute rejection and other hurdles [3, 4]. Xenotransplantation from other species has been proposed to be an alternative method, but it is associated with some concerns including risks of immunologic problems and xenogeneic infections [5]. Drug therapies can help to prevent the development of CVDs and is a major treatment modality [6], yet few new drugs have been approved by the Food and Drug Administration (FDA) for the treatment within the past years [7]. The high cost, ethical concerns and the limited predictive value of animal models slow cardiac drug discovery [8-10]. Furthermore, the traditional therapies are not appropriate for the treatment of end-stage patients [11, 12]. To overcome these limitations, new therapies and more standardized platforms for drug testing are required.

Cardiovascular tissue engineering combines the principles of engineering and life science to create functional heart tissue substitutes that can serve as biological implants or drug testing systems [13]. An engineered cardiac tissue should consist of phenotypically stable cardiac cell populations (cardiomyocytes (CMs), cardiac fibroblasts, vascular cells) within two-dimensional (2D) or three-dimensional (3D) matrices [14]. These matrices are either cultured in vitro inside a bioreactor system with defined mechanical and biochemical conditions to mimic the in vivo physiological environment or under static conditions [15, 16]. Ideally, an engineered cardiac tissue should re-establish normal tissue structure and remodel or self-repair in response to the environmental cues [14].

1.1.1 Challenge #1: Source of cells

1.1.1.1 Primary isolated cardiomyocytes

Although current cardiovascular tissue engineering approaches show promise [17], one of the major issues is to identify a suitable source to generate sufficient and phenotypically stable cardiac cells [18]. CMs are the most important cell type in the heart and are responsible for regular heart contraction [19, 20]. However, the application of primary adult CMs in cardiovascular tissue engineering is hampered by a few obstacles. First, human adult CMs do not proliferate in culture [21-23]. Second, the isolation disrupts the connections between the cells, which leads to hypercontracted cells and cell death [24]. Therefore, CMs can only be maintained in vitro for a rather short time [22, 25]. Furthermore, the possibility to receive healthy heart tissue for isolation is relatively limited.

1.1.1.2 Cardiac progenitor cells

Though adult CMs have very limited potential for self-renewal, evidence indicates the existence of a resident cardiac stem cell or progenitor cell population with a capacity to differentiate into all types of cardiac cells [26-30]. The first endogenous cardiac stem cells reported were the Lin^- $c\text{-}kit^+$ cells isolated from female rats that are self-renewing, multipotent, and had potential to differentiate to all types of cardiac cells including myocytes, smooth muscle cells (SMCs) and endothelial cells (ECs) [26]. In addition, when cardiac $c\text{-}kit^+$ cells were injected into the hearts of syngeneic rats after myocardial infarction, these cells reconstituted the well-differentiated myocardium, differentiated to ECs and SMCs and eventually improved the heart function [26]. Robbin´s group injected Lin^- $c\text{-}kit^+$ cells and $c\text{-}kit^+$ $Thy1.1^{lo}$ Lin^- $Sca\text{-}1^+$ long-term reconstituted haematopoietic stem cells into an infarct model, however, few cells were detected after 30 days [31]. Furthermore, these cells did not express cardiac tissue-specific markers [31]. Recently, $c\text{-}kit^+$ human cardiac progenitor cells were proved to have the potential to differentiate to CMs during the heart development or after injury in adulthood [32, 33]. Nevertheless, the percentage of the new CMs produced by these endogenous $c\text{-}kit^+$ cells after the heart injury is

approximately less than 0.03%, which is insufficient to repair the damaged heart [32]. Cai et al. and Laugwitz et al. identified one cardiac progenitor population in the postnatal rat, mouse and human myocardium expressing homeobox gene islet-1 (isl1) [30, 34, 35]. The isl1 - expressing cells give rise to the outflow tract, right ventricle, and a subset of left ventricular cells during the heart development [30]. When these cells differentiate into cardiac cells, the expression of isl1 is lost [34, 36, 37]. It has been demonstrated that the $isl1^+$ progenitors have the potential for differentiation into CMs, SMCs, and ECs both in vivo and in vitro [34, 36, 37]. Furthermore, the $isl1^+$ progenitors are capable of self-renewal and expansion before differentiation [37]. Though promising, it is well accepted that the acquisition and isolation of the human cardiac progenitor cells from myocardial samples is challenging [36, 38]. Additionally, the number of cardiac progenitor cells distributed in the atrium, ventricle, and epicardium are very small (1 to 1 × 10^3 CMs) [39]. Therefore, the application of the cardiac progenitor cells remains challenging until these limitations are appropriately addressed.

1.1.1.3 Pluripotent stem cells

Pluripotent stem cells (PSCs) are defined based on three characteristics: 1) they are capable of renewing themselves; 2) they can differentiate into specialized cell types of all three germ layers: endoderm, mesoderm, and ectoderm; 3) they are capable of repopulating a tissue in vivo [40]. PSCs include induced pluripotent stem cells (iPSCs) and embryonic stem cells (ESCs) [40, 41]. ESCs are the cells derived from the blastocyst of a 3 to 5 days old embryo [42]. In 2006, iPSCs were generated by Shinya Yamanaka´s group for the first time from somatic cells by the forced expression of up to four stem-cell-related transcription factors (Oct3/4, Sox2, Klf4, and c-Myc) [43]. IPSCs have the advantage of high proliferation capacity and represent one of the most viable cell sources for in vitro generation of a large number of CMs to date [44]. Moreover, iPSCs do not cause the ethical concerns that accompany ESCs [45]. Nevertheless, many hurdles still need to be overcome before iPSC-derived cells can be established for clinical applications [46]. For example, the viruses used to reprogram somatic cells for the generation of iPSCs can trigger the expression of oncogenes (cancer-causing genes) [47, 48]. Other methods for

generation of PSC have been investigated including employing polycistronic reprogramming cassettes [49-51], non-integrating adenoviral vectors [51-56], traditional recombinant DNA transfection [57], transfection of mRNA [57], miRNA [58-60] and minicircle DNA [61] or transfection of episomally maintained EBNA1/OriP plasmids [62-66]. The discovery of the PSCs opened a new opportunity for cardiovascular tissue engineering. Ever since, many methods for CM differentiation from human PSCs (hPSCs) have been investigated, including the monolayer method and embryoid body (EB) method [67-80]. Adding cytokines, growth factors or small molecules to activate or inhibit specific signaling pathways can greatly increase the cardiac differentiation efficiency [81]. For example, regulation of activating bone morphogenetic protein (BMP) signaling by activin A and BMP4 can control cardiac mesendoderm induction [73, 79]. Vascular endothelial growth factor (VEGF) was demonstrated to enhance CM differentiation by the activation of extracellular signal-regulated kinase (ERK) signaling pathway [82]. Inhibition of the WNT signaling with dickkopf-related protein 1 or the small molecule IWR-1 at a later stage was shown to improve the efficiency of differentiation [78]. The optimized protocol allowed the achievement of cardiac differentiation efficiency higher than 60 % [76, 83].

Even though in vitro cardiac differentiation has improved, some limitations still need to be addressed. One of the main challenges is that hPSC-derived CMs (hPSC-CMs) retain a structurally and functionally immature phenotype that closely resembles embryonic or fetal heart cells [83]. Compared to adult CMs, PSC-CMs exhibit a round and irregular shape, low capacitance, lack of well-formed sarcomeres, the absence of T-tubules, poor calcium handling properties, and a relatively low number of mitochondria [84-88]. Researchers have attempted to address these limitations using mechanical cues [44, 89-95], biochemical cues [96-100], extended culture time [101], and electrical stimulations [95, 102-105] amongst others. Beyond the issue of maturation, other existing limitations are heterogeneity of the differentiated cell population and the requirement for a highly reliable and efficient differentiation protocol that can be applied to different cell lines [83].

1.1.2 Challenge #2: Establishing elastin containing extracellular matrix

Cardiovascular tissues are rich in elastin containing extracellular matrix (ECM) [106]. Elastin is crucial during heart development and allows heart valves and blood vessels to accommodate strains by deformation and to endure passive recoil [106]. Thus, to ensure appropriate mechanical function, successful tissue-engineered cardiovascular tissues, specifically heart valve substitutes, must incorporate an elastic component [107]. Research to date highlights the importance of elastin incorporation into tissue engineered heart valve although the synthesis of mature elastic fibers in vitro still remains challenging [107]. As a result, these heart valves substitutes have poor biomechanical behavior compared to native valves after implantation [108-110].

The induction of elastic fibers in vitro is difficult and challenging because of the size, molecular complexity, and the requirement for numerous proteins to facilitate fiber assembly, including fibulin-4, fibulin 5, lysyl oxidase (LOX), elastin microfibril interface located protein-1 (EMILIN1), and microfibril-associated proteins [111]. This challenge has been addressed via multiple approaches, such as scaffolds [112, 113], biomolecules [114-116], and mechanical cues [117-119]. Scaffolds, which are designed to provide a defined structural ECM mimicking microenvironment in vitro, have been used as a strategy to induce elastic fiber assembly in cells. For example, rat arterial SMCs cultured on a planar scaffold displayed a significant increase of elastin-stabilizing desmosine cross-links [112]. This is consistent with the results from another study [120]. Human vascular SMCs cultured on a hybrid electrospun scaffold exhibited ECM deposition containing mature elastic fibers [113]. Besides scaffolds, biomolecules, including growth factors [114, 121], nucleotides [122], vitamins [115] and exogenous enzymes [123], have been shown also to be a potential solution to induce the synthesis of elastin. The use of Vitamin C or its erythorbic acid isomer has been shown to promote elastin synthesis in human dermal fibroblasts [115]. Long-chain hyaluronic acid has been reported to assists in tropoelastin recruitment and crosslinking [124]. Similar to HA, TGF-β also plays an important role in elastin production and assembly [114, 121]. Mechanical stimulation is another important cue that regulates matrix synthesis. The state of art of using mechanical stimuli via bioreactor systems will be discussed in section 1.2.3. Despite these promising results, developing a mature elastic fiber containing tissue engineered constructs with human cells is still an unmet challenge.

1.2 The role of mechanical cues and bioreactors in the cardiovascular system

1.2.1 Mechanotransduction in cardiac cells and tissues

Mechanical forces play a vital role in manipulating cellular behavior and expression. Translation of environmental mechanical cues into a biochemical signal is facilitated via cellular mechanosensors, such as ion channels, integrins, and cell surface receptors [125-128]. These mechanosensors are activated by specific mechanical cues and activate downstream signaling pathways thereby modulating cellular functions [128].

ECs are the main cell type that is exposed to fluid shear stress, and a large number of responses have been described, such as activation of Ras, Erk1/2, focal adhesion kinase (FAK), mitogen-activated protein kinase (MAPK), and Rho family GTPases [129, 130]. Though many of these are specific to ECs, other cells do show some response to fluid flow [131]. Fluid shear stress-stimulated fibroblasts exhibited an increase in matrix assembly, which is mediated by the Rho family of GTPases [132]. The surface glycocalyx, which has been linked to fluid flow mechanotransduction, plays a crucial role in regulating SMC contraction in vitro and modulates the SMC phenotype [133, 134]. Shear stress also stimulates large outward ion channels in CMs and leads to the activation of FAK, which controls the density of repolarizing current and therefore tunes the electrical activity of CMs [135].

Cells respond directly to stretch by opening stretch-activated ion channels in the membranes and allowing the transport of calcium and other ions, such as K^+, and Na^+ [126, 136]. This leads to increase or decrease in ion levels which, in turn, may activate the phosphatidylinositol-4,5-bisphosphate 3-kinase (PI3K)–protein kinase B (Akt) signal transduction pathway [137] and p21 (Ras) / ERK1/2 signaling pathway [138]. Activating these signaling pathways further regulates cell proliferation and apoptosis [139]. Indeed, the mechanical stretch was found to induce transient activation of the Wnt/β-catenin signaling pathway, which is essential for proper cardiac specification, progenitor expansion and myocardial growth and maturation [140-143]. In addition to ion channels, receptor tyrosine kinase is important in

response to stretch-induced mechanotransduction [144]. Stretching of cells induces a rapid phosphorylation of platelet-derived growth factor (PDGF) receptor alpha and epidermal growth factor (EGF) receptor [145-147]. After which, the intracellular ERK1/2 signaling pathway is activated to regulate ECM synthesis and cell proliferation [147, 148]. Integrins and integrin-associated proteins are also involved in mechanotransduction [126, 127, 147]. Stretch induces structural reinforcement of integrin adhesions, such as activation of FAK. As a direct response, the Rho-associated protein kinase (ROCK) signaling pathway is triggered, which in turn regulates the expression of the β-myosin heavy chain (β-MHC) [149, 150]. It was also shown that cyclic stretch can stimulate the MAPK, which leads to the initiation of the RhoA/ ROCK signaling pathway and the Janus kinase/signal transducers and activators of transcription (JAK/STAT) pathway [131, 151]. Consequently, it modulates cell growth and differentiation and induces cardiac hypertrophy [118, 152]. Nevertheless, it has to be recognized that mechanical stimuli often activate multiple signaling pathways at once. It is rather difficult to perform research on one specific pathway since signaling pathways can have significant overlap and crosstalk [126].

1.2.2 The role of bioreactor systems in engineered cardiac muscle

1.2.2.1 The effect of flow on cardiac maturation

A bioreactor was first defined by Martin I. as a device that is used in biological or biochemical processes allows to precisely control and monitor culture environmental and operating conditions such as pressure, nutrient supply, shear stress and waste removal [15]. Compared to traditional static cell culture systems, bioreactors have significant advantages due to higher mass-transfer rates and the ability to monitor and control critical culture parameters [153]. More importantly, the bioreactor allows the mechanical stimulation of cells, providing physiologically relevant biophysical signals [154]. In consideration of the specific role of the hydrodynamics of human circulation and continuous contractions of the heart, the bioreactor system is fundamental for cardiovascular tissue engineering [155]. Perfusion bioreactor is the most commonly used bioreactor in this field. It provides a continuous flow through the construct and promotes the mass transfer in the cell microenvironment by the

continual exchange of cell culture medium [15, 153, 155-157]. Meanwhile, the fluid flow provides shear stress stimulation to the cells [15]. Brown et al applied pulsatile perfusion at a flow rate of 1.5 mL/minute (mL/min) or 0.32 mL/min at 1 Hz to an engineered cardiac patch formed by seeding neonatal rat CMs onto an ultrafoam collagen hemostat disc, which resulted in enhanced contractile properties and an increased hypertrophy index compared to the static controls [158]. More recently, Kenar et al. developed a myocardial 3D patch, which was obtained by seeding human mesenchymal stem cells (MSCs) on electrospun poly(l-lactide) (PLA) and poly(glycerol sebacate) (PGS) scaffolds. The 3D patch was dynamically cultured in a bioreactor, and the cell medium was transiently perfused through the macropores of the scaffolds. After two weeks, 3D constructs from perfused cultures showed an enhanced cell viability and a uniform cell distribution due to an improved nutrient provision in comparison to the static controls [159]. Some groups further studied the combined effects of perfusion flow and growth factors on engineered cardiac tissues [160]. Neonatal rat CMs were cultured on 3D scaffolds in medium supplemented with insulin-like factor-I and in the presence of bi-directional perfusion flow [160]. The multi-factorial simulations resulted in reduced cell apoptosis, increased connexin 43 expression and decreased excitation threshold [160]. However, only a few studies to date have focused on using perfusion bioreactor systems to induce cardiac differentiation and maturation from stem cells.

1.2.2.2 Stretch-induced cardiac maturation

Stretch is also a physiological mechanical cue that modulates cardiac tissue phenotype. Cyclic stretch provides important cues during heart growth and development [44]. Therefore, a variety of stretch regimes have been utilized including static stretch, ramp stretch and cyclic stretch [161, 162]. For example, Fink et al. created a circular engineered heart tissue, which consists of neonatal rat CMs and collagen I [163]. They exposed the engineered heart tissue to a 10% unidirectional cyclic stretch at 2 Hz [163]. After 7 days, the engineered heart tissue displayed structural and functional features of a native differentiated rat myocardium [163]. In contrast, Birla et al. applied short-term cyclic stretch up to 24 hours to neonatal rat CMs and did not detect any significant change in the active force, specific force,

pacing characteristics and morphological features of the tissue [164]. The possible reason for these opposing results is that the parameters of the mechanical stimulation varied between the studies. CMs are highly sensitive to the flow rate, strain magnitude, frequency, and duration [165], thus different stimuli parameters potentially lead to completely different results and cannot be objectively compared with each other. Recently, the effects of stretch on cardiac maturation were further investigated with human stem cells. Mihic et al. seeded human ESC-derived CMs (hESC-CMs) on gelatin-based scaffolds, which underwent a 12% cyclical stretch at 1.25 Hz. After 72 hours, hESC-CMs exhibited a functional maturation in terms of greater cell elongation, increased gap junction formation and better contractile elements as well as improved calcium handling properties [93]. Comparable results were detected by Murry´s group. Cyclic stress conditioning has been shown to increased expression of several cardiac markers, leading to enhanced calcium dynamics and force production [89]. Even though the effect of pulsatile flow or cyclic stretch on cardiac maturation has been investigated, a possible synergistic effect of the combination of pulsatile flow and cyclic strain remains unclear. There are indeed flow/stretch bioreactors exist [166, 167]; nevertheless, they have been mainly used for heart valve studies [166]. Therefore, to assess the effect of the combination of pulsatile flow and cyclic strain on cardiac maturation, a new flow/stretch bioreactor has to be designed specifically for this application.

1.2.3 Effects of fluid flow on elastogenesis

The mechanical stimulations have not only been shown to influence cardiac maturation, but also have been used to induce ECM synthesis, such as elastogenesis [107]. While strain was used as one of the important methods to induce elastogenesis in last decades, few studies focused on the effect of fluid flow on elastogenesis because it was believed that vascular SMCs and fibroblasts are not directly exposed to shear stress in vivo. Nevertheless, Shi et al. suggested that SMCs are exposed to an extremely low interstitial flow (~10^{-6} cm/s) driven by the transvascular pressure differential. They calculated the transmural interstitial shear stress on SMCs is approximately 1 dyne/cm^2 [168]. Qiu et al. demonstrated that low shear stress results in the induction of matrix synthesis, including collagen and

elastin synthesis, whereas high shear stress leads to SMC apoptosis [147]. Other groups have confirmed that applying low shear stress on SMCs resulted in elastin synthesis [169-171]. Zhang et al. seeded human coronary artery SMCs and human aortic ECs on tubular electrospun silk fibroin scaffolds and then exposed the cell-seeded scaffolds to physiological pulsatile flow [170]. They observed an increase in elastin gene expression, but no elastic fibers were detected using Verhoeff's elastic stain [170]. Generation of elastic fibers in a tissue-engineered construct with human cells still proves challenging. Hinderer et al. reported for the first time the generation of maturing elastic fibers utilizing human primary vascular SMCs within a customized fluid-flow bioreactor system [113]. This fluid-flow bioreactor system was designed and characterized in my master thesis (Figure 1) [172]. In this study, the shear stress magnitude of 6-11 × 10^{-5} Pa was applied to the SMCs, which was seeded on a hybrid fibrous 3D polymeric scaffold [113]. The success of this study leads to another question. The SMCs were isolated from veins and arteries, which is a disadvantage when producing patient-tailored models [113]. Fibroblasts, which are the most abundant cell type in the human body, are more suitable to be used to create the tissue engineered in vitro models. Nevertheless, the effect of low shear stress conditioning on elastogenesis in fibroblasts is yet to be investigated.

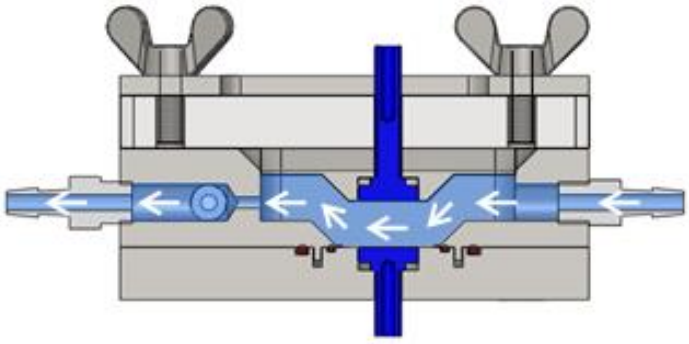

Figure 1: Cross-section view of the fluid flow bioreactor. In detail, this bioreactor system contains a lid, a flow block and a bottom. The lid is placed on the top of a flow block to create a flow chamber. A cell-seeded construct is clamped between the flow block and the bottom. The fluid flow passes the lateral inlet of the flow block and will be distributed on the cell-seeded construct when it reaches the flow chamber [172].

2 Objectives

This PhD thesis aims to 1) identify the role of biophysical signals on murine and human ESC-CM maturation, and 2) study the effect of pulsatile flow on elastogenesis in human fibroblasts using the customized fluid flow bioreactor. It is hypothesized that by applying physiologically relevant mechanical stimuli using bioreactor systems can potentially induce ESC-CM maturation and elstogenesis in fibroblasts. To visualize the activity of cells in a non-invasive fashion, the third objective of this study is to design a flow bioreactor that is compatible with high-resolution imaging. To achieve this, I propose the following

1) Investigate the effect of pulsatile flow and/or cyclic strain on ESC-CM maturation
    a. Design and characterize a flow/stretch bioreactor system
    b. Determine appropriate mechanical stimuli to regulate murine and human ESC-CMs maturation
    c. Investigate if a combination of different cues, such as mechanical stimulations and a prolonged culture period can advance the maturation of ESC-CMs
    d. Characterize the ESC-CM phenotype and compared them with primary CMs
2) Examine whether shear stress promotes elastogenesis in human fibroblasts.
    a. Investigate the gene and protein expression of (tropo)elastin and elastogenesis-associated proteins in shear stress-stimulated fibroblasts and compare to static controls
    b. Investigate the crosslinked level of elastic fibers in shear stress-stimulated human fibroblasts and compare to static controls
3) Design a flow bioreactor that is compatible with high-resolution imaging systems and validate its functions
    a. Design the bioreactor and simulate the hydrodynamics of the bioreactor chamber
    b. Utilize fluorescence lifetime imaging microscopy (FLIM) to investigate the metabolic activity of human umbilical vein endothelial cells (HUVECs) cultured under low shear stress conditions with the aim to show the functionality of the bioreactor in conjunction with high-resolution marker-free imaging

3 Results and discussion

3.1 Step towards maturation of ESC-CMs by defined biophysical cues

3.1.1 Development and characterization of a flow/stretch bioreactor

An autoclavable bioreactor system was designed in this study, which can apply both cyclic strain and pulsatile shear stress to cells without contamination, leakage or shearing off cells (**see publication: Appendix I**). In detail, the flow/stretch bioreactor comprises a liquid block lid, a liquid block, an air block lid, a silicone membrane, and an air block (Figure 2A and **Appendix I**). The liquid block, the air block lid, and the air block were machined from polyether ether ketone (PEEK), which has high resistance to heat (over 250 ºC), strong mechanical properties, and excellent biocompatibility [173]. The liquid block lid is made of polycarbonate, which is a transparent thermoplastic of a considerably high impact-resistance [174]. These components assembled into two chambers, a lower chamber filled with air and an upper chamber filled with cell culture medium. These are separated by a silicone membrane in order to ensure a sterile environment (**Appendix I**). The cells are seeded on a flat membrane, which is clamped between the two chambers on the top of a silicone membrane. Inlet and outlet ports are located on each side of the flow chamber (0.7 mm × 10 mm × 15 mm) (**Appendix I**). The medium flow passes through the lateral inlet and is slowed down when it reaches the flow chamber. The medium flow is equally distributed over the culture area. The port on top of the side of the flow block was implemented as such that can be connected to a tube. The air block lid is placed beneath the flow block to complement the flow chamber and create the air chamber together with an air block (**Appendix I**). The pressure and vacuum controlled air chamber generates a pressure gradient, which transfers strain from the silicone membrane to the cell-seeded membranes and the cells, resulting in a physiological stretch profile (**Appendix I**). Four screws are used to secure the chamber

components and Viton O-rings are included to prevent leakage. Image of the flow/stretch bioreactor system is shown in Figure 2B.

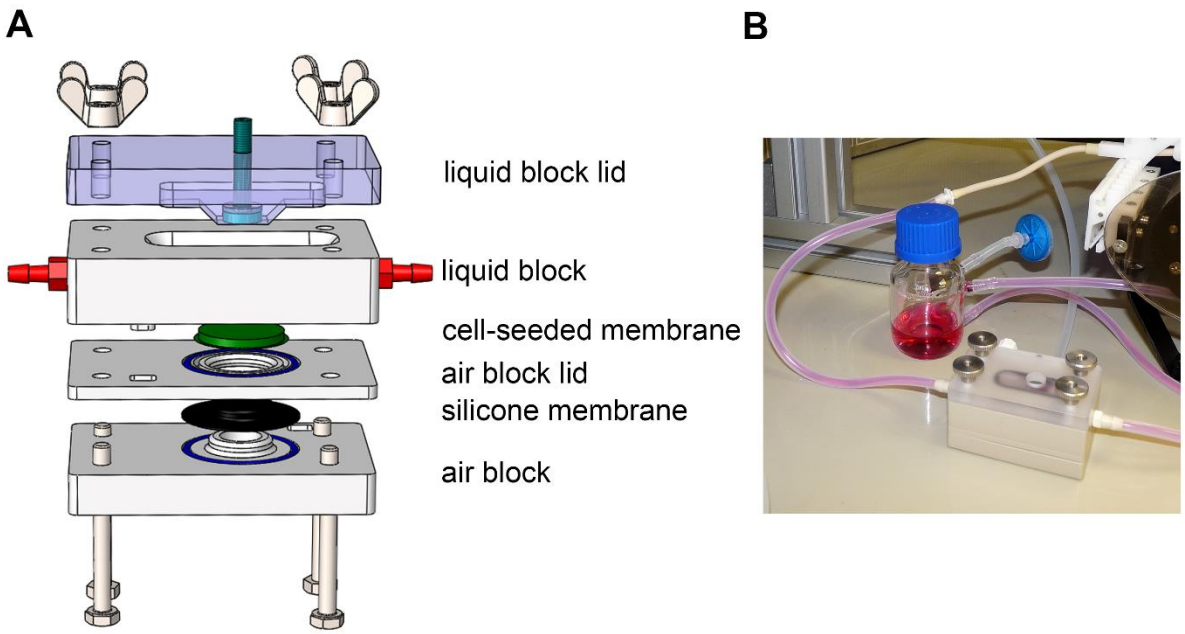

Figure 2: The flow/stretch bioreactor. (A) computer-aided design (CAD) of an exploded view of the flow/strain bioreactor system. The cell-seeded membrane is highlighted in green. The silicone membrane is depicted in black. (B) Photograph of the assembled bioreactor system connected to the medium reservoir.

Computational fluid dynamic modelling was employed to validate that a defined and reproducible shear stress is applied to the cells [175]. A computer-aided design (CAD) simulation was performed based on the geometry of the flow/strain bioreactor using commercially available software COMSOL. The mesh was auto-generated with a ´fine´ mesh size using COMSOL predefined ´fine´ mesh size for meshing the 3D geometries. The global temperature was set to 37°C and the domain material to the medium solution. The fluid dynamics of the medium flow inside the bioreactor was described through the Navier−Stokes equations for incompressible fluids. As illustrated in **Appendix I**, constant shear stresses between 10^{-3} and 4.5×10^{-3} dyne/cm^2 over the entire membrane area were applied to the cells with a flow rate of 1.48 mL/min. Flow rates of 2.96 mL/min and 5.92 mL/min created a shear stress ranging from 10^{-3} to 1.16×10^{-2} dyne/cm^2 and from 10^{-3} to 2.44×10^{-2} dyne/cm^2, respectively. The applied strains were also simulated using COMSOL. Based on the

simulation result, a gradient of strain (up to 5%) on the cell-seeded membrane was created by a 1.35 standard atmospheric pressure. Pneumatic deformation using air or vacuum resulted in a biaxial strain near the center of the membrane, therefore, cells were seeded only in a defined area of the membrane to ensure a homogeneous stretching.

The biocompatibility of the flow/stretch bioreactor was also tested using mESC line CCE. mESCs were seeded on a 2D membrane and placed into the bioreactor system. After 12 days dynamic culture with a flow rate of 5.92 mL/min and 10% cyclic strain, the cells were harvested and calculated the percentage of living cells with live and dead staining assay. As shown in Figure 3, no significant difference of the percentage of live cells was detected between dynamic and static conditions. This result demonstrates that the bioreactor is biocompatible and suitable to be used for stem cell-related study.

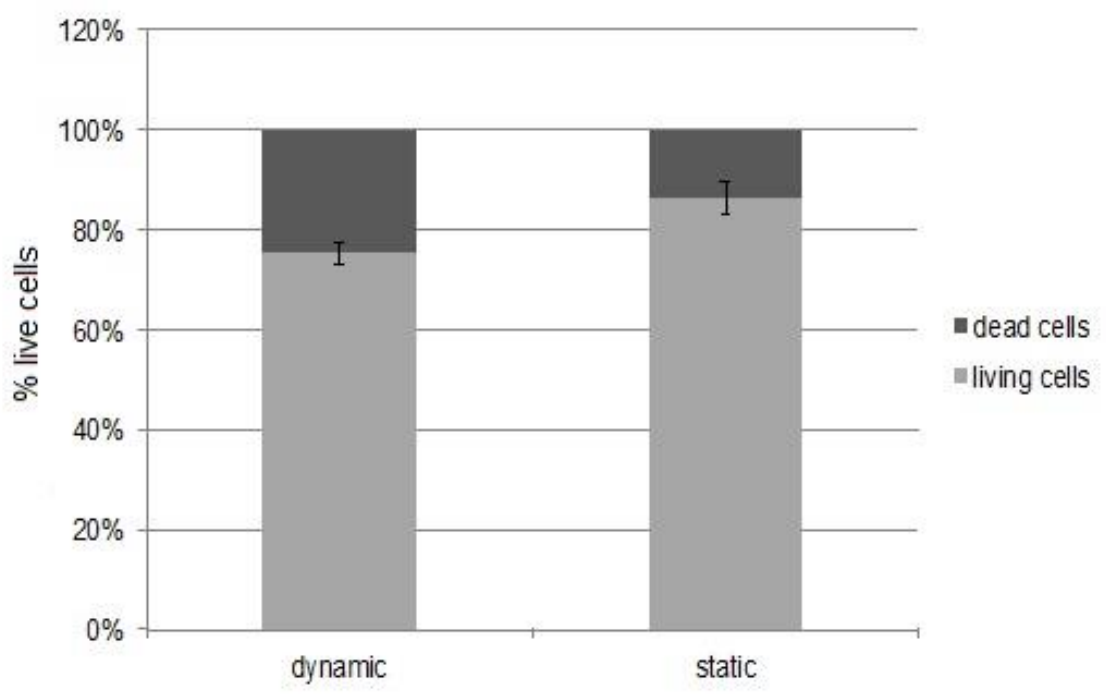

Figure 3: Percentage of live cells after a 12-day culture under dynamic and static condition. Cell viability was quantified using double staining of fluorescein diacetate/propidium iodide (FDA/PI).

3.1.2 Mechanical stimulation-induced maturation of ESC-CMs

After designing and evaluating the bioreactor, the system was utilized to investigate the impact of shear stress and/or cyclic strain on cardiac maturation. ESC-derived cells were seeded on 2D membranes and exposed to nine different dynamic conditions (three different shear stress conditions, three different cyclic strain conditions, and three different shear stress / cyclic strain conditions) **(Appendix I**). The cardiac-associated protein expression indicated that the combination of 5% strain and 1.48 mL/min flow can greatly enhance ESC-CMs maturation. Interestingly, the shear stress induced by 1.48 mL/min flow is approximately 10^{-2} to 10^{-3} according to the simulation result (**Appendix I**). It thus differs from physiological blood luminal flow (~10-20 dyn/cm^2) but corresponds with the in vivo environment, where CMs are exposed to an extremely low transmural flow rather than direct blood luminal flow [176]. Furthermore, the flow also generates continuous medium perfusion to the cells. This process helps can also help to maintain a stable culture environment for the cells by controlling oxygen, pH value, nutrient supply and waste removal [177]. Cardiac cells experience cyclic strains with significant temporal and regional variations (-7.9 ± 3.8% to +11.3 ± 6.4%) in vivo [151, 178]. A few previous studies have exposed PSC-CMs to cyclic strains between 2.5% and 12% [93, 151, 179]. They showed that cyclic strain conditioning can increase the expression of cardiac markers and the organization of sarcomere proteins [93, 151, 179]. Consistently with these studies, a similar result was detected when subjecting ESC-CMs to cyclic strains alone (**Appendix I**). Furthermore, compared to other recent bioreactor-related studies, which focus on either using cyclic strain or electrical stimulation [88, 93, 100, 103, 105, 165, 180-183], this study highlights the importance of combining pulsatile shear stress and cyclic strain to drive ESC-CM maturation. Specifically, an increased cardiac-associated gene expression and an improved alignment of sarcomeric fibers were detected in 12-day dynamically cultured murine ESC-CMs (mESC-CMs) and 10-day dynamically cultured hESC-CMs when compared to static controls. In previous studies, a majority of the ESC-CMs did not respond to caffeine, as they were similar to fetal CMs, which relied on calcium influx from sarcolemma instead of the sarcoplasmic reticulum [184, 185]. Some studies cultured hESC-CMs for 27 days and those CMs were responded to caffeine [103,

186]. However, this study determined that dynamically cultured ESC-CMs responded to caffeine after 12 (mESC-CMs) or 10 days (hESC-CMs) (**Appendix I**).

Nevertheless, 12-day dynamically cultured mESC-CMs and 10-day dynamically cultured hESC-CMs remain non-comparable to adult CMs, due to the difference in the sarcomeric structures and cardiac gene expression (**Appendix I**). As observed from in vivo conditions, human neonatal CMs take approximately six years to reach their adult phenotype [187]. Thus, an extended culture time is necessary in order to obtain CMs of greater maturity. Kamakura et al. reported that long-term cultured (1 year) hiPSC-derived CMs (hiPSC-CMs) exhibited ultrastructural sarcomeric changes compared to short-term cultured hiPSC-CMs (14 days) [101]. Recently, another group have cultured hPSC-CMs for 80-120 days and found dramatic changes in cell size, sarcomere length, electrophysiological, and calcium handling properties [188]. However, the limitation of low throughput and the relatively long culture time requirement have restricted the study´s application. In our study, dynamic culture time was extended to 18 days (mESC-CMs) or 20 days (hESC-CMs) and a further increase in CM maturation-associated markers was observed (**Appendix I**). 18-day dynamically cultured mESC-CMs and 20-day dynamically cultured hESC-CMs exhibited well-organized sarcomeric proteins, an increased gap junction protein expression, an increased cardiac ion channel gene expression and a functional improvement compared to ESC-CMs cultured in a short time or under static conditions (**Appendix I**). It is particularly noteworthy that 20-day dynamically cultured hESC-CMs had an average sarcomere length of 1.97 ± 0.25 mm, which is higher than the average sarcomere length of hESC-CMs reported in other studies and is close to the sarcomere length of relaxed adult CMs [103, 189]. Additionally, the typical systolic calcium transient parameters (e.g. the rate of constant of Ca^{2+} decay, slope, the amplitude), and the caffeine-induced calcium transient parameters (e.g. Ca^{2+} transient duration) were improved through the extension of culture times, suggesting a rapid electromechanical coupling. A concentration-response study was employed using a multi-electrode array system to investigate ion channel properties in hESC-CMs. Interestingly, both 10-day and 20-day statically and dynamically cultured hESC-CMs exhibited a dose-dependent response to nifedipine and dofetilide without any significant differences. This suggests that the calcium and hERG channels in all hESC-CMs were fully functional (**Appendix I**). Raman microspectroscopy, which has shown in the previous study for the marker-free

characterization of CM phenotypes [190], was used to compare dynamically cultured ESC-CMs to primary isolated CMs. Maturation-associated peaks similar to those of primary CMs were detected in 18-day dynamically cultured mESC-CMs and 20-day dynamically cultured hESC-CMs (**Appendix I**, Figure 4). This may indicate that both had a comparable phenotype to primary CMs.

The myocardial differentiation, specification, and maturation are regulated via signaling pathways, such as Wnt/β catenin signaling pathway. These pathways can be activated or inhibited by mechanical stimuli or biochemical cues [191, 192]. As shown by previous studies, the down-regulation of Wnt/β-catenin signaling promotes the maturation of committed CMs [191, 192]. Consequently, a lower expression of β-catenin in 20-day dynamically cultured hESC-CMs was observed when compared with static control (**Appendix I**), indicating that mechanical stimuli may lead to the downregulation of Wnt/β-catenin signaling and, thus regulate the maturation of hESC-CMs.

In summary, our results highlight the importance of combined pulsatile flow, cyclic strain and extended culture time in the maturation process of PSC-CMs. The designed flow/strain bioreactor system can serve as a foundation for the development of human-based cardiac in vitro models to verify drug candidates. Furthermore, it can facilitate the study of cardiovascular development and disease.

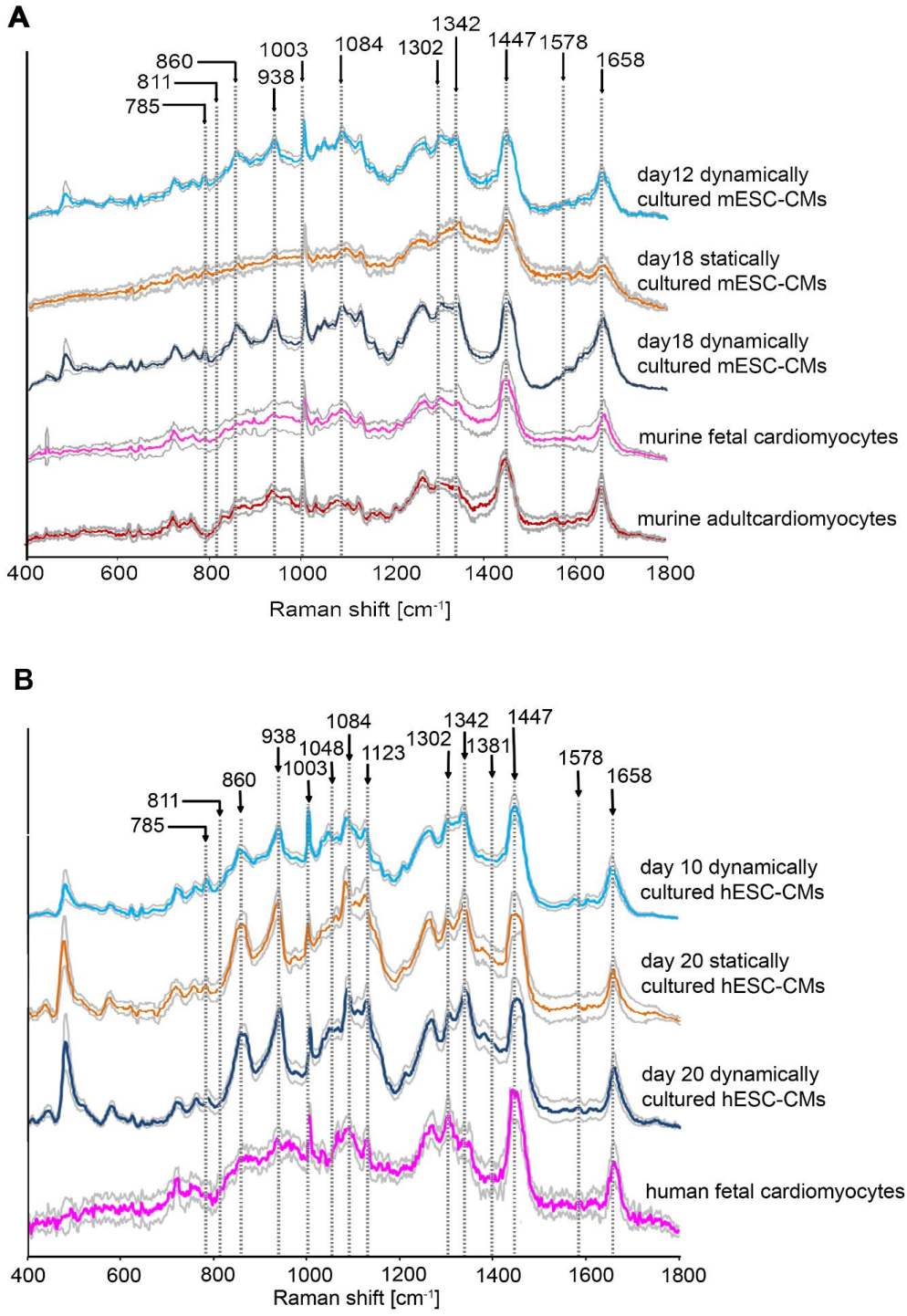

Figure 4: Phenotype characterization of (A) mESC-CMs and (B) hESC-CMs using Raman microspectroscopy. Scores plot demonstrates spectral changes due to cardiac maturation highlighted by the arrow. The responsible peaks were identified both in murine and human cells were 785, 811, 860, 938, 1,003, 1,084, 1,302, 1,342, 1,447, 1,578, 1,578 and 1,658cm^{-1}. Interestingly, different Raman peaks were identified in Raman spectra from murine and human cells (1,048, 1,123, and 1,302 cm^{-1}).

.

3.2 Low shear stress conditioning supports elastogenesis in fibroblasts

Elastin plays a crucial role in organ development and allows heart valves and blood vessels to endure passive recoil and accommodate strains by deformation [106]. Therefore, in order to ensure appropriate mechanical function, tissue-engineered cardiac tissue or blood vessels necessity incorporate an elastic component [107]. However, the induction of elastogensis remains challenging because of the size, molecular complexity of elastic fibers, as well as the requirement for numerous proteins to facilitate fiber assembly. In a previous study, a custom-designed flow bioreactor system was shown to allow the generation of maturing elastic fiber contain ECM in SMCs [113]. Here, the same bioreactor system and the same experimental setting were used to investigate the effect of low shear stress conditioning on elastogenesis in foreskin fibroblasts and adult skin fibroblasts (**see publication: Appendix II**). Fibroblasts are the most abundant cells in human body and are more suitable for cardiac models than SMCs since SMCs are isolated from veins and arteries, which is a disadvantage when producing patient-tailored models [113, 193]. Foreskin fibroblasts obtained from patients in the age range of 1-10 years old and adult skin fibroblasts isolated from 20-40 years old patients were used in this study. In humans, before birth and in the first few years of life, fibroblasts and SMCs produce the elastic fibers required for the tissue or organs to develop [194]. However, elastin gene expression begins to be substantially diminished from a young age [194]. To exclude the differences between different donors, the experiments with the cells isolated from three donors were repeated for each experiment.

Fibroblasts were seeded on hydrophilic electrospun 3D PEGdma and PLA scaffolds [113] and subjected to a shear stress within the bioreactors for 6 days (**Appendix II**). Our results showed that foreskin fibroblasts exposed to shear stress exhibited an upregulation of ELN (elastin) and FBN1 (fibrillin 1) after a six-day culture (**Appendix II**). A shear stress-induced-upregulation of (tropo)elastin synthesis in foreskin fibroblast was observed by comparing the dynamic cultured cells to the static controls (Figure 5). Interestingly, in both dynamic and static cultures, elastin deposition on electrospun PEGdma-PLA scaffolds was observed (**Appendix II**, Figure 5) [113]. A possible explanation is that the fibrous matrix has a higher surface

area that provides a more suitable environment for the attachment of proteins and growth factors [195, 196]. In addition, an increase in elastogenesis-associated-protein expression in dynamically cultured foreskin fibroblasts (including fibrillin-1, fibrillin-2, fibulin-4, fibulin-5 and EMILIN1) was observed in immunofluorescence (IF) staining images when compared to static controls (**Appendix II**, Figure 5). After six days of dynamic culture, these elastogenesis-associated fibers aligned in one direction. This observation of fiber alignment is in agreement with the findings of Ng et al. [197].

To detect the (tropo)elastin expression in adult skin fibroblasts, IF staining on 6-day statically and dynamically cultured samples was performed. The images confirmed the expression of extracellular tropoelastin/elastin in both statically and dynamically cultured adult skin fibroblasts (Figure 6, **Appendix II**). As with foreskin fibroblasts, a deposition of elastin on the electrospun fibers between the cells in both static and dynamic samples was detected. IF staining was performed on statically and dynamically cultured adult skin fibroblasts for fibrillin-1, fibrillin-2, fibulin-4, fibulin-5, EMILIN1 and fibronectin (green; Figure 6, **Appendix II**), all of which are known to be critical for proper matrix assembly and crosslinking [106]. The IF images revealed a positive staining of fibrillin-1 and fibronectin in both statically cultured and dynamically cultured samples. In contrast to dynamic samples, the staining of fibrillin-1 showed a less homogenous expression in the static control (**Appendix II**, Figure 6). Fibrillin-2, fibulin-4, fibulin-5 and EMILIN1 in dynamic samples exhibited an increased expression with a fibrillar structure between the cells (**Appendix II**). Conversely, the expression of the same proteins in the static controls was barely detectable (Figure 6). Furthermore, alignment of the proteins was observed after six days of dynamic culture (**Appendix II**). mRNA expression of ELN and FBN1 were significantly upregulated in foreskin fibroblasts compared to adult skin fibroblasts, which was supported by findings of other studies [198, 199]. Surprisingly, no difference was observed in elastin and elastogenesis-associated protein expressions in both foreskin fibroblasts and normal skin fibroblasts (**Appendix II**, Figure 5, and Figure 6). In contrast, Zheng et al. have detected significantly lower levels of expression of elastin, fibrillin-1, and fibulin-5 in cells with a high passage number [199]. These discrepancies are possibly related to different culture environment (static or dynamic) and cell source.

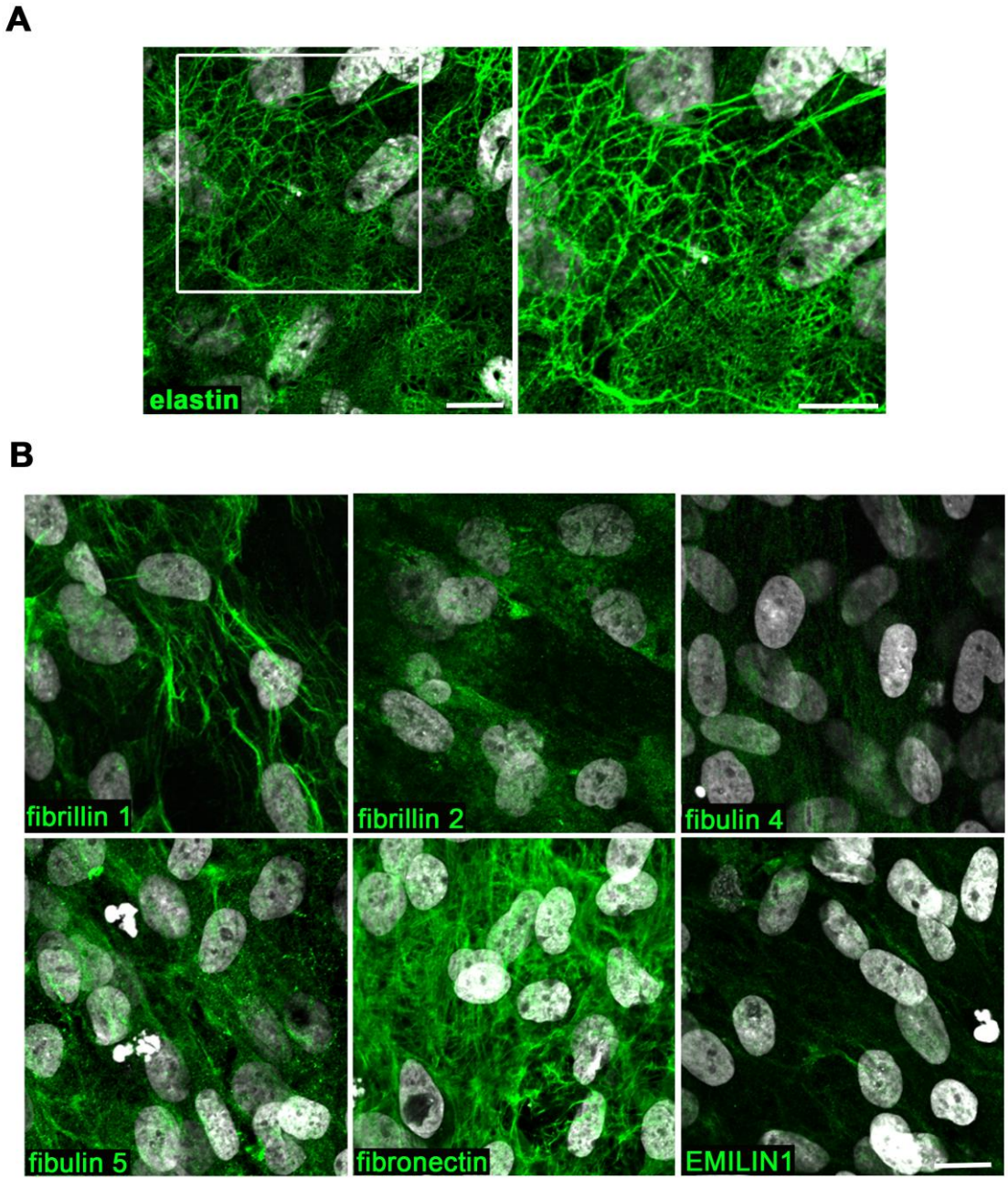

Figure 5: **IF staining of elastin (A) and (B) elastogenesis-associated proteins on statically cultured foreskin fibroblasts.** Elastin is shown in green. Cell nuclei are depicted in white (DAPI). The scale bars equal to 20 µm.

Raman microspectroscopy was employed to detect the crosslinking level of elastic fibers [200-202]. Raman peaks that are previously assigned to two major elastin crosslinks (desmosine and isodesmosine) [201] are significantly higher in dynamically cultured samples than static controls, indicating a higher level of

crosslinking and the presence of properly crosslinked, mature elastic fibers (**Appendix II**).

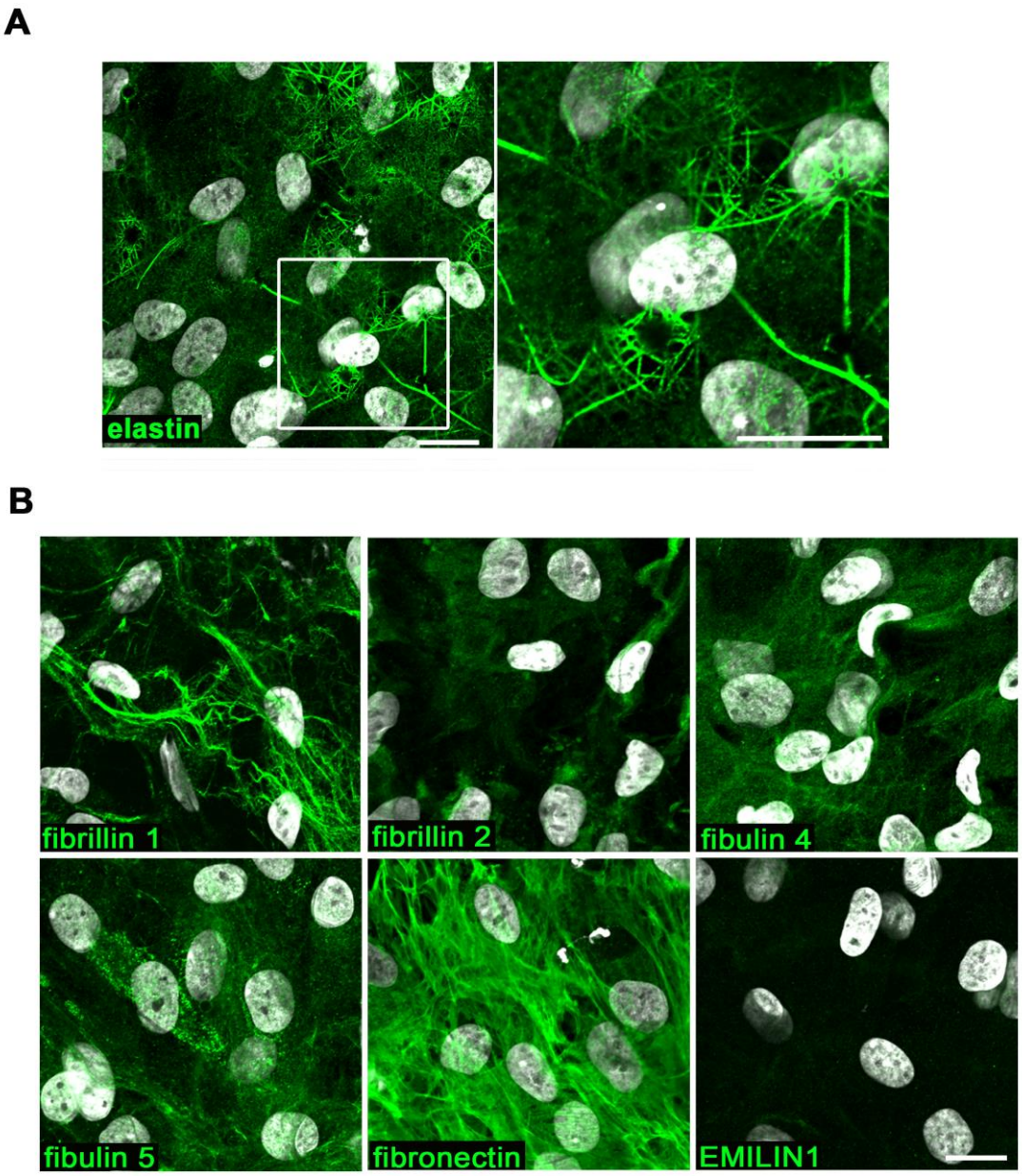

Figure 6: **IF staining of (A) elastin and (B) elastogenesis-associated proteins on statically cultured normal skin fibroblasts.** Elastin is shown in green. Cell nuclei are depicted in white (DAPI). The scale bars equal to 20 µm.

The shear stress applied in this study was relatively low (between 6×10^{-4} and 11×10^{-4} dyne/cm^2) in order to mimic interstitial flow. Interestingly, the interstitial flow has previously been shown to influence fibroblast growth kinetics and morphology [203]. For example, dermal and lung fibroblasts, which were cultured in collagen and exposed to an interstitial flow in a range of 0.1-0.3 dyne/cm^2 for a short time,

.

displayed perpendicular alignment to the direction of fluid flow [197]. Korin et al. have reported that a flow rate of 0.2 mL/hour can promote human foreskin fibroblasts proliferation [203]. Another study showed that shear stress (0.8 dyne/cm^2) can induce rat aortic fibroblast differentiation into myofibroblasts in a 2D culture [204]. Nevertheless, this study has shown for the first time that interstitial flow can enhance elastogenesis in fibroblasts.

The described customized bioreactor system was also used in another study of a project partner to apply flow to hiPSC-derived early SMCs [205]. The usage of pulsatile flow provided by the described bioreactor system resulted in a significantly higher elastin-associated gene expression, a higher concentration of mature elastin, and enhanced maturation of hiPSC derived SMCs. This study further proved that the described customized fluid flow bioreactor is a powerful tool to generate maturing elastic fibers in different types of cells (SMCs [113], fibroblasts (**Appendix II**), hiPSC-derived SMCs [205]) and can serve as a platform to create engineered elastic fiber-rich tissues, as well as organs such as heart valves and vessels.

3.3 A fluid flow bioreactor system that is compatible with real-time high-resolution microscopy

As established in sections 3.1 and 3.2, fluid shear stress plays a crucial role in driving cardiac maturation and elastogenesis. However, to characterize the effect of mechanical stimuli on the cells, the samples have to be sacrificed which does not allow for continuous data sampling. In addition, using multiple samples for various time points may cause high sample variability. Therefore, it would be highly advantageous to develop a system that allows for continuous and non-destructive quantification of biological activities of cells and tissues that are exposed to shear stress in vitro.

To meet this demand, a high-throughput bioreactor system that combines high-resolution marker-free imaging and continuous flow was developed. This bioreactor is in conjunction with various types of imaging modalities, specifically, fluorescence lifetime imaging microscopy (FLIM) was designed and validated (**Appendix III**, Figure 7). FLIM is a non-invasive method that is able to measure intracellular microenvironment change and metabolic shifts within cells [206-210]. As illustrated in Appendix III and Figure 7, the high-resolution imaging bioreactor was designed to be the same size as a cell culture well-plate, thereby ensuring its compatible with various imaging systems. It is composed of four district flow chambers that enable the execution of independent experiments within one system, and thus largely improves the culture´s efficiency (**Appendix III**, Figure 7). Steady-state flow patterns within the fluidic chamber of the bioreactor systems were performed with COMSOL based on the geometry of the bioreactor (**Appendix III**). According to the simulation results, this bioreactor is able to provide reproducible laminar flow conditions with shear stresses of up to 11.2 dyn/cm^2.

To characterize the bioreactor system, HUVECs were cultured for 24 hours under low shear stress conditions to validate the functionality of the bioreactor system. After a 24-hour culture within the bioreactor system, HUVECs retained a high viability, indicating that the bioreactor system is biocompatible (**Appendix III**). To prove the functionality of the bioreactor regarding real-time live cell imaging, HUVECs were subjected to a scratch assay and stimulated with low shear stress or static conditions. 24-hour time lapses imaging were taken and demonstrated that the migration of

HUVECs was decreased under low shear stress conditioning from levels observed in static controls (**Appendix III**). This is in accordance with a previous study, in which Sheikh et al. observed similar characteristics of HUVECs after exposure to a defined shear stress of approximately 0.3 dyn/cm^2 [211]. Finally, FLIM was utilized to investigate the metabolic activity of HUVECs to demonstrate the possibility of high-resolution marker-free imaging. It has previously been shown that shear stress can alter metabolism in endothelial cells from glycolysis to oxidative phosphorylation-dependent mechanisms [116]. Consistent with these findings, a decreased contribution of free-NAD(P)H (α_1) in the 24-hour laminar shear stress-exposed HUVECs was detected when compared with the static controls or HUVECs prior to exposure to shear stress (**Appendix III**). This indicates a metabolic switch from glycolysis to oxidative phosphorylation [212].

Indeed, there are some poly(dimethylsiloxane) (PDMS)-based microfluidic devices that also allow for high-resolution live-cell microscopy. For example, Tonin M. et al have fabricated a hybrid PDMS/glass microfluidic device that facilitates high-resolution microscopy as well as a full control of flow [213]. Another group has also described a similar system that allows for imaging cellular migration at high-resolutions [214]. However, these devices suffer from technical challenges. For example, bubbles in the microchannels are difficult to remove and pose a risk of cell damage [215]. Microfluidic devices are also restricted by their size and are not suitable for larger samples or 3D cultures [215]. Moreover, these microfluidic devices are made by PDMS, a material that absorbs small molecules [216]. This reduces the drug dose, may shift the dose-response curve, and thus limits the predictive value of assays [216].

In sum, this section presented a high-resolution imaging bioreactor system that can provide shear stress while also allowing for successful real-time analysis of cells in culture. Simulation results proved that this system can provide laminar flow in a wide flow range. In addition, it is biocompatible with cells, user-friendly, and compatible high-resolution imaging modalities. Future possibilities for this bioreactor include real-time monitoring in vitro cell fate development, including but not limited to direct cell reprogramming or stem cell differentiation and drug testing.

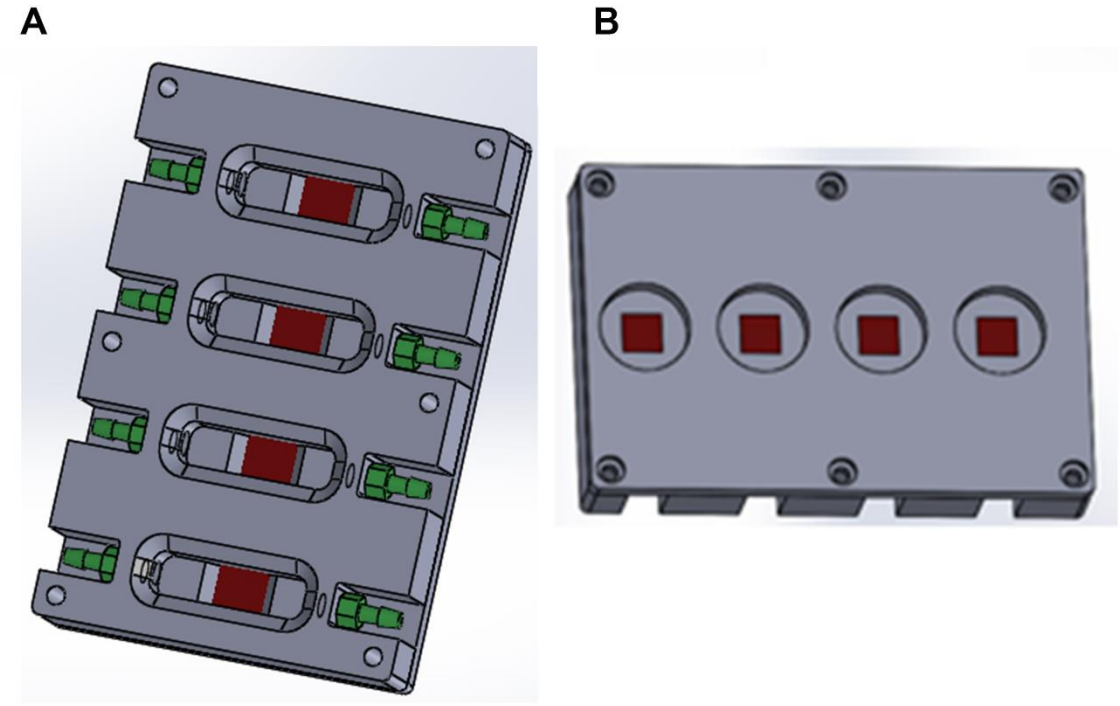

Figure 7: **CAD drawing of new high throughput imaging and flow bioreactor design.** Dimensions are 127 x 85 mm and 21 mm in thickness. (A) is a view of the bioreactor from the top to show the four distinct flow chambers. (B) is a view from the bottom showing where microscope objective can contact cell seeded area for high-resolution imaging.

4 Outlook

Bioreactor systems are fundamental for cardiovascular tissue engineering since it mimics the complexity of the hydrodynamics of the human circulation and continuous contractions of the heart [155]. The results of this thesis emphasize that applying physiologically related mechanical stimulations, including pulsatile flow and cyclic strains, through bioreactor systems can support cell maturation and ECM formation. This conclusion is in agreement with other studies, which also employed bioreactor systems to regulate cell activity [16, 95, 153, 154, 158, 162, 164, 217-219]. Though our studies and studies from others it was confirmed that factors such as amplitude, frequency, and direction of mechanical strains as well as type and amplitude of flow can be critical for the regulation of the cell functions [16, 95, 153, 154, 158, 162, 164, 217-219]. However, the type and parameters of physical stimuli needed to regulate cells remain speculative. Therefore, a systematic study to examine the combination of multiple types of mechanical stimulations across a broad range of magnitude and multiple frequencies is necessary. Moreover, the mechanisms underlying the mechanical force-stimulated changes are not entirely clear. In response to shear stress or cyclic strains, a multitude of intracellular signaling pathways might be triggered in cells, such as the ERK1/2 pathway [220], the MAPK pathway [221], the NFκB pathway [148, 222], and the RhoA/ROCK pathway [223]. It shall be noticed that mechanical stimuli often simultaneously activate multiple signaling pathways [126]. It is relatively difficult to perform research on one specific pathway, as signaling pathways can have significant overlap and crosstalk [126]. Thus, experiments will be conducted to systematically identify the key signaling pathways that are activated when applying the mechanical stimuli in the near future.

Despite the fact that the dynamically cultured ESC-CMs exhibited an increased maturation stage compared to static controls in the context of morphology, calcium handling properties, and gene expression, these dynamically cultured ESC-CMs are not yet completely mature, especially when compared to adult CMs. CMs in vivo are constantly subjected to electrical stimuli, which promote synchronous contractions [88]. Although only limited work has been published, current data suggest that electrical stimuli promote cardiac differentiation and maturation. For example, Radisic

et al. employed electrical pulses on neonatal rat ventricular CMs at 1 Hz for only eight days, which caused a remarkable level of ultrastructural organization and improved conductive and contractile properties [224]. In another study on human iPSC-CMs, pacing with biphasic pulses at 1.5 to 2 Hz for 14 days led to a higher cytoplasm to nucleus ratio, longitudinally oriented CMs, and enhanced calcium transient properties [105]. More recently, Nunes et al. have published a study indicating that a high stimulation frequency of 6 Hz can largely influence the maturation of hPSC-CMs, although a normal human adult heart rate is approximately 1 Hz [103]. Cells stimulated under the 6 Hz regime displayed signs of maturation, such as improved cell and myofilament structure with clearly visible Z discs, H zones and I bands, better electrical properties, improved electrophysiological and calcium handling properties and a greater number of mitochondria and desmosomes compared to static controls or 3 Hz conditions [103]. Based on this background, it would be necessary to design a bioreactor system which combines strain, perfusion flow, and electrical stimulations in order to faithfully mimic the physiology of the cardiovascular system in future studies.

The 2D porous Thincert™ membranes were used in this PhD thesis to study the maturation of ESC-CMs because 2D culture systems are easy to establish and can allow researchers to focus on the influence of mechanical cues with fewer uncontrolled factors than in the case with to 3D cultures. However, 2D cell culture does not represent the physiological environment of cells as cells in vivo reside in a 3D environment that is surrounded by other cells as well [225, 226]. In addition, the 3D cell culture is more reflective of in vivo cellular responses [225, 226]. Previous research efforts have demonstrated that cells in 3D culture environments exhibited improvement in basic biological mechanisms, such as cell proliferation, differentiation, response to stimuli, cell-cell communications, migration, drug metabolism, etc [225, 226]. Thus, it is necessary to further investigate if culturing ESC-CM in the 3D environment could advance the maturation. Scaffolds used in the field of cardiovascular tissue engineering need appropriate mechanical properties to endure cyclic stresses and strains, as well as to be able to support cell infiltration, growth, and cell-to-cell interaction. In addition, scaffolds must have optimal pore sizes, porosity and permeability to allow the diffusion of nutrients and metabolic waste [227]. Various types of scaffolds have been used, such as synthesis scaffolds and natural scaffolds [227]. Among them, our group previously proved that electrospun scaffolds

can create an artificial structure, which mimics the in vivo microenvironment that supports cell adhesion, migration, differentiation, and maturation [228]. Future work includes the characterization of different scaffolds, such as PEGdma and PLA, PLA, and fibronectin-coated PEGdma scaffolds within the stretch flow bioreactor system. This will allow determining the influence of 3D environment in conjunction with mechanical forces on ESC-CM maturation.

In this thesis, a method to use the customized flow bioreactor system to promote elastin and elastic fiber-related proteins synthesis in fibroblasts was described. This technology can be employed to generate engineered elastic-fiber rich tissues in the future, such as blood vessels or heart valves. In order to produce functional elastic-fiber containing engineered tissues, other cell types must be introduced into the system as majority organs or tissues involve more than one cell types in vivo [229]. Furthermore, in tissues or organs, cells are normally subjected to a complex mechanical environment [230]. As an example, the aortic valve experiences tension, stretch, pressure, laminar shear stress and turbulent shear stress during each cardiac cycle [230]. Therefore, this flow bioreactor system must be optimized specifically for each engineered organ or tissue.

In this study, HUVECs were cultured under low shear stress conditions only for 24 hours to prove the functionality of the imaging bioreactor system. Therefore, future studies will need to focus on a long-term culture of HUVECs under different types and magnitude of shear stress. Other application of this imaging bioreactor would be to assess the stem cell commitment and cell maturation process under flow condition. The real-time monitoring of differentiation and maturation can give a more conclusive understanding of the complex biological mechanism to produce mature cardiac tissue. The other potential application of this imaging bioreactor system is to be utilized for drug testing. Compare to static systems, in which cells or tissues are exposed to a constant drug concentration, the continuous flow in the bioreactor system allows cells or tissues to be exposed to an environment, where the concentration of the drug constantly changes. This resembles more the in vivo processes of drug biotransformation [231].

5 References

1. Mendis, S., P. Puska, and B. Norrving, *Global atlas on cardiovascular disease prevention and contro*l, W.W.H.F.W.S. Organization, Editor. 2011.

2. Nichols, M., N. Townsend, P. Scarborough, and M. Rayner, *Cardiovascular disease in Europe 2014: epidemiological update.* European Heart Journal, 2014. 35(42): p. 2950-9.

3. Abouna, G.M., *Organ shortage crisis: problems and possible solutions*. Transplant Proceedings, 2008. 40(1): p. 34-8.

4. Weil, R., D.R. Clarke, Y. Iwaki, K.A. Porter, L.J. Koep, B.C. Paton, P.I. Terasaki, and T.E. Starzl, *Hyperacute rejection of a transplatated human heart.* Transplantation, 1981. 32(1): p. 71-72.

5. Boneva, R.S., T.M. Folks, and L.E. Chapman, *Infectious disease issues in xenotransplantation*. Clinical Microbiology Reviews, 2001. 14(1): p. 1-14.

6. ashid, M.A., D. Edwards, F.M. Walter, and J. Mant, *Medication taking in coronary artery disease: A systematic review and qualitative synthesis.* The Annals of Family Medicine, 2014. 12(3): p. 224-232.

7. Stern, C.S. and J. Lebowitz, *Latest drug developments in the field of cardiovascular disease*. The International Journal of Angiology: Official Publication of the International College of Angiology, Inc, 2010. 19(3): p. e100-e105.

8. McGonigle, P. and B. Ruggeri, *Animal models of human disease: Challenges in enabling translation*. Biochemical Pharmacology, 2014. 87(1): p. 162-171.

9. Denayer, T., T. Stöhr, and M. Van Roy, *Animal models in translational medicine: Validation and predic*tion. New Horizons in Translational Medicine, 2014. 2(1): p. 5-11.

10. Davis, R.P., C.W. van den Berg, S. Casini, S.R. Braam, and C.L. Mummery, *Pluripotent stem cell models of cardiac disease and their implication for drug discovery and development.* Trends in Molecular Medicine, 2011. 17(9): p. 475-484.

11. Johnson, M.J., *Management of end stage cardiac failure*. Postgraduate Medicine Journal. 2007. 83(980): p. 395-401.

12. Adler, E.D., J.Z. Goldfinger, J. Kalman, M.E. Park, and D.E. Meier, *Palliative care in the treatment of advanced heart failure.* Circulation, 2009. 120(25): p. 2597-2606.

13. Badylak, S.F. and R.M. Nerem, *Progress in tissue engineering and regenerative medicine*. Proceedings of the National Academy of Sciences, 2010. 107(8): p. 3285-3286.

14. Vunjak-Novakovic, G., N. Tandon, A. Godier, R. Maidhof, A. Marsano, T.P. Martens, and M. Radisic, *Challenges in cardiac tissue engineering.* Tissue Engineering Part B Review, 2010. 16(2): p. 169-87.

15. Martin, I., D. Wendt, and M. Heberer, *The role of bioreactors in tissue engineerin*g. Trends in Biotechnology, 2004. 22(2): p. 80-6.

16. Chen, H.-C. and Y.-C. Hu, *Bioreactors for tissue engineering*. Biotechnology Letters, 2006. 28(18): p. 1415-1423.

17. Emmert, M.Y., E.S. Fioretta, and S.P. Hoerstrup, *Translational challenges in cardiovascular tissue engineering*. Journal of Cardiovascular Translational Research, 2017. 10(2): p. 139-149.

18. Chen, Q.-Z., S.E. Harding, N.N. Ali, A.R. Lyon, and A.R. Boccaccini, *Biomaterials in cardiac tissue engineering: Ten years of research survey.* Materials Science and Engineering: R: Reports, 2008. 59(1–6): p. 1-37.

19. van Spreeuwel, A.C., et al., *The influence of matrix (an)isotropy on cardiomyocyte contraction in engineered cardiac microtissues*. Integrative Biology, 2014. 6(4): p. 422-9.

20. Kolwicz, S.C., S. Purohit, and R. Tian, *Cardiac metabolism and its interactions with contraction, growth, and survival of cardiomyocytes*. Circulation Research, 2013. 113(5): p. 603-616.

21. Smits, A.M., P. van Vliet, C.H. Metz, T. Korfage, J.P.G. Sluijter, P.A. Doevendans, and M.-J. Goumans, *Human cardiomyocyte progenitor cells differentiate into functional mature cardiomyocytes: an in vitro model for studying*

human cardiac physiology and pathophysiology. Nature Protocols, 2009. 4(2): p. 232-243.

22. Louch, W.E., K.A. Sheehan, and B.M. Wolska, *Methods in cardiomyocyte isolation, culture, and gene transfe*r. Journal of Molecular and Cellular Cardiology, 2011. 51(3): p. 288-298.

23. Schluter, K.D. and D. Schreiber, *Adult ventricular cardiomyocytes: isolation and culture*. Methods in Molecular Biology, 2005. 290: p. 305-14.

24. Woodcock, E.A. and S.J. Matkovich, *Cardiomyocytes structure, function and associated pathologie*s. The International Journal of Biochemistry & Cell Biology, 2005. 37(9): p. 1746-1751.

25. O'Connell, T.D., M.C. Rodrigo, and P.C. Simpson, *Isolation and culture of adult mouse cardiac myocyte*s. Methods in Molecular Biology, 2007. 357: p. 271-96.

26. Beltrami, A.P., et al., *Adult cardiac stem cells are multipotent and support myocardial regeneration*. Cell, 2003. 114(6): p. 763-776.

27. Messina, E., et al., *Isolation and expansion of adult cardiac stem cells from human and murine heart*. Circulation Research, 2004. 95(9): p. 911-921.

28. Garbern, J C. and R T. Lee, *Cardiac stem cell therapy and the promise of heart regeneration*. Cell Stem Cell, 2013. 12(6): p. 689-698.

29. Segers, V.F.M. and R.T. Lee, *Stem-cell therapy for cardiac disease*. Nature, 2008. 451(7181): p. 937-942.

30. Cai, C.-L., X. Liang, Y. Shi, P.-H. Chu, S.L. Pfaff, J. Chen, and S. Evans, *Isl1 identifies a cardiac progenitor population that proliferates prior to differentiation and contributes a majority of cells to the heart*. Developmental Cell, 2003. 5(6): p. 877-889.

31. Balsam, L.B., A.J. Wagers, J.L. Christensen, T. Kofidis, I.L. Weissman, and R.C. Robbins, *Haematopoietic stem cells adopt mature haematopoietic fates in ischaemic myocardium*. Nature, 2004. 428(6983): p. 668-673.

32. van Berlo, J.H., O. Kanisicak, M. Maillet, R.J. Vagnozzi, J. Karch, S.C. Lin, R.C. Middleton, E. Marban, and J.D. Molkentin, *c-kit+ cells minimally contribute cardiomyocytes to the heart*. Nature, 2014. 509(7500): p. 337-41.

33. Bolli, R., et al., *Cardiac stem cells in patients with ischaemic cardiomyopathy (SCIPIO): initial results of a randomised phase 1 tria*l. Lancet, 2011. 378(9806): p. 1847-57.

34. Laugwitz, K.L., et al., *Postnatal isl1+ cardioblasts enter fully differentiated cardiomyocyte lineages*. Nature, 2005. 433(7026): p. 647-53.

35. Ahuja, P., P. Sdek, and W.R. Maclellan, *Cardiac myocyte cell cycle control in development, disease and regeneratio*n. Physiological Reviews, 2007. 87(2): p. 521-544.

36. Sun, Q., Z. Zhang, and Z. Sun*, The potential and challenges of using stem cells for cardiovascular repair and regeneration*. Genes & Diseases, 2014. 1(1): p. 113-119.

37. Bu, L., et al., *Human ISL1 heart progenitors generate diverse multipotent cardiovascular cell lineage*s. Nature, 2009. 460(7251): p. 113-117.

38. Leri, A., J. Kajstura, P. Anversa, and W.H. Frishman, *Myocardial regeneration and stem cell repair*. Current Problems in Cardiology, 2008. 33(3): p. 91-153.

39. Urbanek, K., et al., *Intense myocyte formation from cardiac stem cells in human cardiac hypertrophy*. Proceedings of the National Academy of Sciences of the United States of America, 2003. 100(18): p. 10440-5.

40. Verfaillie, C., *Pluripotent stem cell*s. Transfusion Clinique et Biologique, 2009. 16(2): p. 65-69.

41. Chong, J.J.H., et al., *Human embryonic-stem-cell-derived cardiomyocytes regenerate non-human primate hearts*. Nature, 2014. 510(7504): p. 273-277.

42. Thomson, J.A., J. Itskovitz-Eldor, S.S. Shapiro, M.A. Waknitz, J.J. Swiergiel, V.S. Marshall, and J.M. Jones, *Embryonic stem cell lines derived from human blastocysts*. Science, 1998. 282(5391): p. 1145-7.

43. Takahashi, K. and S. Yamanaka, *Induction of pluripotent stem cells from mouse embryonic and adult fibroblast cultures by defined factors*. Cell, 2006. 126(4): p. 663-676.

44. Zhu, R., A. Blazeski, E. Poon, K.D. Costa, L. Tung, and K.R. Boheler, *Physical developmental cues for the maturation of human pluripotent stem cell-derived cardiomyocytes*. Stem Cell Research & Therapy, 2014. 5(5): p. 117.

45. Du, M., X. Duan, and P. Yang, *Induced pluripotent stem cells and periodontal regeneration*. Current Oral Health Reports, 2015. 2(4): p. 257-265.

46. Egashira, T., S. Yuasa, and K. Fukuda, *Novel insights into disease modeling using induced pluripotent stem cells*. Biological & Pharmaceutical Bulletin, 2013. 36(2): p. 182-8.

47. Medvedev, S.P., A.I. Shevchenko, and S.M. Zakian, *Induced pluripotent stem cells: Problems and advantages when applying them in regenerative medicin*e. Acta Naturae, 2010. 2(2): p. 18-28.

48. Lin, Y.-C., et al*., Role of tumor suppressor genes in the cancer-associated reprogramming of human induced pluripotent stem cells*. Stem Cell Research & Therapy, 2014. 5(2): p. 58-58.

49. Papapetrou, E.P., et al., *Stoichiometric and temporal requirements of Oct4, Sox2, Klf4, and c-Myc expression for efficient human iPSC induction and differentiation*. Proceedings of the National Academy of Sciences of the United States of America, 2009. 106(31): p. 12759-64.

50. Carey, B.W., S. Markoulaki, J. Hanna, K. Saha, Q. Gao, M. Mitalipova, and R. Jaenisch, *Reprogramming of murine and human somatic cells using a single polycistronic vector*. Proceedings of the National Academy of Sciences of the United States of America, 2009. 106(1): p. 157-162.

51. Chang, C.W., Y.S. Lai, K.M. Pawlik, K. Liu, C.W. Sun, C. Li, T.R. Schoeb, and T.M. Townes, *Polycistronic lentiviral vector for "hit and run" reprogramming of adult skin fibroblasts to induced pluripotent stem cells*. Stem Cells, 2009. 27(5): p. 1042-9.

52. Stadtfeld, M., M. Nagaya, J. Utikal, G. Weir, and K. Hochedlinger, *Induced pluripotent stem cells generated without viral integration*. Science, 2008. 322(5903): p. 945-9.

53. Zhou, W. and C.R. Freed, *Adenoviral gene delivery can reprogram human fibroblasts to induced pluripotent stem cells*. Stem Cells, 2009. 27(11): p. 2667-74.

54. Fusaki, N., H. Ban, A. Nishiyama, K. Saeki, and M. Hasegawa, *Efficient induction of transgene-free human pluripotent stem cells using a vector based on Sendai virus, an RNA virus that does not integrate into the host genome*.

Proceedings of the Japan Academy. Series B, Physical and Biological Sciences, 2009. 85(8): p. 348-62.

55. Seki, T., et al., *Generation of induced pluripotent stem cells from human terminally differentiated circulating T cells.* Cell Stem Cell, 2010. 7(1): p. 11-14.

56. Zhou, H., et al., *Generation of induced pluripotent stem cells using recombinant protein*s. Cell Stem Cell, 2009. 4(5): p. 381-4.

57. Warren, L., et al., *Highly efficient reprogramming to pluripotency and directed differentiation of human cells with synthetic modified mRNA*. Cell Stem Cell, 2010. 7(5): p. 618-30.

58. ubramanyam, D., S. Lamouille, R.L. Judson, J.Y. Liu, N. Bucay, R. Derynck, and R. Blelloch, *Multiple targets of miR-302 and miR-372 promote reprogramming of human fibroblasts to induced pluripotent stem cells*. Nature Biotechnology, 2011. 29(5): p. 443-8.

59. Anokye-Danso, F., et al., *Highly efficient miRNA-mediated reprogramming of mouse and human somatic cells to pluripotency*. Cell Stem Cell. 8(4): p. 376-388.

60. Miyoshi, N., et al., *Reprogramming of mouse and human cells to pluripotency using mature microRNAs*. Cell Stem Cell, 2011. 8(6): p. 633-8.

61. Narsinh, K.H., F. Jia, R.C. Robbins, M.A. Kay, M.T. Longaker, and J.C. Wu, *Generation of adult human induced pluripotent stem cells using nonviral minicircle DNA vectors*. Nature Protocols, 2011. 6(1): p. 78-88.

62. Okita, K., M. Nakagawa, H. Hyenjong, T. Ichisaka, and S. Yamanaka, *Generation of mouse induced pluripotent stem cells without viral vector*s. Science, 2008. 322(5903): p. 949-53.

63. Yu, J., et al., *Induced pluripotent stem cell lines derived from human somatic cells*. Science, 2007. 318(5858): p. 1917-20.

64. Hu, K., J. Yu, K. Suknuntha, S. Tian, K. Montgomery, K.D. Choi, R. Stewart, J.A. Thomson, and Slukvin, II, *Efficient generation of transgene-free induced pluripotent stem cells from normal and neoplastic bone marrow and cord blood mononuclear cells*. Blood, 2011. 117(14): p. e109-19.

65. Chou, B.-K., et al., *Efficient human iPS cell derivation by a non-integrating plasmid from blood cells with unique epigenetic and gene expression signatures*. Cell Research, 2011. 21(3): p. 518-529.

66. Chen, G., et al., *Chemically defined conditions for human iPSC derivation and culture*. Nature Methods, 2011. 8(5): p. 424-9.

67. Mummery, C., et al., *Differentiation of human embryonic stem cells to cardiomyocytes: role of coculture with visceral endoderm-like cel*ls. Circulation, 2003. 107(21): p. 2733-40.

68. Passier, R., D.W. Oostwaard, J. Snapper, J. Kloots, R.J. Hassink, E. Kuijk, B. Roelen, A.B. de la Riviere, and C. Mummery, *Increased cardiomyocyte differentiation from human embryonic stem cells in serum-free cultures*. Stem Cells, 2005. 23(6): p. 772-80.

69. Graichen, R., et al., *Enhanced cardiomyogenesis of human embryonic stem cells by a small molecular inhibitor of p38 MAP*K. Differentiation, 2008. 76(4): p. 357-70.

70. Xu, X.Q., et al., *Chemically defined medium supporting cardiomyocyte differentiation of human embryonic stem cell*s. Differentiation, 2008. 76(9): p. 958-70.

71. Tran, T.H., X. Wang, C. Browne, Y. Zhang, M. Schinke, S. Izumo, and M. Burcin, *Wnt3a-induced mesoderm formation and cardiomyogenesis in human embryonic stem cells*. Stem Cells, 2009. 27(8): p. 1869-78.

72. Yang, L., et al., *Human cardiovascular progenitor cells develop from a KDR+ embryonic-stem-cell-derived population*. Nature, 2008. 453(7194): p. 524-8.

73. Kattman, S.J., A.D. Witty, M. Gagliardi, N.C. Dubois, M. Niapour, A. Hotta, J. Ellis, and G. Keller, *Stage-specific optimization of activin/nodal and BMP signaling promotes cardiac differentiation of mouse and human pluripotent stem cell lines*. Cell Stem Cell, 2011. 8(2): p. 228-40.

74. Willems, E., S. Spiering, H. Davidovics, M. Lanier, Z. Xia, M. Dawson, J. Cashman, and M. Mercola, *Small-molecule inhibitors of the Wnt pathway potently promote cardiomyocytes from human embryonic stem cell-derived mesoderm*. Circulation Research, 2011. 109(4): p. 360-4.

75. urridge, P.W., D. Anderson, H. Priddle, M.D. Barbadillo Munoz, S. Chamberlain, C. Allegrucci, L.E. Young, and C. Denning, *Improved human embryonic stem cell embryoid body homogeneity and cardiomyocyte differentiation from a novel V-96 plate aggregation system highlights interline variabili*ty. Stem Cells, 2007. 25(4): p. 929-38.

76. Zhang, J., et al., *Extracellular matrix promotes highly efficient cardiac differentiation of human pluripotent stem cells: the matrix sandwich method*. Circulation Research, 2012. 111(9): p. 1125-36.

77. Lian, X., et al., *Robust cardiomyocyte differentiation from human pluripotent stem cells via temporal modulation of canonical Wnt signaling*. Proceedings of the National Academy of Sciences of the United States of America, 2012. 109(27): p. E1848-57.

78. Karakikes, I., et al., *Small molecule-mediated directed differentiation of human embryonic stem cells toward ventricular cardiomyocytes*. Journal of Stem Cells Translational Medicine, 2014. 3(1): p. 18-31.

79. Ren, Y., et al., *Small molecule Wnt inhibitors enhance the efficiency of BMP-4-directed cardiac differentiation of human pluripotent stem cells*. Journal of Molecular and Cellular Cardiology, 2011. 51(3): p. 280-7.

80. Lian, X., J. Zhang, S.M. Azarin, K. Zhu, L.B. Hazeltine, X. Bao, C. Hsiao, T.J. Kamp, and S.P. Palecek, *Directed cardiomyocyte differentiation from human pluripotent stem cells by modulating Wnt/beta-catenin signaling under fully defined conditions*. Nature Protocols, 2013. 8(1): p. 162-75.

81. Mummery, C.L., J. Zhang, E.S. Ng, D.A. Elliott, A.G. Elefanty, and T.J. Kamp, *Differentiation of human ES and iPS cells to cardiomyocytes: A methods overview*. Circulation Research, 2012. 111(3): p. 344-358.

82. Chen, Y., I. Amende, T.G. Hampton, Y. Yang, Q. Ke, J.Y. Min, Y.F. Xiao, and J.P. Morgan, *Vascular endothelial growth factor promotes cardiomyocyte differentiation of embryonic stem ce*lls. American journal of physiology. Heart and circulatory physiology, 2006. 291(4): p. H1653-8.

83. Sirabella, D., E. Cimetta, and G. Vunjak-Novakovic*, "The state of the heart": Recent advances in engineering human cardiac tissue from pluripotent stem ce*lls. Experimental biology and medicine, 2015. 240(8): p. 1008-18.

84. Sayed, N., C. Liu, and J.C. Wu, *Translation of human-induced pluripotent stem cells from clinical trial in a dish to precision medicine*. Journal of the American College of Cardiology, 2016. 67(18): p. 2161-2176.

85. Gherghiceanu, M., L. Barad, A. Novak, I. Reiter, J. Itskovitz-Eldor, O. Binah, and L.M. Popescu, *Cardiomyocytes derived from human embryonic and induced pluripotent stem cells: comparative ultrastructure*. Journal of Cellular and Molecular Medicine, 2011. 15(11): p. 2539-51.

86. Snir, M., I. Kehat, A. Gepstein, R. Coleman, J. Itskovitz-Eldor, E. Livne, and L. Gepstein, *Assessment of the ultrastructural and proliferative properties of human embryonic stem cell-derived cardiomyocyte*s. American journal of physiology. Heart and circulatory physiology, 2003. 285(6): p. H2355-63.

87. Satin, J., et al., *Calcium handling in human embryonic stem cell-derived cardiomyocyte*s. Stem Cells, 2008. 26(8): p. 1961-72.

88. Yang, X., L. Pabon, and C.E. Murry, *Engineering adolescence: maturation of human pluripotent stem cell-derived cardiomyocytes*. Circulation Research, 2014. 114(3): p. 511-23.

89. Ruan, J.L., et al., *Mechanical stress promotes maturation of human myocardium from pluripotent stem cell-derived progenitors*. Stem Cells, 2015. 33(7): p. 2148-57.

90. Chun, Y.W., et al., *Differential responses of induced pluripotent stem cell-derived cardiomyocytes to anisotropic strain depends on disease status*. Journal of Biomechanics, 2015. 48(14): p. 3890-3896.

91. Schmelter, M., B. Ateghang, S. Helmig, M. Wartenberg, and H. Sauer*, Embryonic stem cells utilize reactive oxygen species as transducers of mechanical strain-induced cardiovascular differentiation*. The FASEB Journal, 2006. 20(8): p. 1182-4.

92. Gwak, S.J., S.H. Bhang, I.K. Kim, S.S. Kim, S.W. Cho, O. Jeon, K.J. Yoo, A.J. Putnam, and B.S. Kim, *The effect of cyclic strain on embryonic stem cell-derived cardiomyocytes*. Biomaterials, 2008. 29(7): p. 844-56.

93. Mihic, A., J. Li, Y. Miyagi, M. Gagliardi, S.H. Li, J. Zu, R.D. Weisel, G. Keller, and R.K. Li, *The effect of cyclic stretch on maturation and 3D tissue formation of human embryonic stem cell-derived cardiomyocytes*. Biomaterials, 2014. 35(9): p. 2798-808.

94. Lux, M., B. Andree, T. Horvath, A. Nosko, D. Manikowski, D. Hilfiker-Kleiner, A. Haverich, and A. Hilfiker, *In vitro maturation of large-scale cardiac patches based on a perfusable starter matrix by cyclic mechanical stimulation*. Acta Biomaterialia, 2016. 30: p. 177-87.

95. Jason, W.M., S.N. Sara, S. Aarash, A.R. Lewis, P. Aric, X. Yun, L. Carol, and R. Milica, *Bioreactor for modulation of cardiac microtissue phenotype by combined static stretch and electrical stimulation*. Biofabrication, 2014. 6(2): p. 024113.

96. Zhang, D., I.Y. Shadrin, J. Lam, H.Q. Xian, H.R. Snodgrass, and N. Bursac, *Tissue-engineered cardiac patch for advanced functional maturation of human ESC-derived cardiomyocytes*. Biomaterials, 2013. 34(23): p. 5813-20.

97. Valderrabano, M., *Influence of anisotropic conduction properties in the propagation of the cardiac action potential*. Progress in Biophysics and Molecular Biology, 2007. 94(1-2): p. 144-68.

98. Lieu, D.K., J.D. Fu, N. Chiamvimonvat, K.C. Tung, G.P. McNerney, T. Huser, G. Keller, C.W. Kong, and R.A. Li, *Mechanism-based facilitated maturation of human pluripotent stem cell-derived cardiomyocyte*s. Circulation: Arrhythmia and Electrophysiology, 2013. 6(1): p. 191-201.

99. Rao, C., et al., *The effect of microgrooved culture substrates on calcium cycling of cardiac myocytes derived from human induced pluripotent stem cells*. Biomaterials, 2013. 34(10): p. 2399-411.

100. Wang, J., et al., *Effect of engineered anisotropy on the susceptibility of human pluripotent stem cell-derived ventricular cardiomyocytes to arrhythmias*. Biomaterials, 2013. 34(35): p. 8878-86.

101. Kamakura, T., et al., *Ultrastructural maturation of human-induced pluripotent stem cell-derived cardiomyocytes in a long-term culture*. Circulation Journal, 2013. 77(5): p. 1307-14.

102. Tan, Y., D. Richards, R. Xu, S. Stewart-Clark, S.K. Mani, T.K. Borg, D.R. Menick, B. Tian, and Y. Mei, *Silicon nanowire-induced maturation of cardiomyocytes derived from human induced pluripotent stem cel*ls. Nano letters, 2015. 15(5): p. 2765-2772.

103. Nunes, S.S., et al., *Biowire: a platform for maturation of human pluripotent stem cell-derived cardiomyocyte*s. Nature Methods, 2013. 10(8): p. 781-787.

104. Xiao, Y., et al., *Microfabricated perfusable cardiac biowire: a platform that mimics native cardiac bundle*. Lab Chip, 2014. 14(5): p. 869-82.

105. Hirt, M.N., et al., *Functional improvement and maturation of rat and human engineered heart tissue by chronic electrical stimulation*. Journal of Molecular and Cellular Cardiology, 2014. 74: p. 151-161.

106. Wagenseil, J.E. and R.P. Mecham, *New insights into elastic fiber assembly*. Birth Defects Research. Part C, Embryo Today: Reviews., 2007. 81(4): p. 229-40.

107. Patel, A., B. Fine, M. Sandig, and K. Mequanint, *Elastin biosynthesis: The missing link in tissue-engineered blood vessels*. Cardiovascular Research, 2006. 71(1): p. 40-9.

108. Vesely, I., *Heart valve tissue engineering*. Circulation Research, 2005. 97(8): p. 743-755.

109. Anita Mol, A.I.S., Carlijn VC Bouten and Frank PT Baaijens, *Tissue engineering of heart valves: advances and current challenges*. Expert Review of Medical Devices, 2009. 6(3): p. 259-275.

110. Mendelson, K. and F.J. Schoen*, Heart valve tissue engineering: concepts, approaches, progress, and challenges*. Annals of Biomedical Engineering, 2006. 34(12): p. 1799-1819.

111. Shifren, A. and R.P. Mecham, *The stumbling block in lung repair of emphysema: elastic fiber assembly*. Proceedings of the American Thoracic Society, 2006. 3(5): p. 428-33.

112. Keire, P.A., N. L'Heureux, R.B. Vernon, M.J. Merrilees, B. Starcher, E. Okon, N. Dusserre, T.N. McAllister, and T.N. Wight, *Expression of versican isoform V3 in the absence of ascorbate improves elastogenesis in engineered vascular constructs*. Tissue Engineering Part A, 2009. 16(2): p. 501-512.

113. Hinderer, S., N. Shen, L.J. Ringuette, J. Hansmann, D.P. Reinhardt, S.Y. Brucker, E.C. Davis, and K. Schenke-Layland, *In vitro elastogenesis – Instructing human vascular smooth muscle cells to generate an elastic fiber-containing extracellular matrix scaffold*. Biomedical Materials, 2015. 10(3): p. 034102.

114. Heise, R.L., A. Parekh, E.M. Joyce, M.B. Chancellor, and M.S. Sacks, *Strain history and TGF-β1 induce urinary bladder wall smooth muscle remodeling and elastogenesis*. Biomechanics and Modeling in Mechanobiology, 2012. 11(1-2): p. 131-145.

115. Farris, P.K., *Topical vitamin C: a useful agent for treating photoaging and other dermatologic conditions*. Dermatologic Surgery, 2005. 31(7 Pt 2): p. 814-7; discussion 818.

116. Kim, B., H. Lee, K. Kawata, and J.-Y. Park, *Exercise-mediated wall shear stress increases mitochondrial biogenesis in vascular endothelium*. PLoS ONE, 2014. 9(11): p. e111409.

117. Gupta, V. and K.J. Grande-Allen, *Effects of static and cyclic loading in regulating extracellular matrix synthesis by cardiovascular cells*. Cardiovascular Research, 2006. 72(3): p. 375-83.

118. Gambillara, V., T. Thacher, P. Silacci, and N. Stergiopulos, *Effects of reduced cyclic stretch on vascular smooth muscle cell function of pig carotids perfused ex vivo*. American Journal of Hypertension 2008. 21(4): p. 425-31.

119. Choe, M.M., P.H. Sporn, and M.A. Swartz, *Extracellular matrix remodeling by dynamic strain in a three-dimensional tissue-engineered human airway wall model*. American Journal of Respiratory Cell and Molecular Biology, 2006. 35(3): p. 306-313.

120. Joddar, B. and A. Ramamurthi, *Elastogenic effects of exogenous hyaluronan oligosaccharides on vascular smooth muscle cells*. Biomaterials, 2006. 27(33): p. 5698-5707.

121. Noda, K., et al., *Latent TGF-β binding protein 4 promotes elastic fiber assembly by interacting with fibulin-5*. Proceedings of the National Academy of Sciences of the United States of America, 2013. 110(8): p. 2852-2857.

122. Mecham, R.P., B.D. Levy, S.L. Morris, J.G. Madaras, and D.S. Wrenn, *Increased cyclic GMP levels lead to a stimulation of elastin production in ligament fibroblasts that is reversed by cyclic AMP. The Journal of biological chemistry*, 1985. 260(6): p. 3255-8.

123. Kothapalli, C.R. and A. Ramamurthi*, Lysyl oxidase enhances elastin synthesis and matrix formation by vascular smooth muscle cells*. Journal of tissue engineering and regenerative medicine, 2009. 3(8): p. 655-661.

124. Joddar, B. and A. Ramamurthi, *Fragment size- and dose-specific effects of hyaluronan on matrix synthesis by vascular smooth muscle cells*. Biomaterials, 2006. 27(15): p. 2994-3004.

125. Shi, Z.D., X.Y. Ji, H. Qazi, and J.M. Tarbell, *Interstitial flow promotes vascular fibroblast, myofibroblast, and smooth muscle cell motility in 3-D collagen I via upregulation of MMP-1. American journal of physiology*. Heart and Circulatory Physiology, 2009. 297(4): p. H1225-34.

126. Jaalouk, D.E. and J. Lammerding, *Mechanotransduction gone awry*. Nature Reviews Molecular Cell Biology, 2009. 10(1): p. 63-73.

127. Haga, J.H., Y.S. Li, and S. Chien, *Molecular basis of the effects of mechanical stretch on vascular smooth muscle cells*. Journal of Biomechanics, 2007. 40(5): p. 947-960.

128. Brosig, M., *Mechanotransduction in fibroblasts*. 2011, Universität Basel.

129. Davies, P.F., *Flow-mediated endothelial mechanotransduction*. Physiological Reviews, 1995. 75(3): p. 519-60.

130. Takahashi, M., T. Ishida, O. Traub, M.A. Corson, and B.C. Berk, *Mechanotransduction in endothelial cells: temporal signaling events in response to shear stress*. Journal of Vascular Research, 1997. 34(3): p. 212-9.

131. Orr, A.W., B.P. Helmke, B.R. Blackman, and M.A. Schwartz, *Mechanisms of mechanotransduction*. Developmental Cell, 2006. 10(1): p. 11-20.

132. Sit, S.-T. and E. Manser, *Rho GTPases and their role in organizing the actin cytoskeleton*. Journal of Cell Science, 2011. 124(5): p. 679-683.

133. Kang, H., Y. Fan, and X. Deng, *Vascular smooth muscle cell glycocalyx modulates shear-induced proliferation, migration, and NO production responses*. American Journal of Physiology. Heart and Circulatory Physiology, 2011. 300(1): p. H76-83.

134. Shi, Q., et al., *In vitro effects of pirfenidone on cardiac fibroblasts: proliferation, myofibroblast differentiation, migration and cytokine secretion*. PLoS ONE, 2011. 6(11): p. e28134.

135. Boycott, H.E., et al., *Shear stress triggers insertion of voltage-gated potassium channels from intracellular compartments in atrial myocytes*. Proceedings of the National Academy of Sciences of the United States of America, 2013. 110(41): p. e3955-e3964.

136. Davis, M.J., G.A. Meininger, and D.C. Zawieja, *Stretch-induced increases in intracellular calcium of isolated vascular smooth muscle cells*. American Journal of Physiology, 1992. 263(4 Pt 2): p. H1292-9.

137. Haga, M., A. Yamashita, J. Paszkowiak, B.E. Sumpio, and A. Dardik, *Oscillatory shear stress increases smooth muscle cell proliferation and Akt phosphorylation*. Journal of Vascular Surgery, 2003. 37(6): p. 1277-84.

138. Iwasaki, H., S. Eguchi, H. Ueno, F. Marumo, and Y. Hirata, *Mechanical stretch stimulates growth of vascular smooth muscle cells via epidermal growth factor receptor*. American Journal of Physiology, 2000. 278(2): p. H521-H529.

139. Iwasaki, H., T. Yoshimoto, T. Sugiyama, and Y. Hirata, *Activation of cell adhesion kinase β by mechanical stretch in vascular smooth muscle cells*. Endocrinology, 2003. 144(6): p. 2304-2310.

140. Lavery, D.L., J. Martin, Y.D. Turnbull, and S. Hoppler, *Wnt6 signaling regulates heart muscle development during organogenesis*. Developmental Biology, 2008. 323(2): p. 177-188.

141. Alfieri, C.M., J. Cheek, S. Chakraborty, and K.E. Yutzey, *Wnt signaling in heart valve development and osteogenic gene induction*. Developmental Biology, 2010. 338(2): p. 127-35.

142. Hurlstone, A.F., et al., *The Wnt/beta-catenin pathway regulates cardiac valve formation*. Nature, 2003. 425(6958): p. 633-7.

143. Gessert, S. and M. Kuhl, *The multiple phases and faces of wnt signaling during cardiac differentiation and development*. Circulation Research, 2010. 107(2): p. 186-99.

144. Katsumi, A., A.W. Orr, E. Tzima, and M.A. Schwartz, *Integrins in mechanotransductio*n. Journal of Biological Chemistry, 2004. 279(13): p. 12001-04.

145. Hu, Y., G. Böck, G. Wick, and Q. Xu, *Activation of PDGF receptor α in vascular smooth muscle cells by mechanical stress*. The FASEB Journal, 1998. 12(12): p. 1135-42.

146. Balestreire, E.M. and G. Apodaca, *Apical epidermal growth factor receptor signaling: regulation of stretch-dependent exocytosis in bladder umbrella cells*. Molecular Biology of the Cell, 2007. 18(4): p. 1312-1323.

147. Qiu, J., Y. Zheng, J. Hu, D. Liao, H. Gregersen, X. Deng, Y. Fan, and G. Wang, *Biomechanical regulation of vascular smooth muscle cell functions: From in vitro to in vivo understanding*. Interface, 2013. 11(90).

148. Lehoux, S., Y. Castier, and A. Tedgui, *Molecular mechanisms of the vascular responses to haemodynamic forces*. Journal of Internal Medicine, 2006. 259(4): p. 381-92.

149. Torsoni, A.S., T.M. Marin, L.A. Velloso, and K.G. Franchini, *RhoA/ROCK signaling is critical to FAK activation by cyclic stretch in cardiac myocytes*. American Journal of Physiology. Heart and Circulatory Physiology, 2005. 289(4): p. H1488-96.

150. Fonseca, P.M., R.Y. Inoue, C.B. Kobarg, D.P. Crosara-Alberto, J. Kobarg, and K.G. Franchini, *Targeting to C-terminal myosin heavy chain may explain mechanotransduction involving focal adhesion kinase in cardiac myocytes*. Circulation Research, 2005. 96(1): p. 73-81.

151. Shyu, K.-G., B.-W. Wang, C.-M. Lin, and H. Chang, *Cyclic stretch enhances the expression of Toll-like Receptor 4 gene in cultured cardiomyocytes via p38 MAP kinase and NF-κB pathway*. Journal of Biomedical Science, 2010. 17(1): p. 15-15.

152. Pan, J., K. Fukuda, M. Saito, J. Matsuzaki, H. Kodama, M. Sano, T. Takahashi, T. Kato, and S. Ogawa, Mechanical *stretch activates the JAK/STAT pathway in rat cardiomyocytes*. Circulation Research, 1999. 84(10): p. 1127-1136.

153. Rodrigues, C.A., T.G. Fernandes, M.M. Diogo, C.L. da Silva, and J.M. Cabral, *Stem cell cultivation in bioreactors*. Biotechnology Advances, 2011. 29(6): p. 815-29.

154. Tandon, N., D. Marolt, E. Cimetta, and G. Vunjak-Novakovic, *Bioreactor engineering of stem cell environments*. Biotechnology Advances, 2013. 31(7): p. 1020-1031.

155. Vunjak-Novakovic, G., *The fundamentals of tissue engineering: scaffolds and bioreactors*. Novartis Foundation Symposia, 2003. 249: p. 34-46.

156. Portner, R., S. Nagel-Heyer, C. Goepfert, P. Adamietz, and N.M. Meenen, *Bioreactor design for tissue engineerin*g. Journal of Bioscience and Bioengineering, 2005. 100(3): p. 235-45.

157. Ellis, M., M. Jarman-Smith, and J.B. Chaudhuri, *Bioreactor systems for tissue engineering: A four-dimensional challenge*. Bioreactors for Tissue Engineering: Principles, Design and Operation, J. Chaudhuri and M. Al-Rubeai, Editors. 2005, Springer Netherlands: Dordrecht. p. 1-18.

158. Brown, M.A., R.K. Iyer, and M. Radisic, *Pulsatile perfusion bioreactor for cardiac tissue engineering*. Biotechnology Progress, 2008. 24(4): p. 907-20.

159. Kenar, H., G.T. Kose, M. Toner, D.L. Kaplan, and V. Hasirci, *A 3D aligned microfibrous myocardial tissue construct cultured under transient perfusio*n. Biomaterials, 2011. 32(23): p. 5320-5329.

160. Cheng, M., M. Moretti, G.C. Engelmayr, and L.E. Freed, *Insulin-like growth factor-I and slow, bi-directional perfusion enhance the formation of tissue-engineered cardiac grafts*. Tissue Engineering. Part A, 2009. 15(3): p. 645-653.

161. Fink, C., S. Ergün, D. Kralisch, U. Remmers, J. Weil, and T. Eschenhagen, *Chronic stretch of engineered heart tissue induces hypertrophy and functional improvement*. The FASEB Journal, 2000. 14(5): p. 669-679.

162. Rangarajan, S., L. Madden, and N. Bursac, *Use of flow, electrical, and mechanical stimulation to promote engineering of striated muscles*. Annals of biomedical engineering, 2014. 42(7): p. 1391-405.

163. Zimmermann, W.-H., K. Schneiderbanger, P. Schubert, M. Didié, F. Münzel, J.F. Heubach, S. Kostin, W.L. Neuhuber, and T. Eschenhagen, *Tissue engineering of a differentiated cardiac muscle construct*. Circulation Research, 2002. 90(2): p. 223-230.

164. Birla, R.K., Y.C. Huang, and R.G. Dennis, *Development of a novel bioreactor for the mechanical loading of tissue-engineered heart muscl*e. Tissue Engineering, 2007. 13(9): p. 2239-48.

165. Cao, H., B.J. Kang, C.A. Lee, K.K. Shung, and T.K. Hsiai, *Electrical and mechanical strategies to enable cardiac repair and regeneration*. IEEE reviews in biomedical engineering, 2015. 8: p. 114-24.

166. Engelmayr, G.C., Jr., L. Soletti, S.C. Vigmostad, S.G. Budilarto, W.J. Federspiel, K.B. Chandran, D.A. Vorp, and M.S. Sacks, *A novel flex-stretch-flow bioreactor for the study of engineered heart valve tissue mechanobiology*. Annals of Biomedical Engineering, 2008. 36(5): p. 700-12.

167. Galie, P.A. and J.P. Stegemann, *Simultaneous application of interstitial flow and cyclic mechanical strain to a three-dimensional cell-seeded hydrogel*. Tissue Engineering. Part C, Methods, 2011. 17(5): p. 527-536.

168. Shi, Z.D. and J.M. Tarbell, *Fluid flow mechanotransduction in vascular smooth muscle cells and fibroblasts*. Annals of Biomedical Engineering, 2011. 39(6): p. 1608-19.

169. Iwasaki, K., K. Kojima, S. Kodama, A.C. Paz, M. Chambers, M. Umezu, and C.A. Vacanti, *Bioengineered three-layered robust and elastic artery using hemodynamically-equivalent pulsatile bioreactor*. Circulation, 2008. 118(14 Suppl): p. S52-7.

170. Zhang, X., X. Wang, V. Keshav, X. Wang, J.T. Johanas, G.G. Leisk, and D.L. Kaplan, *Dynamic culture conditions to generate silk-based tissue-engineered vascular grafts*. Biomaterials, 2009. 30(19): p. 3213-23.

171. Gao, J., P. Crapo, R. Nerem, and Y. Wang, *Co-expression of elastin and collagen leads to highly compliant engineered blood vessels*. Journal of Biomedical Materials Research Part A, 2008. 85(4): p. 1120-8.

172. Shen, N., *Development of a bioreactor system for tissue engineering, in Medical department*. 2013, RWTH Aachen.

173. Kurtz, S.M. and J.N. Devine, *PEEK biomaterials in trauma, orthopedic, and spinal implan*ts. Biomaterials, 2007. 28(32): p. 4845-4869.

174. Platt, D.K., *Other markets for engineering and high performance plastics*, in Engineering and High Performance Plastics Market Report: A Rapra Market Report. 2003, Smithers Rapra Technology.

175. Kayser, M., *Design of enabling tools for the engineering of elastin structures for application in cardiovascular regenerative medicine*, in Institute for interfacial engineering. 2011, University of Stuttgart: Stuttgart. p. 52.

176. Andrés-Delgado, L. and N. Mercader, *Interplay between cardiac function and heart developmen*t. BBA-Molecular Cell Research, 2016. 1863(7, Part B): p. 1707-1716.

177. Guan, J., F. Wang, Z. Li, J. Chen, X. Guo, J. Liao, and N.I. Moldovan, *The stimulation of the cardiac differentiation of mesenchymal stem cells in tissue constructs that mimic myocardium structure and biomechanics*. Biomaterials, 2011. 32(24): p. 5568-80.

178. Tsamis, A., W. Bothe, J.-P.E. Kvitting, J.C. Swanson, D.C. Miller, and E. Kuhl*, Active contraction of cardiac muscle: In vivo characterization of mechanical activation sequences in the beating heart*. Journal of The Mechanical Behavior of Biomedical Materials, 2011. 4(7): p. 1167-1176.

179. Huang, Y., L. Zheng, X. Gong, X. Jia, W. Song, M. Liu, and Y. Fan, *Effect of cyclic strain on cardiomyogenic differentiation of rat bone marrow derived mesenchymal stem cells*. PLoS ONE, 2012. 7(4): p. e34960.

180. Stoppel, W.L., D.L. Kaplan, and L.D. Black, 3rd, *Electrical and mechanical stimulation of cardiac cells and tissue constructs*. Advanced Drug Delivery Reviews, 2016. 96: p. 135-55.

181. Hirt, M.N., A. Hansen, and T. Eschenhagen, *Cardiac tissue engineering: State of the art*. Circulation Research, 2014. 114(2): p. 354-367.

182. Chan, Y.C., S. Ting, Y.K. Lee, K.M. Ng, J. Zhang, Z. Chen, C.W. Siu, S.K. Oh, and H.F. Tse, *Electrical stimulation promotes maturation of cardiomyocytes derived*

.

from human embryonic stem cells. Journal of Cardiovascular Translational Research, 2013. 6(6): p. 989-99.

183. Blazeski, A., R. Zhu, D.W. Hunter, S.H. Weinberg, K.R. Boheler, E.T. Zambidis, and L. Tung, *Electrophysiological and contractile function of cardiomyocytes derived from human embryonic stem cells*. Progress in Biophysics and Molecular Biology, 2012. 110(0): p. 178-195.

184. Khan, J.M., A.R. Lyon, and S.E. Harding, *The case for induced pluripotent stem cell-derived cardiomyocytes in pharmacological screening.* British Journal of Pharmacology, 2013. 169(2): p. 304-17.

185. Li, S., G. Chen, and R.A. Li, *Calcium signalling of human pluripotent stem cell-derived cardiomyocytes*. The Journal of Physiology, 2013. 591(21): p. 5279-90.

186. Kosmidis, G., M. Bellin, M.C. Ribeiro, B. van Meer, D. Ward-van Oostwaard, R. Passier, L.G.J. Tertoolen, C.L. Mummery, and S. Casini, *Altered calcium handling and increased contraction force in human embryonic stem cell derived cardiomyocytes following short term dexamethasone exposure*. Biochemical and Biophysical Research Communications, 2015. 467(4): p. 998-1005.

187. Peters, N.S., N.J. Severs, S.M. Rothery, C. Lincoln, M.H. Yacoub, and C.R. Green, *Spatiotemporal relation between gap junctions and fascia adherens junctions during postnatal development of human ventricular myocardium*. Circulation, 1994. 90(2): p. 713-725.

188. Lundy, S.D., W.Z. Zhu, M. Regnier, and M.A. Laflamme, *Structural and functional maturation of cardiomyocytes derived from human pluripotent stem cells*. Stem Cells and Development, 2013. 22(14): p. 1991-2002.

189. Borg, T.K., E.C. Goldsmith, R. Price, W. Carver, L. Terracio, and A.M. Samarel, *Specialization at the Z line of cardiac myocytes*. Cardiovascular Research, 2000. 46(2): p. 277-85.

190. Brauchle, E., et al., *Non-invasive chamber-specific identification of cardiomyocytes in differentiating pluripotent stem cells*. Stem Cell Reports, 2016. 6(2): p. 188-199.

191. Naito, A.T., I. Shiojima, H. Akazawa, K. Hidaka, T. Morisaki, A. Kikuchi, and I. Komuro, *Developmental stage-specific biphasic roles of Wnt/β-catenin signaling in*

*cardiomyogenesis and hematopoiesi*s. Proceedings of the National Academy of Sciences, 2006. 103(52): p. 19812-19817.

192. Pohjoismaki, J.L.O., M. Kruger, N. Al-Furoukh, A. Lagerstedt, P.J. Karhunen, and T. Braun, *Postnatal cardiomyocyte growth and mitochondrial reorganization cause multiple changes in the proteome of human cardiomyocyte*s. Molecular BioSystems, 2013. 9(6): p. 1210-1219.

193. Dan, L., C.K. Chua, and K.F. Leong, *Fibroblast response to interstitial flow: A state-of-the-art revie*w. Biotechnology and Bioengineering, 2010. 107(1): p. 1-10.

194. Pasquali-Ronchetti, I. and M. Baccarani-Contri, *Elastic fiber during development and aging.* Microscopy Research and Technique, 1997. 38(4): p. 428-435.

195. Bashur, C.A., L. Venkataraman, and A. Ramamurthi, *Tissue engineering and regenerative strategies to replicate biocomplexity of vascular elastic matrix assembly*. Tissue engineering. Part B, Reviews, 2012. 18(3): p. 203-17.

196. Agarwal, S., J.H. Wendorff, and A. Greiner, *Progress in the field of electrospinning for tissue engineering applications*. Advanced Material, 2009. 21(32-33): p. 3343-51.

197. Ng, C.P., B. Hinz, and M.A. Swartz, *Interstitial fluid flow induces myofibroblast differentiation and collagen alignment in vitro*. Journal of Cell Science, 2005. 118(20): p. 4731-4739.

198. Swee, M.H., W.C. Parks, and R.A. Pierce, *Developmental Regulation of Elastin Production.: Expression of tropoelastin pre-mRNA persists after down-regulation of steady-state mRNA levels.* Journal of Biological Chemistry, 1995. 270(25): p. 14899-14906.

199. Zheng, Q., S. Chen, Y. Chen, J. Lyga, R. Wyborski, and U. Santhanam, *Investigation of age-related decline of microfibril-associated glycoprotein-1 in human skin through immunohistochemistry study.* Clinical, Cosmetic and Investigational Dermatology, 2013. 6: p. 317-323.

200. Yeo, G.C., A. Tarakanova, C. Baldock, S.G. Wise, M.J. Buehler, and A.S. Weiss, *Subtle balance of tropoelastin molecular shape and flexibility regulates dynamics and hierarchical assembly*. Science Advances, 2016. 2(2): p. e1501145.

201. Frushour, B.G. and J.L. Koenig, *Raman scattering of collagen, gelatin, and elastin*. Biopolymers, 1975. 14(2): p. 379-391.

202. Green, E.M., J.C. Mansfield, J.S. Bell, and C.P. Winlove, *The structure and micromechanics of elastic tissu*e. Interface Focus, 2014. 4(2): p. 20130058.

203. Korin, N., A. Bransky, U. Dinnar, and S. Levenberg, *A parametric study of human fibroblasts culture in a microchannel bioreactor.* Lab Chip, 2007. 7(5): p. 611-7.

204. Shi, Z.D., R.A. Mathura, J.S. Garanich, G. Abraham, and J.M. Tarbell. *Shear stress plays a role in differentiation and migration of adventitial fibroblasts*. in 2007 IEEE 33rd Annual Northeast Bioengineering Conference. 2007.

205. Eoh, J.H., N. Shen, J.A. Burke, S. Hinderer, Z. Xia, K. Schenke-Layland, and S. Gerecht, *Enhanced elastin synthesis and maturation in human vascular smooth muscle tissue derived from induced-pluripotent stem cells*. Acta Biomaterialia, 2017. 52: p. 49-59.

206. Sanders, R., A. Draaijer, H.C. Gerritsen, P.M. Houpt, and Y.K. Levine, *Quantitative pH imaging in cells using confocal fluorescence lifetime imaging microscopy*. Analytical Biochemistry, 1995. 227(2): p. 302-8.

207. Szmacinski, H., I. Gryczynski, and J.R. Lakowicz, *Three-photon induced fluorescence of the calcium probe Indo-1*. Biophysical Journal, 1996. 70(1): p. 547-55.

208. Szmacinski, H. and J.R. Lakowicz, *Sodium Green as a potential probe for intracellular sodium imaging based on fluorescence lifetime*. Analytical Biochemistry, 1997. 250(2): p. 131-8.

209. Gerritsen, H.C., R. Sanders, A. Draaijer, C. Ince, and Y.K. Levine, *Fluorescence lifetime imaging of oxygen in living cell*s. Journal of Fluorescence, 1997. 7(1): p. 11-15.

210. Murata, S., P. Herman, and J.R. Lakowicz, *Texture analysis of fluorescence lifetime images of nuclear DNA with effect of fluorescence resonance energy transfer*. Cytometry, 2001. 43(2): p. 94-100.

211. Sheikh, S., G.E. Rainger, Z. Gale, M. Rahman, and G.B. Nash, *Exposure to fluid shear stress modulates the ability of endothelial cells to recruit neutrophils in*

response to tumor necrosis factor-alpha: a basis for local variations in vascular sensitivity to inflammation. Blood, 2003. 102(8): p. 2828-34.

212. Meleshina, A.V., V.V. Dudenkova, M.V. Shirmanova, V.I. Shcheslavskiy, W. Becker, A.S. Bystrova, E.I. Cherkasova, and E.V. Zagaynova, *Probing metabolic states of differentiating stem cells using two-photon FLIM*. Scientific Reports, 2016. 6: p. 21853.

213. Tonin, M., N. Descharmes, and R. Houdre, *Hybrid PDMS/glass microfluidics for high resolution imaging and application to sub-wavelength particle trappin*g. Lab on a Chip, 2016. 16(3): p. 465-70.

214. Funamoto, K., I.K. Zervantonakis, Y. Liu, C.J. Ochs, C. Kim, and R.D. Kamm, *A novel microfluidic platform for high-resolution imaging of a three-dimensional cell culture under a controlled hypoxic environment*. Lab on a Chip, 2012. 12(22): p. 4855-63.

215. Bhatia, S.N. and D.E. Ingber, *Microfluidic organs-on-chi*ps. Nature Biotechnology, 2014. 32(8): p. 760-772.

216. van Meer, B.J., et al., *Small molecule absorption by PDMS in the context of drug response bioassays*. Biochemical Biophysical Research Communications, 2017. 482(2): p. 323-328.

217. Hinderer, S., J. Seifert, M. Votteler, N. Shen, J. Rheinlaender, T.E. Schäffer, and K. Schenke-Layland, *Engineering of a bio-functionalized hybrid off-the-shelf heart valve.* Biomaterials, 2014. 35(7): p. 2130-2139.

218. Kensah, G., et al., *A novel miniaturized multimodal bioreactor for continuous in situ assessment of bioartificial cardiac tissue during stimulation and maturation*. Tissue Engineering. Part C, Methods, 2011. 17(4): p. 463-73.

219. Zhao, F. and T. Ma, *Perfusion bioreactor system for human mesenchymal stem cell tissue engineering: dynamic cell seeding and construct development*. Biotechnology and Bioengineering, 2005. 91(4): p. 482-93.

220. Shi, Z.D., X.Y. Ji, D.E. Berardi, H. Qazi, and J.M. Tarbell, *Interstitial flow induces MMP-1 expression and vascular SMC migration in collagen I gels via an ERK1/2-dependent and c-Jun-mediated mechanism*. American Journal of Physiology. Heart and Circulatory Physiology, 2010. 298(1): p. H127-35.

221. Raffetto, J.D., R. Vasquez, D.G. Goodwin, and J.O. Menzoian, *Mitogen-activated protein kinase pathway regulates cell proliferation in venous ulcer fibroblasts.* Vascular Endovascular Surgery, 2006. 40(1): p. 59-66.

222. Inoh, H., N. Ishiguro, S. Sawazaki, H. Amma, M. Miyazu, H. Iwata, M. Sokabe, and K. Naruse, Uni-axial cyclic stretch induces the activation of transcription factor nuclear factor kappaB in human fibroblast cells. The FASEB Journal, 2002. 16(3): p. 405-7.

223. Sarasa-Renedo, A., V. Tunc-Civelek, and M. Chiquet, *Role of RhoA/ROCK-dependent actin contractility in the induction of tenascin-C by cyclic tensile strai*n. Experimental Cell Research, 2006. 312(8): p. 1361-70.

224. Radisic, M., H. Park, H. Shing, T. Consi, F.J. Schoen, R. Langer, L.E. Freed, and G. Vunjak-Novakovic, *Functional assembly of engineered myocardium by electrical stimulation of cardiac myocytes cultured on scaffolds*. Proceedings of the National Academy of Sciences, 2004. 101(52): p. 18129-18134.

225. Antoni, D., H. Burckel, E. Josset, and G. Noel, *Three-dimensional cell culture: A breakthrough in vivo*. International Journal of Molecular Sciences, 2015. 16(3): p. 5517-5527.

226. Edmondson, R., J.J. Broglie, A.F. Adcock, and L. Yang, *Three-dimensional cell culture systems and their applications in drugdiscovery and cell-based biosensors*. Assay and Drug Development Technologies, 2014. 12(4): p. 207-218.

227. Generali, M., P.E. Dijkman, and S.P. Hoerstrup, *Bioresorbable scaffolds for cardiovascular tissue engineering*. European Medical Journal, 2014. 1: p. 91-99.

228. Chan, B.P. and K.W. Leong, *Scaffolding in tissue engineering: general approaches and tissue-specific considerations*. European Spine Journal, 2008. 17(Suppl 4): p. 467-479.

229. Goers, L., P. Freemont, and K.M. Polizzi, *Co-culture systems and technologies: taking synthetic biology to the next level*. Journal of the Royal Society Interface, 2014. 11(96): p. 20140065.

230. Arjunon, S., S. Rathan, H. Jo, and A.P. Yoganathan, *Aortic valve: mechanical environment and mechanobiology*. Annals of Biomedical Engineering, 2013. 41(7): p. 1331-1346.

231. Rebelo, S.P., E.M. Dehne, C. Brito, R. Horland, P.M. Alves, and U. Marx, *Validation of bioreactor and human-on-a-chip devices for chemical safety assessmen*t. Advances in Experimental Medicine and Biology, 2016. 856: p. 299-316.

Declaration

I declare that this dissertation is my own original work, except where indicated through the proper use of citations and references. I used no sources or aids other than those explicitly mentioned. Support provided by third parties is clearly marked as such in this dissertation.

Tübingen, November 7, 2017

Acknowledgements

These four years of Ph.D. has been a wonderful experience and a valuable journey in my life. During these few years, I have received a lot of support and help from my supervisors, colleagues, friends, and family. I would like to use this opportunity to thank everyone who helped me to make this work possible. I particularly thank

- **Prof. Dr. Katja Schenke-Layland** for the great support, the encouragement, the patience, the constructive advice and the guidance during this work. I also want to thank you for your help with all the experimental design and writing. Thanks for giving me the opportunity to work in this wonderful team and conduct this great project. You have been tremendous mentors to me.

- **Prof. Dr. Garry Duffy** for being the second supervisor and examiner of my thesis. Thanks for your advice and trust in my scientific work.

- **Dr. Svenja Hinderer** for giving me the support, all the useful advices for my experiments and personally, help me to correct abstracts, posters, manuscripts, the book chapter and the grand application.

- **Shannon Layland** for the constructive talks and suggestions. Every time after talking to you, I always full of energy and motivation.

- Stem cell group, **Anne Knopf,** and **Claas Westendorf**. Thanks for the fun and the happiness during the cell culture.

- I would like to thank **Dr. Michael Monaghan** for the valuable suggestions about my career and taught me to do right things at the right time.

- My special thanks to my lovely colleagues as well as friends **Anne Knopf**, **Daniel Carvajal**, **Eva Brauchle**, **Hannah Bauer, Julia Riedl, Simone Liebscher** and **the salad group**, as well as all the members of Fraunhofer

IGB and Tübingen AG Schenke-Layland lab membranes that made the lab a great working atmosphere and fun. Without all of you, I would not have enjoyed my time at here so much.

- Of course, I also want to give my great thanks to **Diana Holzer** for assisting me with my visa and making this work possible.

- I would like to express my special gratitude to **Simone Poeschel**, who helped me with imaging flow cytometry.

- I would also like to thanks, **Anne Knopf**, **Eva Brauchle, Svenja Hinderer, Monika Holeiter**, **Julia Riedl** for taking time out from their busy schedule to proofread my thesis.

- My friends **Yang Xu**, **Junwen Cai**, **Zhicheng Chen**, and **Junyuan Ma**, my husband **Sili Yao**, and My family, whose love, understanding, supporting was important for the completion of this thesis.

Curriculum Vitae

Personal Information

Name	Nian Shen
Address:	Grosse fleischergasse 11 04109 Leipzig, Germany
Date and Place of Birth:	11.06.1988, Henan, PR China
Nationality:	Chinese
E-Mail:	shennian23@gmail.com

Education

01.2013 – Present Eberhard-Karls Universität Tübingen, Tübingen, Germany
Ph.D. Candidate in Biology

09.2011 – 12.2012 RWTH Aachen, Aachen, Germany
M. Sc. in Biomedical Engineering, Dept. of Medical

09.2010 – 08.2011 Trinity College University of Dublin, Dublin, Ireland
M. Sc. in Bioengineering, Dept. of Mechanical Engineering

09.2006 – 06.2010 Shanghai Jiao Tong University, Shanghai, PR China
B. Sc in Biomedical Engineering

Research experience

09.2017– present **Trinity College Dublin, Dublin, Ireland**
Post-doc researcher, Dept. of Mechanics and Manufacturing Engineering

06.2015 – 03.2017 **University Women's Hospital of the Eberhard Karls University Tübingen, Tübingen, Germany**

Research Associate, Dept. of Biology

01.2013 – 05.2015 **Fraunhofer Institute for Interfacial Engineering and Biotechnology (IGB), Stuttgart, Germany**

Research Associate

06.2012 – 12.2012 **Fraunhofer Institute for Interfacial Engineering and Biotechnology (IGB), Stuttgart, Germany**

2nd Master Thesis

Title ´Development of a bioreactor system for tissue engineering.

03.2011 – 08.2011 **Royal College of Surgeons (RCSI), Dublin, Ireland**

1st Master Thesis, Dept. of Anatomy

Patents

1. Li G, Chen Q, **Shen N**, Zhao JL (2011). *A method to manufacture three-dimensional smooth curved surface microelectrode using SU-8 photolithography.* Patent No. CN 201010275953.0
2. Sui XH, Chai XY, Ren QS, **Shen N** (2010). *Silicone microelectrode surface coating method based on micro-electromechanical system (MEMS).* Patent No. CN 201010510589.1

Oral presentations

1. **Shen N,** Westendorf C, Brauchle E, Brekke J, Hinderer S, Schenke-Layland K, *Maturation of embryonic stem cell-derived cardiomyocytes using mechanical cues*, SCeNT retreat, Eglof, Germany, February 03-05, 2016.
2. Lee A, **Shen N,** Brauchle E, Schenke-Layland K. *Raman microspectroscopy assesses human embryonic stem cell cardiac differentiation and maturation*. BMES 2015 Annual Meeting, Tampa, USA. October 7-10, 2015.

Poster presentations

1. **Shen N,** Hinderer S, Westendorf C, Brekke J, Lee A, Bauer H, Layland S, Brauchle E, Schenke-Layland K. *Maturation of embryonic stem cell-derived cardiomyocytes using defined mechanical cues,* Leiden, Netherlands, March 17-19, 2016.
2. **Shen N**, Knopf A, Westendorf C, Schenke-Layland K, *Exposure to ECM and biophysical signals support maturation of ESC-derived cardiomyocytes,* Extracellular matrix: new perspectives for translational medicine, Freiburg, Germany, March 03-05, 2016.
3. **Shen N,** Westendorf C, Brauchle E, Brekke J, Hinderer S, Schenke-Layland K, *Maturation of embryonic stem cell-derived cardiomyocytes using mechanical cues*, Stem cell mechanobiology in development and disease, Capri, Italy, October 18-21, 2015.
4. **Shen N,** Westendorf C, Hansmann J, Hinderer S, Schenke-Layland K, *Bioreactor induced cardiomyogenic differentiation of pluripotent stem cells*, From stem cells to human development workshop, Dorking, UK, September 21-24, 2014.
5. **Shen N,** Hinderer S, Hansmann J, Schenke-Layland S, *Development of a bioreactor system for 2D and 3D elastogenesis,* TERMIS AM, TERMIS AM, Atlanta, USA, November 10-13, 2013.
6. **Shen N,** Hinderer S, Hansmann J, Schenke-Layland S, *Upregulation of elastin gene expression in the dynamic bioreactor system,* Annual Meeting of the German Society for Matrix Biology, Tübingen, March 7-9, Germany, 2013.

Awards and scholarships

03.2016	GSMB Travel Grant
10.2015	EMBO Travel Grant
09.2010 – 08.2011	Erasmus Mundus Scholarship of CEMACUBE; €42,000
2007 – 2009	Excellent Academic Scholarship

Appendices

Appendix I: Shen N, Knopf A., Westendorf C, Knopf A., Kraushaar U., Riedl. J, Bauer,…,Schenke-Layland K., et al. Stem Cell Report. 9 (1):122-135. 2017.

Appendix II: Shen N, Hinderer S, Schenke-Layland K, *Scaffold and biomechanical transductive approaches to elastic tissue engineering,* in A. Ramamurthi and C. Kothapalli (Eds), Elastic fiber matrices: biomimetic approaches to regeneration and repair. Taylor & Francis Group, 2016.

Appendix III: Shen N, Riedl J, Carvajal Berrio D.A., Davis Z., Monaghan M.G., Shannon S.L., Hinderer S., Schenke-Layland K, *A flow bioreactor compatible with real-time marker free fluorescence lifetime imaging microscopy.* Biomedical Materials. 13(2). https://doi.org/10.1088/1748-605X/aa9b3c 2018.

Appendix I: Shen et al. 2017

Highlights:

- Custom-made bioreactor exposes ESC-CMs to defined shear stress and cyclic stretch.
- Physical signals and extended culture significantly improve maturation of ESC-CMs.
- Biochemical fingerprint of dynamically cultured ESC-CMs is similar to primary CMs.

eTOC blurb:

In this study, we induce differentiation and maturation of mouse and human embryonic stem cell (ESC)-derived cardiomyocytes (CMs) by the application of defined pulsatile flow and cyclic strain in a custom-made bioreactor. The ESC-CMs cultured under dynamic conditions and extended culture time showed significantly faster calcium decay, increased SERCA activities and sarcomeric lengths, as well as protein and gene expression patterns, and biochemical fingerprints comparable to primary CMs.

Steps towards maturation of embryonic stem cell-derived cardiomyocytes by defined physical signals

Nian Shen[1,2], Anne Knopf[1,2], Claas Westendorf[1], Udo Kraushaar[3], Julia Riedl[1,2], Hannah Bauer[2], Simone Pöschel[2], Shannon Lee Layland[1,2], Monika Holeiter[1,2], Stefan Knolle[1,3], Eva Brauchle[1,2], Ali Nsair[4,5], Svenja Hinderer[1,2], Katja Schenke-Layland [1,2,4#]

[1] Department of Cell and Tissue Engineering, Fraunhofer Institute for Interfacial Engineering and Biotechnology IGB, Stuttgart, 70569, Germany

[2] Department of Women's Health, Research Institute of Women's Health, University Hospital of the Eberhard Karls University Tübingen, 72076, Germany

[3] Department of Cell Biology, Electrophysiology, Natural and Medical Sciences Institute at the University of Tübingen, Reutlingen, 72770, Germany

[4] Department of Medicine/ Cardiology, Cardiovascular Research Laboratories (CVRL) at David Geffen School of Medicine, University of California Los Angeles (UCLA), Los Angeles, CA, 90095, USA

[5] Broad Stem Cell Research Center, David School of Medicine at UCLA, Los Angeles, CA, 90095, USA

Correspondence and requests for materials should be addressed to K.S.L. (katja.schenke-layland@med.uni-tuebingen.de, Tel: +49-7071-2985205, www.schenke-layland-lab.de)

Running title: ESC-derived cardiomyocyte maturation by defined physical signals

Summary

Cardiovascular disease remains a leading cause of mortality and morbidity worldwide. Embryonic stem cell-derived cardiomyocytes (ESC-CMs) may offer significant advances in creating in vitro cardiac tissues for disease modelling, drug testing, and elucidating developmental processes; however, the induction of ESCs to a more adult-like CM phenotype remains challenging. In this study, we developed a bioreactor system to employ combining pulsatile flow (1.48 mL per minute), cyclic strain (5%) and extended culture time to improve the maturation of murine and human ESC-CMs. Dynamically-cultured ESC-CMs showed an increased expression of cardiac-associated proteins and genes, cardiac ion channel genes, as well as increased SERCA activity and a Raman fingerprint with the presence of maturation-associated peaks similar to primary CMs. We present a bioreactor platform that can serve as a foundation for the development of human-based cardiac in vitro models to verify drug candidates, as well as the study of cardiovascular development and disease.

Introduction

Pluripotent stem cells (PSCs) hold immense therapeutic potential (Passier, van Laake et al. 2008, Masumoto, Matsuo et al. 2012). PSC-derived cardiomyocytes (PSC-CMs) may offer significant advances towards creating novel pre-clinical in vitro test systems for disease modelling, drug toxicity screening and drug sensitivity identification (Braam, Passier et al. 2009, Ebert, Liang et al. 2012, Yang, Pabon et al. 2014). A number of research groups have established methods for the differentiation of PSCs into CMs (Zhang, Klos et al. 2012, Lundy, Zhu et al. 2013, Nunes, Miklas et al. 2013); however, the PSC-CMs displayed an immature phenotype when compared with adult CMs with respect to sarcomere structure (Yang, Soonpaa et al. 2008), calcium handling properties (Li, Chen et al. 2013) and electrophysiology (Blazeski, Zhu et al. 2012, Ribeiro, Tertoolen et al. 2015). PSC-CMs that are not fully matured may reduce their usability for drug testing and disease modelling, particularly when the disease-causing mutation affects a gene that is not expressed until later in development or if the disease occurs postnatally (Braam, Passier et al. 2009, Passier, van Laake et al. 2008).

Cytoskeletal and rhythmic contraction, and pulsatile laminar shear stress are mechanical forces that have been suggested to play a crucial role in heart development and growth (Taber 2001, Zhu, Blazeski et al. 2014, Andrés-Delgado and Mercader 2016). Cytoskeletal contraction is involved in several morphogenetic processes in the embryo (Taber 2001). Rhythmic contraction is the exposure of CMs to regular cyclic stretch (Zhu, Blazeski et al. 2014). The heart is exposed to blood flow during most heart developmental stages and throughout adult life (Andrés-Delgado and Mercader 2016). Pulsatile laminar shear stress generated by blood flow in healthy hearts influences heart chamber formation and maturation, trabeculation, CM proliferation and valvulogenesis (Andrés-Delgado and Mercader 2016). Employing physical signals to mimic cardiogenesis in vitro is a potential strategy to achieve PSC-CM maturation. Several groups have developed methods to apply uniaxial stress to PSCs (Tulloch, Muskheli et al. 2011, Wan, Chung et al. 2011, Mihic, Li et al. 2014). Although uniaxial stress can promote PSC-CM maturation, applying stretch alone does not mimic in vivo physical signals that act on CMs within the heart (Guan, Wang et al. 2011). In 2002, Carrier et al. demonstrated that perfusion flow leads to continuous medium change and therefore increases the spatial uniformity of CMs by improving the control of oxygen, pH, nutrients and metabolites in the cellular microenvironment (Carrier, Rupnick et al. 2002); however, the impact of pulsatile flow on PSC-CM maturation, or a possible synergistic effect of the combination of pulsatile flow and cyclic strain has not been investigated.

In the present study, we designed and evaluated a bioreactor system to expose mouse embryonic stem cell (mESC)- and human ESC (hESCs)-derived cells to defined mechanical

stimuli. We investigated the impact of pulsatile flow-induced shear stress and physiological stretch on murine and human ESC-CM maturation in vitro by extensively analyzing cardiac protein and gene expression patterns. We analyzed the calcium handling properties and sarco-endoplasmic reticulum Ca^{2+}-ATPase (SERCA) activities in dynamically-cultured CMs. In addition, we characterized the phenotype of ESC-CMs employing marker-free Raman microspectroscopy. Elucidating the effect of defined mechanical forces on the maturation of ESC-CMs is an essential step towards developing fully matured and functional cardiovascular tissues in vitro that can be used to study cardiovascular diseases and investigate potential drug candidates.

Results

Bioreactor design, in silico and functional evaluation

A bioreactor system was designed and manufactured to induce a defined shear stress by exposing cells that were seeded on a membrane to laminar flow and a physiological strain. A computer-aided design (CAD) schematic of the bioreactor is displayed in **Figure 1A**, **1C-E**. Computer simulations were performed based on the geometry of the bioreactor using COMSOL. Simulations showed that a flow rate of 1.48 mL per minute (mL/min) created a constant shear stress between 10^{-3} and 5.6×10^{-3} dyn/cm^2 over the entire cell-seeded membrane (**Figure 1B**). Flow rates of 2.96 mL/min and 5.92 mL/min resulted in a shear stress ranging from 10^{-3} to 1.16×10^{-2} dyn/cm^2 and 10^{-3} to 2.44×10^{-2} dyn/cm^2 respectively. A vacuum- (**Figure 1C**) and pressure- (**Figure 1D, E**) controlled air chamber generated a cyclic strain on the cell-seeded membrane that was placed on a silicone membrane, which separated the flow from the air chamber. **Figure 1F** illustrates the distribution of a gradient of strain (up to 5%) on the cell-seeded membrane created by a 1.35 standard atmosphere. Based on the simulation results, we seeded cells in the center of the membrane within a defined area to ensure a homogeneous stretching. The bioreactor system set up is illustrated in **Figure 1G**.

The combination of a 1.48 mL/min pulsatile flow and 5% cyclic strain increases cardiac gene and protein expression patterns in mESC-derived cells after 12 days in culture

After confirming pluripotency of mESCs by immunofluorescence (IF) staining (**Figure S1**), cells were transferred to fibronectin-coated membranes for one day to allow cell attachment, before being exposed to static or dynamic culture conditions. To determine the appropriate mechanical stimuli required to induce cardiac differentiation and maturation, we subjected

mESC-derived cells to an initial flow rate of 0.74 mL/min, and then increased the flow rates to 1.48 mL/min, 2.96 mL/min or 5.92 mL/min from the second day to day 12, a time-point that been previously described as appropriate to mimic early cardiogenesis (Davis, Casini et al. 2012). In parallel, we tested cyclic strains of 2.5%, 5% or 10% at 0.33 Hz without flow for 12 days. Subsequently, cells were harvested for gene and protein expression analyses. The 1.48 mL/min flow rate led to significantly increased *Nkx2-5, Actc1, Myh6,* and *Myh7* gene expression and a higher number of sarcomeric myosin-positive ($MF20^+$) cells when compared to other flow conditions or static controls (**Figure S2A-E** and **S2P**). All strain conditions significantly increased the expression of cardiac-associated genes when compared with static controls (**Figure S2F**). No significant change in the number of $MF20^+$ cells was detected amongst the different strain settings (**Figure S2G-J**).

To investigate a possible synergistic effect of both pulsatile flow and cyclic strain, we exposed the mESC-derived cells to an initial flow rate of 0.74 mL/min, which was then increased to 1.48 mL/min on day 2 with simultaneous exposure to cyclic strain of 2.5%, 5% or 10% (all at a frequency of 0.33 Hz). The combination of pulsatile flow and strain resulted in a significant increase in cardiac-associated gene expression when compared with the static controls (**Figure S2K and S2P**). $MF20^+$ cells cultured under flow and cyclic strain conditions displayed a more rod-like morphology (**Figure S2L-N**). The combination of 1.48 mL/min flow and 5% strain resulted in >20% increase in $MF20^+$ cells, which was the highest among all conditions and led to spontaneously beating clusters (**Figure S2O**). Therefore, further experiments were performed using 1.48 mL/min pulsatile flow and 5% strain, to which we refer to as the dynamic condition in the following paragraphs.

Combination of prolonged culture time and dynamic conditions results in advanced maturation of mESC-CMs

To verify whether exposure to prolonged dynamic conditions can further advance the maturation of mESC-CMs, we continuously cultured the cells for another 6 days (a total of 18 days in dynamic culture (d18 dyn mESC-CMs)). The d18 dyn mESC-CMs were then compared to day 12 dynamically-cultured cells (d12 dyn mESC-CMs) and static controls (d12 stat mESC-CMs and d18 stat mESC-CMs). d12 and d18 dyn mESC-CMs showed well-defined and aligned cross-striated sarcomeric structures as determined by the expression of MF20 and cTNT (**Figure 2A**). Randomly aligned fibers with no striated sarcomeric structures were seen in mESC-CMs cultured for either 12 or 18 days under static conditions (**Figure 2A**). Connexin 43 (CX43) IF staining of d18 dyn mESC-CMs indicated an increase in plasma membrane gap junctions when compared with the d12 stat and dyn mESC-CMs, and d18

stat mESC-CMs (**Figure 2A**). Sarcomere length was also increased in d18 dyn mESC-CMs when compared with d12 dyn mESC-CMs (**Figure 2B**). Sarcomeric structures were not detectable in either the d12 or d18 stat mESC-CMs (**Figure 2B**). cTNT expression in d18 stat and dyn mESC-CMs was examined using imaging flow cytometry to confirm IF staining results. To ensure only viable cells were used for analysis, we exclude dead cells using Zombie Red™ dye (ZR). We observed a significant increase in the median fluorescence intensity (MFI) of cTNT in d18 dyn mESC-CMs when normalized to MFI of cTNT in d18 stat mESC-CMs (**Figure 2C, D**). In addition, a significant upregulation of cardiac-associated genes including myosin heavy chain α (*Myh6*) and β (*Myh7*), cardiac myosin binding protein C (*Mybpc3*), troponin I1 (*Tnni1*), and troponin T2 (*Tnnt2*) was detected in d18 dyn mESC-CMs when compared with d18 stat mESC-CMs (normalized to *Gapdh* or *Rplp0*, **Figure S3**, **Table S1**).

Adult CMs express high levels of cardiac-specific ion channels, which contribute to the propagation of action potentials and contraction (Mihic, Li et al. 2014). Therefore, we evaluated transcript levels of several cardiac ion channel genes in d18 stat and dyn mESC-CMs (**Figure S3**). A significant upregulation of the delayed-rectifier voltage-gated potassium hERG channel (*Kcnh2; 6.3-fold normalized to Gapdh; 4.6-fold normalized to Rplp0*) and α1c subunit L-type calcium channel (*Cacna1c*; *3.6-fold normalized to Gapdh*) was detected in d18 dyn mESC-CMs when compared with d18 stat mESC-CMs. We identified a significant downregulation of sarco/endoplasmic reticulum calcium ATPase 2 (*Atp2a2,* normalized to *Gapdh*) expression in d18 dyn mESC-CMs. Interestingly, when normalized to *Rplp0*, we saw that *Atp2a2* was 1.5-fold up-regulated in d18 dyn mESC-CMs when compared with the static controls. An increase in the expression of inward-rectifier potassium channel Kir2.2 (*Kcnj12*) and sodium voltage-gated channel alpha subunit (*Scn5a*) was observed in d18 dyn mESC-CMs (both normalized to *Gapdh* or *Rplp0*); however, no statistical significance was detected (**Figure S3, Table S1**).

As shown before, Raman microspectroscopy allows the label-free monitoring of cardiac maturation (Brauchle, Knopf et al. 2016). Thus, Raman spectra of the 18-day statically- and dynamically-cultured mESC-CMs were recorded and analyzed using principle component analysis (PCA). The loadings of the principal component (PC) values exhibited spectral changes due to the different phenotypes. Plotting of PC-1 and PC-2 score values depicted two clearly distinguishable populations (**Figure 2D**). The investigation of the correlated PC-1 loading patterns elucidated a stronger impact of peaks at 860 cm^{-1} (glycogen), 938 cm^{-1} (glycogen), 1003 cm^{-1} (phenylalanine), 1123 cm^{-1} (glycogen) and 1658 cm^{-1} (amide I) on the spectra of d18 dyn mESC-CMs when compared with those from d18 stat mESC-CMs. These peaks were all previously associated with postnatal maturation of CMs (**Figure 2E**)

(Notingher, Green et al. 2004, Movasaghi, Rehman et al. 2007, Pascut, Kalra et al. 2013, Brauchle, Knopf et al. 2016). In contrast, Raman peaks at 785 cm^{-1} (phosphodiester bonds of DNA) and 1342 cm^{-1} (guanine) were more predominant in d18 stat mESC-CMs.

We further investigated the calcium handling properties of d12 and d18 dyn mESC-CMs (**Figure 3A-D**). No significant changes of the slope of Ca^{2+} transient and relative amplitude values were detected, whereas transient duration (CaT_{90}) and time constant (tau) were both significantly shorter in d18 dyn mESC-CMs when compared with d12 dyn mESC-CMs (**Figure 3B**). To quantify the sarcoplasmic reticulum (SR) stores and SERCA function, d12 and d18 dyn mESC-CMs were subjected to rapid puffs of a caffeine-containing solution. Typical caffeine-induced Ca^{2+} transients with a sharp peak followed by a gradual return to diastolic levels were detected (**Figure 3C**). An increase of caffeine-induced transient duration (CaT_{90}) was observed in d18 dyn mESC-CMs (**Figure 3D**). The SERCA activity, which was calculated by subtracting the decay rate from the systolic Ca^{2+} transient as previously reported (Kosmidis, Bellin et al. 2015), was significantly increased in d18 dyn mESC-CMs, indicating an enhanced SERCA function (**Figure 3D**).

D18 dyn mESC-CMs express a similar phenotype to adult murine CMs

To further explore the maturation status of d18 dyn mESC-CMs, the Raman spectra of d18 dyn mESC-CMs were recorded and compared with the Raman spectra of murine fetal CMs (fCMs; age: E15.5) and adult CMs (aCMs; age: 3 months) using PCA (**Figure 4A**). The cluster of d18 dyn mESC-CMs showed a partial overlap with the clusters of fCMs and aCMs. When analyzing the PC-5 loading, we identified that Raman bands at 860, 938, 1003, and 1658 cm^{-1} were decreased, most likely due to the degree of maturation of the CMs (**Figure 4B**). The nucleic acid-specific bands at 785, 1342 and 1578 cm^{-1} (guanine and adenine), and the protein-specific band 1437 (acyl chains in lipids) were more predominant in fCMs (Notingher, Green et al. 2004, Movasaghi, Rehman et al. 2007, Pascut, Kalra et al. 2013).

Extended dynamic culture significantly increases cardiac-associated protein and gene expression in hESC-CMs that is controlled by the Wnt/β-catenin pathway

To investigate the effect of an extended dynamic culture on cardiac maturation in hESC-CMs, we utilized a previously established protocol (Satin, Kehat et al. 2004, Lundy, Zhu et al. 2013, Brauchle, Knopf et al. 2016). We chose day 10 and day 20 for analyses since these time points have been previously reported to be crucial for early-stage and mid-stage assessment of cardiac maturation (Satin, Kehat et al. 2004, Lundy, Zhu et al. 2013, Brauchle, Knopf et al.

2016). The differentiation efficiency using this protocol was confirmed by imaging flow cytometry (**Figure S4**). After 20 days of dynamic culture, 18.4% of the cells were $cTNT^+$; whereas only 7.2% of the cells were $cTNT^+$ in the static controls (**Figure S4**). Similar to our findings utilizing mESC-derived cells, IF staining showed well-defined, aligned, cross-striated MF20 and cTNT patterns in both CMs derived from day 10 (d10 dyn hESC-CMs) and day 20 (d20 dyn hESC-CMs) dynamically-cultured populations (**Figure 5A**). In contrast, no striated sarcomeric structures were seen in CMs derived from day 10 (d10 stat hESC-CMs) or day 20 (d20 stat hESC-CMs) static controls (**Figure 5A**). Aligned rod-shaped myofilaments were observed in d20 dyn hESC-CMs (**Figure 5A**). In contrast, d10 dyn hESC-CMs, as well as d10 and d20 stat hESC-CMs exhibited random arrays of myofilaments (**Figures 5A**). CX43 staining in d10 dyn hESC-CMs and d20 stat hESC-CMs appeared diffuse (**Figures 5A**), whereas d20 dyn hESC-CMs displayed a strong CX43 expression along the sarcolemma or at the intercalated discs (**Figure 5A**). Overall, CX43 was more abundant in the d20 dyn hESC-CMs when compared with the d10 dyn hESC-CMs, d10 and d20 stat hESC-CMs (**Figures 5A**). In addition, the sarcomere length of d20 dyn hESC-CMs was significantly increased when compared with d20 stat hESC-CMs and d10 dyn hESC-CMs (**Figure 5B**). Imaging flow cytometry was used to validate the IF staining data. ZR was used to select viable cells for cTNT expression analysis (**Figure 5A**). There was a statistically significant increase in the MFI of cTNT expression in the d20 dyn hESC-CMs when normalized to the d20 stat hESC-CMs (**Figure 5C, D**). We examined the cardiac-associated gene expression in d20 dyn hESC-CMs and compared it to d20 stat hESC-CMs (**Figure S5, Table S1**). *MYH7* was significantly up-regulated in d20 dyn hESC-CMs compared to d20 stat hESC-CMs (normalized to *RPLP0*). The expression of other cardiac-associate genes, such as alpha-actinin 2 (*ACTN2*), *TNNT2* and troponin I3 (*TNNI3*) were increased in d20 dyn hESC-CMs (normalized to either *GAPDH* or *RPLP0*); however, this increase was not statistically significant (**Figure S5**). It has been proposed that maturation of hESC-CMs is related to changes in ion channel expression, with relevant electrophysiological properties (Bosman, Sartiani et al. 2013). Expression of *CACNA1C* (5.6-fold normalized to *GAPDH*; 10.2-fold normalized to *RPLP0*) and *ATP2A2* (4.0-fold normalized to *GAPDH*; 6.9-fold normalized to *RPLP0*) increased significantly in d20 dyn hESC-CMs when compared with d20 stat hESC-CMs (**Figure S5**). No significant changes in the expression of sodium/ potassium-related ion channels including *SCN5A*, *HCN4, KCNH2*, *KCNJ12* and the slowly activating delayed rectifier potassium channel subfamily (*KCNQ1*) were observed in d20 dyn hESC-CMs when normalized to *GAPDH*. In contrast, when normalized to *RPLP0*, we saw that *KCNJ12* (2.4-fold), *SCN5A* (4.1-fold), and *HCN4* (5.0-fold) were significantly up-regulated in d20 dyn hESC-CMs when compared with d20 stat hESC-CMs (**Figure S5**).

We acquired and compared Raman spectral fingerprints of d20 stat and d20 dyn hESC-CMs (**Figure 5E**). Although PC score plots depicted two distinct populations, an intermediate zone was also visible where both populations overlapped. The responsible peaks for the population separation were 785, 860, 1003, 1048 (glycogen), 1066 (cholesterol), 1084 (glycogen), 1342, 1437, and 1658 cm^{-1} (**Figure 5E**). d20 dyn hESC-CMs exhibited stronger signals at 860, 1066, 1084, 1437, and 1658 cm^{-1} (Brauchle, Knopf et al. 2016). Signals at 785, 1003, 1048, and 1342 cm^{-1} were more pronounced in Raman spectra of d20 stat hESC-CMs (**Figure 5F**).

The Wnt/β-catenin signaling pathway has been shown to play a prominent role in regulating cardiogenesis (Hurlstone, Haramis et al. 2003, Naito, Shiojima et al. 2006, Tzahor 2007, Alfieri, Cheek et al. 2010, Gessert and Kühl 2010, Piven, Palchevska et al. 2014). In the early phase of cardiogenesis, the activation of Wnt/β-catenin signaling promotes the commitment of mesodermal cells to the cardiac lineage, which is in great contrast to the late phase of cardiac development, where a down-regulation of β-catenin promotes the maturation of committed CMs (Naito, Shiojima et al. 2006). Based on these studies, we examined whether this pathway also mediates the mechanical stimuli-induced hESC-CM maturation. As depicted in **Figure S6**, d20 dyn hESC-CMs expressed a lower level of β-catenin compared with d20 stat hESC-CMs, indicating an inhibition of the Wnt/β-catenin signaling pathway due to the impact of mechanical forces.

Dynamically-cultured hESC-CMs exhibit proper cardiac electrophysiology and Ca^{2+} handling

Ca^{2+} handling was assessed in d10 and d20 dyn hESC-CMs paced at 2 Hz. Typical systolic Ca^{2+} transient traces were recorded in both d10 and d20 dyn hESC-CMs (**Figure 6A**). When compared with d10 dyn hESC-CMs, the d20 dyn hESC-CMs showed a significantly higher transient amplitude, a higher slope, a shorter CaT_{90} and a smaller time constant (**Figure 6B**). To investigate the SR storage and release capacity, caffeine puffs (10 mM) were applied to d10 and d20 dyn hESC-CMs (**Figure 6C**). Both d10 and d20 dyn hESC-CMs exhibited caffeine-releasable SR Ca^{2+} stores (**Figure 6C**). The caffeine-induced Ca^{2+} transient amplitude in d20 dyn hESC-CMs was higher when compared with d10 dyn hESC-CMs, suggesting an increased SR storage capacity in the d20 dyn hESC-CMs (**Figure 6D**). d20 dyn hESC-CMs also exhibited a decrease in caffeine-induced transient duration (CaT_{90}) and a faster transient decay (**Figure 6D**). SERCA activity was significantly increased in d20 dyn hESC-CMs, indicating an enhanced SERCA function.

Nifedipine, an L-type calcium channel blocker, induced a dose-dependent shortening of the field action potential duration (fPd) in d10 stat and dyn, as well as d20 stat and dyn hESC-CMs (**Figure S7A-B**). The shortening of the fPd was initiated at 10 nM and saturated at 1 µM (**Figure S7A**). No significant differences in response to Nifedipine were detected in static versus dynamic hESC-CMs. When exposed to the hERG K^+ channel blocker dofetilide, all hESC-CMs displayed a dose-dependent prolongation of fPd (**Figure S7C-D**), which was seen by others before (Harris, Aylott et al. 2013). Dofetilide is known as a high-risk drug to evoke arrhythmia of the torsade-de-pointes type (Jaiswal and Goldbarg 2014). Interestingly, in some of the measurements, we observed that dofetilide induced early after depolarizations (EAD) in hESC-CMs at higher concentrations.

Phenotype characterization of dynamically-cultured hESC-CMs

To identify maturation stages of dynamically-cultured hESC-CMs, the Raman spectra of d10 and d20 dyn hESC-CMs were compared with the Raman spectra of primary isolated human fCMs (**Figure 7A**). The loading spectrum of PC-4 highlights that the observed bands at 785, 1003, 1048, 1342 and 1578 cm^{-1} decreased and the bands at 860, 1066, 1084, 1437, and 1658 cm^{-1} increased due to the stage of maturation of the CMs (**Figure 7B**), which is similar to what had been previously reported by others (Notingher, Green et al. 2004, Movasaghi, Rehman et al. 2007). Interestingly, PCA of d20 dyn hESC-CMs and human fCMs alone revealed molecular similarities of the two cell types (**Figure 7C, D**).

Discussion

Mechanical signals play a crucial regulatory role in cardiac growth, development, and maintenance (Happe and Engler 2016). Here, we developed a bioreactor system that exposes ESC-derived cells to defined pulsatile flow and cyclic strain, thereby mimicking in vivo physical signals that are important for normal cardiac development (Andrés-Delgado and Mercader 2016). Compared to other recent bioreactor-related studies, which focused on either using cyclic strain or cyclic strain and electrical stimulation (Torsoni, Marin et al. 2005, Gwak, Bhang et al. 2008, Tulloch, Muskheli et al. 2011, Huang, Zheng et al. 2012, Nunes, Miklas et al. 2013, Mihic, Li et al. 2014), we highlight the importance of combining pulsatile flow and cyclic stain to drive ESC-CM maturation in vitro. The applied shear stresses induced by pulsatile flow in this study (~10^{-2} to 10^{-3} dyn/cm^2) differ from physiological blood luminal flow (~10-20 dyn/cm^2) (Butcher and Nerem 2007, Chiu and Chien 2011), but instead correspond to the in vivo environment, where CMs are exposed to an extremely low transmural flow rather than direct shear stress (Andrés-Delgado and Mercader 2016). Of note, cardiac wall strains display significant temporal and regional variations (-7.9 ± 3.8% to

+11.3 ± 6.4% in vivo (Tsamis, Bothe et al. 2011)). To mimic cardiac strain, previous studies applied cyclic strain between 2.5-12% to PSC-CMs, and demonstrated that cyclic strain conditioning can increase the expression of cardiac-associated markers and improve organization of sarcomere proteins (Shyu, Wang et al. 2010, Huang, Zheng et al. 2012, Mihic, Li et al. 2014). In accordance to these studies, culturing mESC-derived cells for 12 days in the presence of cyclic strains alone led to a significant upregulation of cardiac-associated genes and an increased number of $MF20^+$ cells when compared with static controls. We further observed a synergistic effect of the combination of 1.48 mL/min pulsatile flow with 5% cyclic strain, that led to a significant increase of cardiac-associated gene expression and an improved alignment of sarcomeric fibers. When then extending the culture time, markers associated with CM maturation were further increased in both murine and human ESC-CMs. In detail, d18 dyn mESC-CMs and d20 dyn hESC-CMs displayed well-organized sarcomeric proteins, a higher gap junction protein expression, and an increased cardiac ion channel gene expression. d20 dyn hESC-CMs exhibited an average sarcomere length of 1.97 ± 0.25 µm, which is higher than the average sarcomere length of hESC-CMs reported in other studies and similar to the sarcomere length of relaxed adult CMs (Borg, Goldsmith et al. 2000, Feinberg, Ripplinger et al. 2013, Nunes, Miklas et al. 2013). Maturation of ESC-CMs is often accompanied by increased ion channel expression. Our data showed an increase in relevant ion channel genes in d18 dyn mESC-CMs and d20 dyn hESC-CMs when compared with d18 stat mESC-CMs or d20 stat hESC-CMs (normalized to either *Gapdh* (mouse)/*GAPDH* (human) or *Rplp0* (mouse)/*RPLP0* (human)). Raman microspectroscopy was employed in a previous study for the marker-free characterization of different CM phenotypes (Brauchle, Knopf et al. 2016). Here, we compared Raman spectra and identified that structural protein- and lipid-related peaks were more prominent in d18 dyn mESC-CMs when compared with d18 stat mESC-CMs. The stronger protein-related peaks in d18 dyn mESC-CMs had been previously identified as glycogen (Pascut, Goh et al. 2011, Pascut, Kalra et al. 2013). A higher presence of glycogen in ESC-CMs was previously attributed to an increased glycolytic metabolism in CMs, which is required to produce myofibril contractions (Pascut, Goh et al. 2011, Pascut, Kalra et al. 2013). Lipids have been described to play an important role in energy storage and homeostasis in cardiac muscle (Chung, Dzeja et al. 2007). The increase in lipid-related bands in d18 dyn mESC-CMs might be attributed to a metabolic shift towards β-oxidation of fatty acids (Chung, Dzeja et al. 2007, Brauchle, Knopf et al. 2016). The comparison of mESC-CMs and primary isolated fCMs and aCMs revealed that d18 dyn mESC-CMs exhibited a phenotype closer to murine aCMs. Similar to murine aCMs, human aCMs exhibit a lower nuclear and higher mitochondrial density as well as a metabolic shift (Pohjoismaki, Kruger et al. 2013). In accordance, d20 dyn hESC-CMs and human fCMs showed stronger structural protein- and lipid-related peak

intensities, but decreased signals of nucleotide bands when compared with hESC-CMs cultured for only 10 days or under static conditions. The observed differences in protein-assigned bands are possibly due to the sarcomeric organization and increasing myofibril densities in the d20 dyn hESC-CMs as it was confirmed by IF staining in this study and as previously hypothesized (Brauchle, Knopf et al. 2016). These findings highlight the importance of combined pulsatile flow and cyclic strain in the maturation process of PSC-CMs.

In our study, we revealed that d18 dyn mESC-CMs and d20 dyn hESC-CMs showed a functional improvement as the typical systolic calcium transient parameters, the *rate of constant* of Ca^{2+} *decay* (tau), slope, and amplitude improved with extended culture times, indicating rapid electromechanical coupling. This change could be the result of structural changes in the contractile apparatus, the better orientation of the myocyte network associated with enhanced expression of gap junctions, or alterations in the balance of cardiac ion channels (Zhu, Blazeski et al. 2014). In previous studies, most of the ESC-CMs did not respond to caffeine as they relied on calcium influx from sarcolemma instead of the sarcoplasmic reticulum as seen in adult CMs (Khan, Lyon et al. 2013, Li, Chen et al. 2013). In a few studies, hESC-CMs cultured for more than 27 days showed a response to caffeine (Nunes, Miklas et al. 2013, Kosmidis, Bellin et al. 2015). Here, ESC-CMs responded to caffeine after 12 (mESC-CMs) or 10 (hESC-CMs) days, as shown by an increased Ca^{2+} handling consistent with a functional SR. Furthermore, when compared with d12 dyn mESC-CMs and d10 hESC-CMs, d18 dyn mESC-CMs and d20 dyn hESC-CMs exhibited a higher store of Ca^{2+} and an improved SERCA function. We further performed concentration-response studies employing nifedipine and dofetilide. Although hESC-CMs exhibited a dose-dependent response to nifedipine and dofetilide, no significant differences were seen between stat and dyn hESC-CMs. The electrophysiology was stable throughout the recordings. This indicates that the calcium and hERG channels in all hESC-CMs were fully functional without any limitation.

In concert with biochemical cues, mechanical stimuli can activate or inhibit signaling pathways and thus regulate transcription factor expression to drive myocardial differentiation, specification, and maturation (Van Vliet, Wu et al. 2012, Happe and Engler 2016). As shown by others (Gessert and Kühl 2010), we also detected a lower expression of β-catenin in d20 dyn hESC-CMs when compared with d20 stat hESC-CMs. Wnt/β-catenin signaling has been reported to have a stage-dependent, paradoxical effect on cardiogenesis. We hypothesize that the low expression of β-catenin seen in d20 dyn hESC-CMs was due to late-phase cardiac maturation (Gessert and Kühl 2010). A stretch-induced down-regulation of Wnt/β-catenin was described in other studies using human osteoblastic cells (Jansen, Eijken et al.

2010). The Wnt/β-catenin signaling pathway is one of many pathways regulated by mechanical stimuli. Other mechanically-induced signaling pathways may also play a role in regulating cardiac differentiation and maturation (Fonseca, Inoue et al. 2005, Torsoni, Marin et al. 2005, Jaalouk and Lammerding 2009). Future work will focus on the systematical identification of the signaling pathways that are activated when applying different mechanical stimuli. In addition, development of the existing bioreactor towards a high-throughput system would be beneficial since this would allow studies with increased numbers of experimental conditions and replicates while reducing the amounts of cell and culture materials.

Experimental procedures

Detailed information on the Experimental Procedures can be found in the Supplemental Information file.

Design and simulation of a multi-functional bioreactor system

A custom-built, bioreactor system was designed using Solidworks for CAD (Solidworks2010, Dassault Systemes SolidWorks Corporation, Ludwigsburg, Germany). It is composed of an air and fluid chamber that are separated by a silicone membrane in order to ensure a sterile environment (**Figure 1**). A computational model was developed to assess the designed bioreactor system performance in silico. Meshing and calculations were performed in COMSOL 4.3a based on the bioreactor geometry and dimensions (COMSOL Multiphysics GmbH, Berlin, Germany). The detailed experimental set-up description is provided in the Supplemental Data file.

mESC and hESC cultures

CCE mESCs (ATCC, USA) and H9 hESCs were employed in this study. The use of human embryonic stem cells for this study was approved by the Robert Koch-Institute, Berlin, Germany (AZs: 3.04.02/0086 and 3.04.02/0111). For experiments, 1.18 x 10^6 CCE mESCs/ 9.5 cm^2 were seeded on the center area of fibronectin-coated Thincert™ six-well culture inserts (Greiner Bio-One, Frickenhausen, Germany), followed by transfer into the bioreactor system and exposure to pulsatile flow-induced shear stress or/and strain for 12 or 18 days. hESC differentiation was performed based on a protocol that was previously reported (Brauchle, Knopf et al. 2016). After 4 days of differentiation, 200 EBs/ 9.5 cm^2 were seeded on the center of gelatin-coated Thincert™ inserts, which were subsequently transferred into the bioreactor and exposed to pulsatile flow-induced shear stress and strain for 5 or 15 days

(in total d10 and d20 of culture, counted from the undifferentiated cell stage). See the Supplemental Data file for details.

IF staining

All cells were fixed directly on the membranes with 4% paraformaldehyde (PFA). The mESC-CMs were further processed for staining as previously described (Hinderer, Shen et al. 2015). For hESC-CMs samples, Histogel (American MasterTech, USA) was dispensed on the samples after PFA was removed, followed by embedding in paraffin. IF staining of 3 µm sections was performed as previously described (Votteler, Carvajal Berrio et al. 2013). All antibodies are listed in the Supplemental Data file. DAPI was used to visualize cell nuclei. A confocal microscope LSM710 (Carl Zeiss GmbH, Jena, Germany) was used for imaging. Sarcomere length was analyzed using ImageJ (version 1.46r, Wayne Rasband, NIH) (Wang, Wu et al. 2013, Nance, Whitfield et al. 2015).

Calcium transient recordings

mESC-CMs and hESC-CMs were transferred to fibronectin-coated plastic bottom petri dishes and the fluorescence intensity of Ca520-AM dye was measured using a Confocal LSM710 microscope with controlled temperature 37 ºC and 5% CO_2. Electrical field stimulation was applied to evoke Ca^{2+} transients at the stimulation frequencies of 3 Hz (hESC-CMs) or 2 Hz (hESC-CMs) using bipolar electrodes attached to an STG-2004 stimulator (Multi Channel Systems MCS, Germany). Systolic and caffeine-induced Ca^{2+} transient duration (from peak amplitude until 90% return to base level, CaT_{90}), decay, amplitude, and slope were assessed as previously published (Kosmidis, Bellin et al. 2015)

Raman microspectroscopy

A custom-built Raman microspectroscope was used to acquire Raman spectra of mESC-CMs and hESC-CMs as previously described in detail (Brauchle, Knopf et al. 2016). A detailed description of the experimental set-up, including Raman spectra processing and principal component analysis is provided in the Supplemental Data file. Additional details on these pre-processing steps were previously described in detail (Pudlas, Berrio et al. 2011, Votteler, Carvajal Berrio et al. 2012a, Votteler, Carvajal Berrio et al. 2012b, Brauchle, Thude et al. 2014, Brauchle, Knopf et al. 2016).

Statistical analysis

Except stated otherwise, data are shown in mean ± standard deviation. One-way analysis of variance (ANOVA) was performed to compare data groups. Student's t-test was performed to compare between two data groups. A probability value of 95% ($p < 0.05$) was used to determine significance.

Author contributions

N.S., E.B., U.K., and K.S.-L. designed experiments. N.S. and J.R. designed the bioreactor. N.S., A.K., C.W., U.K., H.B., S.P. and S.K. performed experiments, collected and analyzed data. S.L.L., M.H. and A.N. gave conceptual advice. N.S., S.H., S.L.L. and K.S.-L. wrote the manuscript.

Acknowledgements

We thank Adrienne Lee (Fraunhofer IGB) for her assistance with the Raman measurements. This work was financially supported by CIRM (RB3-05086 to A.N.), Fraunhofer-Gesellschaft (Attract to K.S.-L., FFE to S.L.L., Talenta to S.H.), DAAD RISE and US Fulbright Student Scholarships (both to J.R.), as well as the BMBF (0316059), Ministry of Science, Research and Arts of Baden-Württemberg (Az.: SI-BW 01222-91, 33-729.55-3/214), and the DFG (INST 2388/33-1, SCHE 701/7-1, SCHE 701/10-1) (all to K.S.-L).

References

Alfieri, C. M., Cheek, J., Chakraborty, S., and Yutzey, K. E. (2010). Wnt signaling in heart valve development and osteogenic gene induction. Dev Biol *338*, 127-135.

Andrés-Delgado, L., and Mercader, N. (2016). Interplay between cardiac function and heart development. Biochim Biophys Acta *1863*, 1707-1716.

Blazeski, A., Zhu, R., Hunter, D. W., Weinberg, S. H., Boheler, K. R., Zambidis, E. T., and Tung, L. (2012). Electrophysiological and contractile function of cardiomyocytes derived from human embryonic stem cells. Prog Biophys Mol Biol *110*, 178-195.

Borg, T. K., Goldsmith, E. C., Price, R., Carver, W., Terracio, L., and Samarel, A. M. (2000). Specialization at the Z line of cardiac myocytes. Cardiovasc Res *46*, 277-285.

Bosman, A., Sartiani, L., Spinelli, V., Del Lungo, M., Stillitano, F., Nosi, D., Mugelli, A., Cerbai, E., and Jaconi, M. (2013). Molecular and functional evidence of HCN4 and caveolin-3 interaction during cardiomyocyte differentiation from human embryonic stem cells. Stem Cells Dev *22*, 1717-1727.

Braam, R., Passier, R., and Mummery, C. L. (2009). Cardiomyocytes from human pluripotent stem cells in regenerative medicine and drug discovery. Trends Pharmacol Sci *30*, 536-545.

Brauchle, E., Knopf, A., Bauer, H., Shen, N., Linder, S., Monaghan, M. G., Ellwanger, K., Layland, S. L., Brucker, S. Y., Nsair, A., et al. (2016). Novel non-invasive identification of chamber specific cardiomyocytes in differentiating pluripotent stem cells. Stem Cell Reports *6*, 188-199.

Brauchle, E., Thude, S., Brucker, S. Y., and Schenke-Layland, K. (2014). Cell death stages in single apoptotic and necrotic cells monitored by Raman microspectroscopy. Sci Rep *4*, 4698.

Butcher, J. T., and Nerem, R. M. (2007). Valvular endothelial cells and the mechanoregulation of valvular pathology. Philos Trans R Soc Lond B Biol Sci *362*, 1445-1457.

Carrier, R. L., Rupnick, M., Langer, R., Schoen, F. J., Freed, L. E., and Vunjak-Novakovic, G. (2002). Perfusion improves tissue architecture of engineered cardiac muscle. Tissue Eng *8*,175-188.

Chiu, J. J., and Chien, S. (2011). Effects of disturbed flow on vascular endothelium: pathophysiological basis and clinical perspectives. Physiol Rev *91*, 327-387.

Chung, S., Dzeja, P. P., Faustino, R. S., Perez-Terzic, C., Behfar, A., and Terzic, A. (2007). Mitochondrial oxidative metabolism is required for the cardiac differentiation of stem cells. Nat Clin Pract Cardiovasc Med *4*, S60-S67.

Davis, R. P., Casini, S., van den Berg, C. W., Hoekstra, M., Remme, C. A., Dambrot, C., Salvatori, D., Oostwaard, D. W.-v., Wilde, A. A. M., Bezzina, C. R., et al. (2012). Cardiomyocytes derived from pluripotent stem cells recapitulate electrophysiological characteristics of an overlap syndrome of cardiac sodium channel disease. Circulation *125*, 3079-3091.

Ebert, A. D., Liang, P., and Wu, J. C. (2012). Induced pluripotent stem cells as a disease modeling and drug screening platform. J Cardiovasc Pharmacol *60*, 408-416.

Feinberg, A. W., Ripplinger, C. M., van der Meer, P., Sheehy, S. P., Domian, I., Chien, K. R., and Parker, K. K. (2013). Functional differences in engineered myocardium from embryonic stem cell-derived versus neonatal cardiomyocytes. Stem Cell Reports *1*, 387-396.

Fonseca, P. M., Inoue, R. Y., Kobarg, C. B., Crosara-Alberto, D. P., Kobarg, J., and Franchini, K. G. (2005). Targeting to C-terminal myosin heavy chain may explain mechanotransduction involving focal adhesion kinase in cardiac myocytes. Circ Res *96*, 73-81.

Gessert, S., and Kühl, M. (2010). The multiple phases and faces of Wnt signaling during cardiac differentiation and development. Circ Res *107*, 186-199.

Guan, J., Wang, F., Li, Z., Chen, J., Guo, X., Liao, J., and Moldovan, N. I. (2011). The stimulation of the cardiac differentiation of mesenchymal stem cells in tissue constructs that mimic myocardium structure and biomechanics. Biomaterials *32*, 5568-5580.

Gwak, S. J., Bhang, S. H., Kim, I. K., Kim, S. S., Cho, S. W., Jeon, O., Yoo, K. J., Putnam, A. J., and Kim, B. S. (2008). The effect of cyclic strain on embryonic stem cell-derived cardiomyocytes. Biomaterials *29*, 844-856.

Happe, C. L., and Engler, A. J. (2016). Mechanical forces reshape differentiation cues that guide cardiomyogenesis. Circ Res *118*, 296-310.

Harris, K., Aylott, M., Cui, Y., Louttit, J. B., McMahon, N. C., and Sridhar, A. (2013). Comparison of electrophysiological data from human-induced pluripotent stem cell–derived cardiomyocytes to functional preclinical safety assays. Toxicol Sci *134*, 412-426.

Hinderer, S., Shena, N., Ringuette, L. J., Hansmann, J., Reinhardt, D. P., Brucker, S. Y., Davis, E. C., and Schenke-Layland, K. (2015). In vitro elastogenesis: instructing human vascular smooth muscle cells to generate an elastic fiber-containing extracellular matrix scaffold. Biomed Mater. *10*, 034102

.

Huang, Y., Zheng, L., Gong, X., Jia, X., Song, W., Liu, M., and Fan, Y. (2012). Effect of cyclic strain on cardiomyogenic differentiation of rat bone marrow derived mesenchymal stem cells. PLoS ONE *7*, e34960.

Hurlstone, A. F., Haramis, A. P., Wienholds, E., Begthel, H., Korving, J., Van Eeden, F., Cuppen, E., Zivkovic, D., Plasterk, R. H., and Clevers, H. (2003). The Wnt/beta-catenin pathway regulates cardiac valve formation. Nature *425*, 633-637.

Jaalouk, D. E., and Lammerding, J. (2009). Mechanotransduction gone awry. Nat Rev Mol Cell Biol *10*, 63-73.

Jaiswal, A., and Goldbarg, S. (2014). Dofetilide induced torsade de pointes: Mechanism, risk factors and management strategies. Indian Heart J *66*, 640-648.

Jansen, J. H., Eijken, M., Jahr, H., Chiba, H., Verhaar, J. A., van Leeuwen, J. P., and Weinans, H. (2010). Stretch-induced inhibition of Wnt/beta-catenin signaling in mineralizing osteoblasts. J Orthop Res *28*, 390-396.

Khan, J. M., Lyon, A. R., and Harding, S. E. (2013). The case for induced pluripotent stem cell-derived cardiomyocytes in pharmacological screening. Br J Pharmacol *169*, 304-317.

Kosmidis, G., Bellin, M., Ribeiro, M. C., van Meer, B., Ward-van Oostwaard, D., Passier, R., Tertoolen, L. G. J., Mummery, C. L., and Casini, S. (2015). Altered calcium handling and increased contraction force in human embryonic stem cell derived cardiomyocytes following short term dexamethasone exposure. Biochem Biophys Res Commun *467*, 998-1005.

Li, S., Chen, G., and Li, R. A. (2013). Calcium signalling of human pluripotent stem cell-derived cardiomyocytes. J Physiol *591*, 5279-5290.

Lundy, S. D., Zhu, W. Z., Regnier, M., and Laflamme, M. A. (2013). Structural and functional maturation of cardiomyocytes derived from human pluripotent stem cells. Stem Cells Dev *22*, 1991-2002.

Masumoto, H., Matsuo, T., Yamamizu, K., Uosaki, H., Narazaki, G., Katayama, S., Marui, A., Shimizu, T., Ikeda, T., Okano, T., et al. (2012). Pluripotent stem cell-engineered cell sheets reassembled with defined cardiovascular populations ameliorate reduction in infarct heart function through cardiomyocyte-mediated neovascularization. Stem Cells *30*, 1196-1205.

Mihic, A., Li, J., Miyagi, Y., Gagliardi, M., Li, S. H., Zu, J., Weisel, R. D., Keller, G., and Li, R. K. (2014). The effect of cyclic stretch on maturation and 3D tissue formation of human embryonic stem cell-derived cardiomyocytes. Biomaterials *35*, 2798-2808.

Movasaghi, Z., Rehman, S., and Rehman, I. U. (2007). Raman spectroscopy of biological tissues. Appl Spectrosc Rev *42*, 493-541.

Naito, A. T., Shiojima, I., Akazawa, H., Hidaka, K., Morisaki, T., Kikuchi, A., and Komuro, I. (2006). Developmental stage-specific biphasic roles of Wnt/β-catenin signaling in cardiomyogenesis and hematopoiesis. Proc Natl Acad Sci U S A *103*, 19812-19817.

Nance, M. E., Whitfield, J. T., Zhu, Y., Gibson, A. K., Hanft, L. M., Campbell, K. S., Meininger, G. A., McDonald, K. S., Segal, S. S., and Domeier, T. L. (2015). Attenuated sarcomere lengthening of the aged murine left ventricle observed using two-photon fluorescence microscopy. AM J Physiol Heart Circ Physiol *309*, H918-H925.

Notingher, I., Green, C., Dyer, C., Perkins, E., Hopkins, N., Lindsay, C., and Hench, L. L. (2004). Discrimination between ricin and sulphur mustard toxicity in vitro using Raman spectroscopy. J R Soc Interface *1*, 79-90.

Nunes, S. S., Miklas, J. W., Liu, J., Aschar-Sobbi, R., Xiao, Y., Zhang, B., Jiang, J., Masse, S., Gagliardi, M., Hsieh, A., et al. (2013). Biowire: a platform for maturation of human pluripotent stem cell-derived cardiomyocytes. Nat Methods *10*, 781-787.

Pascut, F. C., Goh, H. T., Welch, N., Buttery, L. D., Denning, C., and Notingher, I. (2011). Noninvasive detection and imaging of molecular markers in live cardiomyocytes derived from human embryonic stem cells. Biophys J *100*, 251-259.

Pascut, F. C., Kalra, S., George, V., Welch, N., Denning, C., and Notingher, I. (2013). Non-invasive label-free monitoring the cardiac differentiation of human embryonic stem cells in-vitro by Raman spectroscopy. Biochim Biophys Acta *1830*, 3517-3524.

Passier, R., van Laake, L. W., and Mummery, C. L. (2008). Stem-cell-based therapy and lessons from the heart. Nature *453*, 322-329.

Piven, O. O., Palchevska, O. L., and Lukash, L. L. (2014). The Wnt/beta-catenin signaling in embryonic cardiogenesis, postnatal development and myocardium reconstruction. Tsitol Genet *48*, 72-83.

Pohjoismaki, J. L. O., Kruger, M., Al-Furoukh, N., Lagerstedt, A., Karhunen, P. J., and Braun, T. (2013). Postnatal cardiomyocyte growth and mitochondrial reorganization cause multiple changes in the proteome of human cardiomyocytes. Molecular BioSystems *9*, 1210-1219.

Pudlas, M., Berrio, D. A. C., Votteler, M., Koch, S., Thude, S., Walles, H., and Schenke-Layland, K. (2011). Non-contact discrimination of human bone marrow-derived mesenchymal stem cells and fibroblasts using Raman spectroscopy. Med Laser Appl *26*, 119-125.

Ribeiro, M. C., Tertoolen, L. G., Guadix, J. A., Bellin, M., Kosmidis, G., D'Aniello, C., Monshouwer-Kloots, J., Goumans, M. J., Wang, Y. L., Feinberg, A. W., et al. (2015). Functional maturation of human pluripotent stem cell derived cardiomyocytes in vitro--correlation between contraction force and electrophysiology. Biomaterials *51*, 138-150.

.

Satin, J., Kehat, I., Caspi, O., Huber, I., Arbel, G., Itzhaki, I., Magyar, J., Schroder, E. A., Perlman, I., and Gepstein, L. (2004). Mechanism of spontaneous excitability in human embryonic stem cell derived cardiomyocytes. J Physiol *559*, 479-496.

Shyu, K. G., Wang, B. W., Lin, C. M., and Chang, H. (2010). Cyclic stretch enhances the expression of Toll-like Receptor 4 gene in cultured cardiomyocytes via p38 MAP kinase and NF-κB pathway. J Biomed Sci *17*, 1-13.

Taber, L. A. (2001). Biomechanics of cardiovascular development. Annu Rev Biomed Eng *3*, 1-25.

Torsoni, A. S., Marin, T. M., Velloso, L. A., and Franchini, K. G. (2005). RhoA/ROCK signaling is critical to FAK activation by cyclic stretch in cardiac myocytes. Am J Physiol Heart Circ Physiol *289*, H1488-H1496.

Tsamis, A., Bothe, W., Kvitting, J.-P. E., Swanson, J. C., Miller, D. C., and Kuhl, E. (2011). Active contraction of cardiac muscle: In vivo characterization of mechanical activation sequences in the beating heart. J Mech Behav Biomed Mater *4*, 1167-1176.

Tulloch, N. L., Muskheli, V., Razumova, M. V., Korte, F. S., Regnier, M., Hauch, K. D., Pabon, L., Reinecke, H., and Murry, C. E. (2011). Growth of engineered human myocardium with mechanical loading and vascular coculture. Circ Res *109*, 47-59.

Tzahor, E. (2007). Wnt/beta-catenin signaling and cardiogenesis: timing does matter. Dev Cell *13*, 10-13.

Van Vliet, P., Wu, S. M., Zaffran, S., and Puceat, M. (2012). Early cardiac development: a view from stem cells to embryos. Cardiovasc Res *96*, 352-362.

Votteler, M., Carvaja Berrio, D. A., Horke, A., Sabatier, L., Reinhardt, D. P., Nsair, A., Aikawa, E., and Schenke-Layland, K. (2013). Elastogenesis at the onset of human cardiac valve development. Development *140*, 2345-2353.

Votteler, M., Carvajal Berrio, D. A., Pudlas, M., Walles, H., and Schenke-Layland, K. (2012a). Non-contact, label-free monitoring of cells and extracellular matrix using Raman spectroscopy. J Vis Exp. *63*, pii: 3977.

Votteler, M., Carvajal Berrio, D. A., Pudlas, M., Walles, H., Stock, U. A., and Schenke-Layland, K. (2012b). Raman spectroscopy for the non-contact and non-destructive monitoring of collagen damage within tissues. J Biophotonics *5*, 47-56.

Wan, C. R., Chung, S., and Kamm, R. D. (2011). Differentiation of embryonic stem cells into cardiomyocytes in a compliant microfluidic system. Ann Biomed Eng *39*, 1840-1847.

Wang, Y., Wu, Z., Liu, X., and Fu, Q. (2013). Gastrodin ameliorates Parkinson's disease by downregulating connexin 43. Mol Med Rep *8*, 585-590.

Yang, L., Soonpaa, M. H., Adler, E. D., Roepke, T. K., Kattman, S. J., Kennedy, M., Henckaerts, E., Bonham, K., Abbott, G. W., Linden, R. M., et al. (2008). Human cardiovascular progenitor cells develop from a KDR+ embryonic-stem-cell-derived population. Nature *453*, 524-528.

Yang, X., Pabon, L., and Murry, C. E. (2014). Engineering adolescence: maturation of human pluripotent stem cell-derived cardiomyocytes. Circ Res *114*, 511-523.

Zhang, J., Klos, M., Wilson, G. F., Herman, A. M., Lian, X., Raval, K. K., Barron, M. R., Hou, L., Soerens, A. G., Yu, J., et al. (2012). Extracellular matrix promotes highly efficient cardiac differentiation of human pluripotent stem cells: The matrix sandwich method. Circ Res 111, 1125-1136.

Zhu, R., Blazeski, A., Poon, E., Costa, K. D., Tung, L., and Boheler, K. R. (2014). Physical developmental cues for the maturation of human pluripotent stem cell-derived cardiomyocytes. Stem Cell Res Ther 5, 117.

Figures

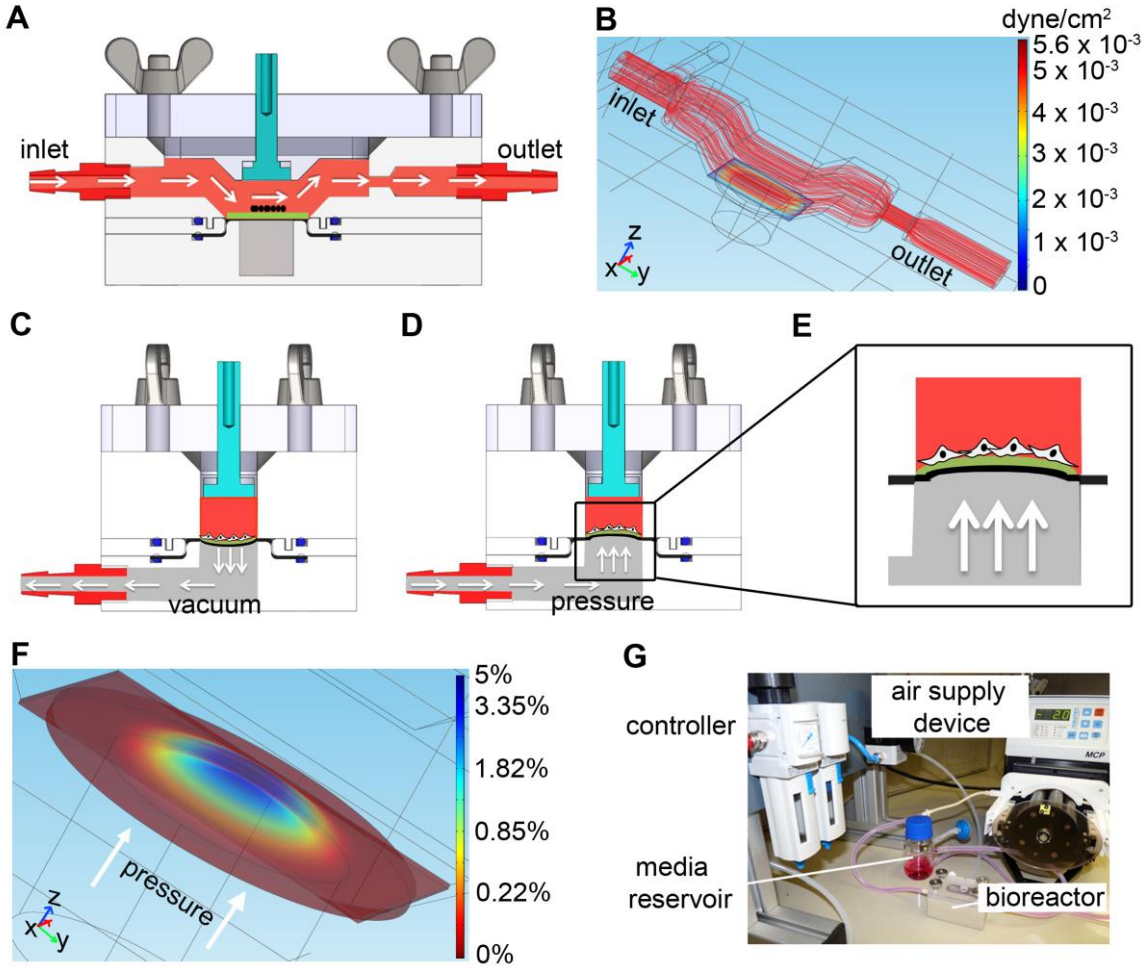

Figure 1. Bioreactor system design and evaluation. (A) Computer-aided design of the flow chamber (red) in a cross-sectional view. White arrows point in flow direction. Cell-seeded membrane in green. Silicone membrane is indicated in black. (B) Representative simulation of wall shear stress distribution in the bioreactor system. Red stream lines indicate laminar flow. (C) Vacuum- and (D, E) pressure-driven mechanism to enable a physiological stretch profile. Pressure gradient is induced in the air chamber (grey) using a controller. White arrows show the direction of air. Cell-seeded membrane is depicted in green, and the silicone membrane is indicated in black. (F) Representative strain distribution simulation of the cell-seeded membrane with 1.35 standard atmosphere pressure applied. White arrows show the direction of pressure. (G) Photograph of the experimental set up. The bioreactor is coupled to a culture medium reservoir, an air supply device, and a controller.

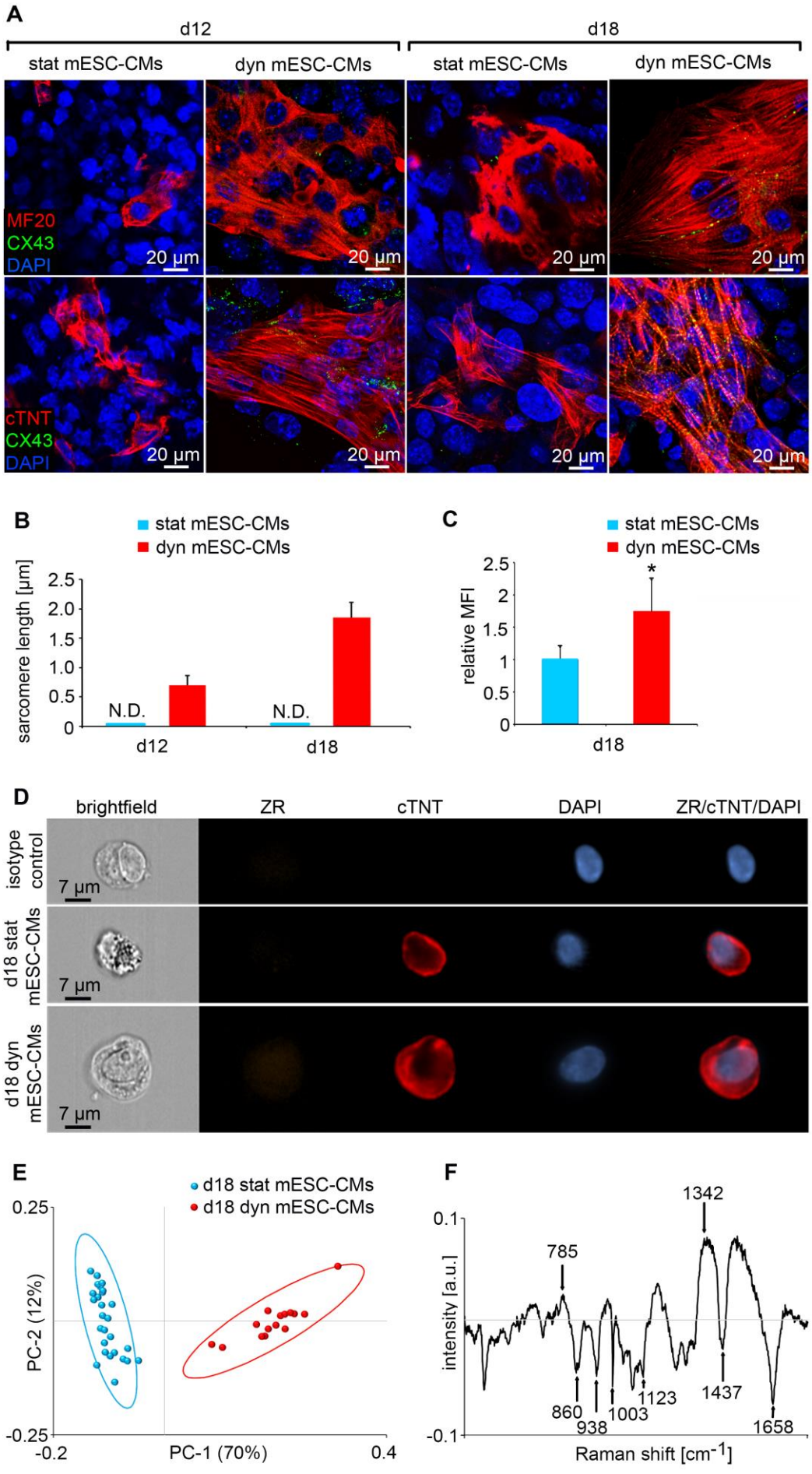
A
d12
d18
stat mESC-CMs
dyn mESC-CMs
stat mESC-CMs
dyn mESC-CMs
MF20
CX43
DAPI
cTNT
CX43
DAPI
20 µm
B
stat mESC-CMs
dyn mESC-CMs
sarcomere length [µm]
N.D.
N.D.
d12
d18
C
stat mESC-CMs
dyn mESC-CMs
relative MFI
*
d18
D
brightfield
ZR
cTNT
DAPI
ZR/cTNT/DAPI
isotype control
d18 stat mESC-CMs
d18 dyn mESC-CMs
7 µm
E
d18 stat mESC-CMs
d18 dyn mESC-CMs
PC-2 (12%)
PC-1 (70%)
F
intensity [a.u.]
Raman shift [cm-1]
785
860
938
1003
1123
1342
1437
1658

Figure 2. Mechanical forces enhance cardiac protein expression patterns in mESC-CMs. (A) IF staining of d12 stat and dyn, d18 stat and dyn mESC-CMs using MF20 (red), CX43 (green) and cTNT (red), DAPI (blue). (B) Sarcomere length in d12 and d18 mESC-CMs was quantified using ImageJ (n=20 cells from 3 independent cultures each). N.D. indicates not detectable. (C) Relative median fluorescence intensity (MFI) of cTNT expression in d18 stat mESC-CMs and d18 dyn mESC-CMs (n=3). *p=0.0490. (D) Representative images of d18 stat mESC-CMs and d18 dyn mESC-CMs stained with ZR (orange), cTNT (red), and DAPI (blue) as well as the isotype control. ZR/cTNT/DAPI represents an overlay. (E) Raman microspectroscopy results. Plotting of PC-1 and PC-2 score values depicts a distinction between d18 stat and d18 dyn mESC-CMs (n=30 measurements from 3 independent cultures each). The ellipses mark the 95% confidence region for each sample. (F) PC-1 loading describes the Raman shifts that vary in d18 dyn mESC-CMs when compared with d18 stat mESC-CMs. Differences between d18 stat and dyn mESC-CMs were identified at wavenumbers indicated by arrows. (See also Figures S2 and S3).

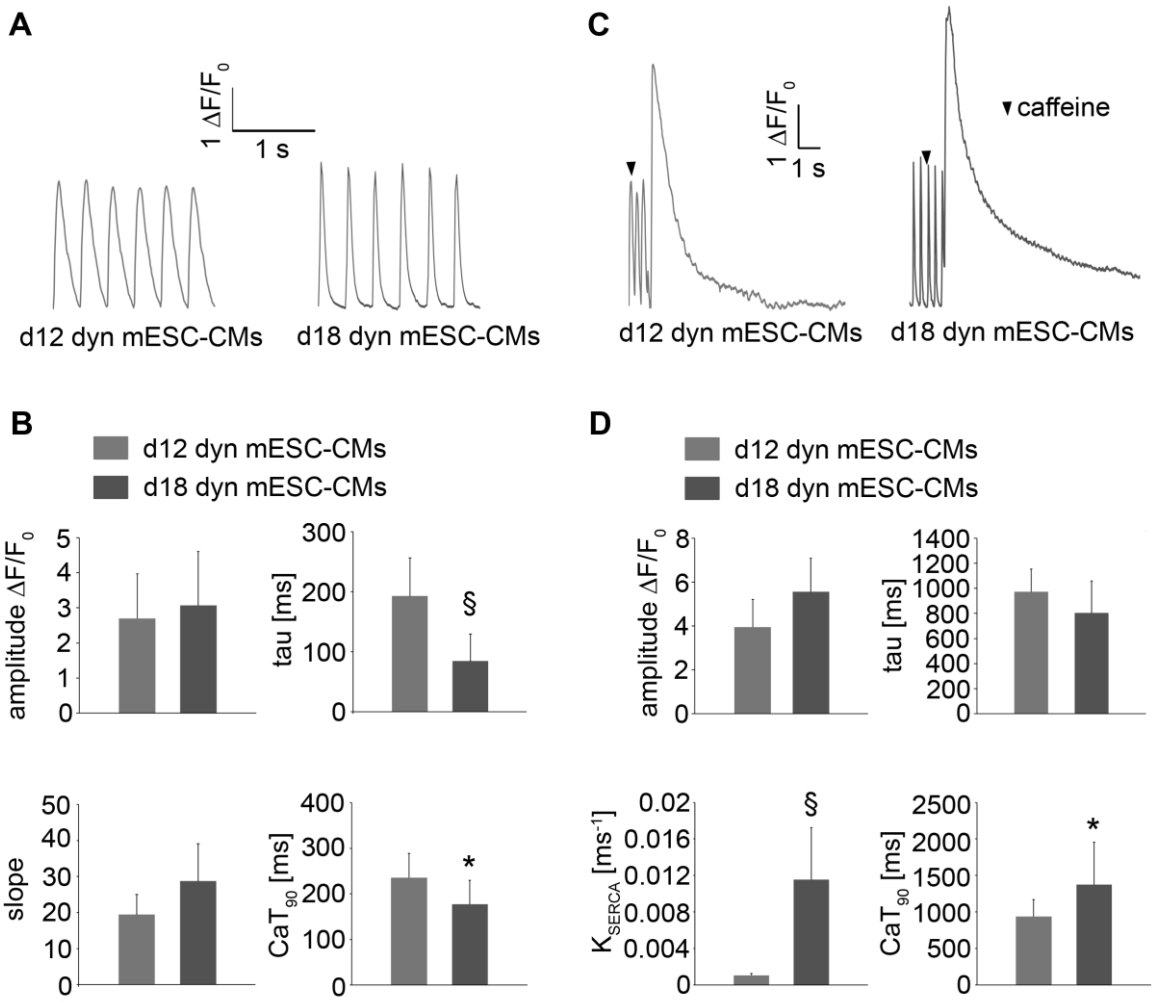

Figure 3. Calcium transient assessment of dynamically-cultured mESC-CMs. (A) Representative systolic Ca^{2+} transient traces recorded at the stimulation frequency of 3 Hz in d12 and d18 dyn mESC-CMs. Fluorescence intensities are displayed in arbitrary units (a.u.). (B) Average amplitude, time constant of decay (tau), slope and Ca^{2+} transient duration (CaT_{90}) in d12 (n=9) and d18 dyn (n=11) mESC-CMs. (C) Representative caffeine-induced changes in Ca^{2+} transient traces in d12 and d18 dyn mESC-CMs. (D) Average caffeine-induced amplitude, time constant of decay (tau), SERCA activity and Ca^{2+} transient duration (CaT_{90}) in d12 (n=9) and d18 dyn (n=11) mESC-CMs. * $p < 0.05$, # $p < 0.05$, § $p < 0.001$.

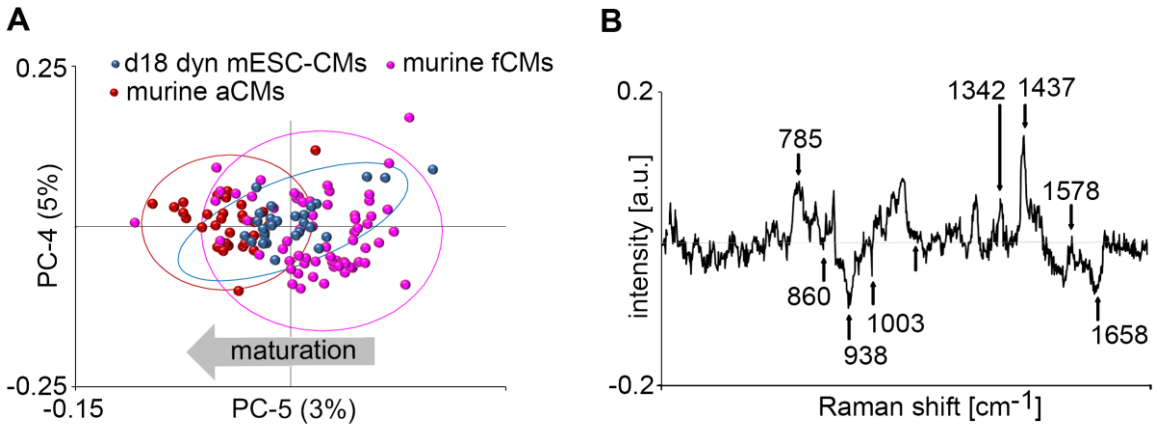

Figure 4. Phenotype characterization of d18 dyn mESC-CMs using Raman microspectroscopy. (A) Scores plot demonstrates spectral changes due to cardiac maturation (n=30 measurements from 3 independent cultures for d18 dyn mESC-CMs and murine aCMs, n=60 measurements from 3 independent cultures for murine fCMs). (B) Corresponding PC-5 loading spectrum describes the differences between the murine CM-phenotypes. Arrows highlight the wavenumbers of the prominent differences.

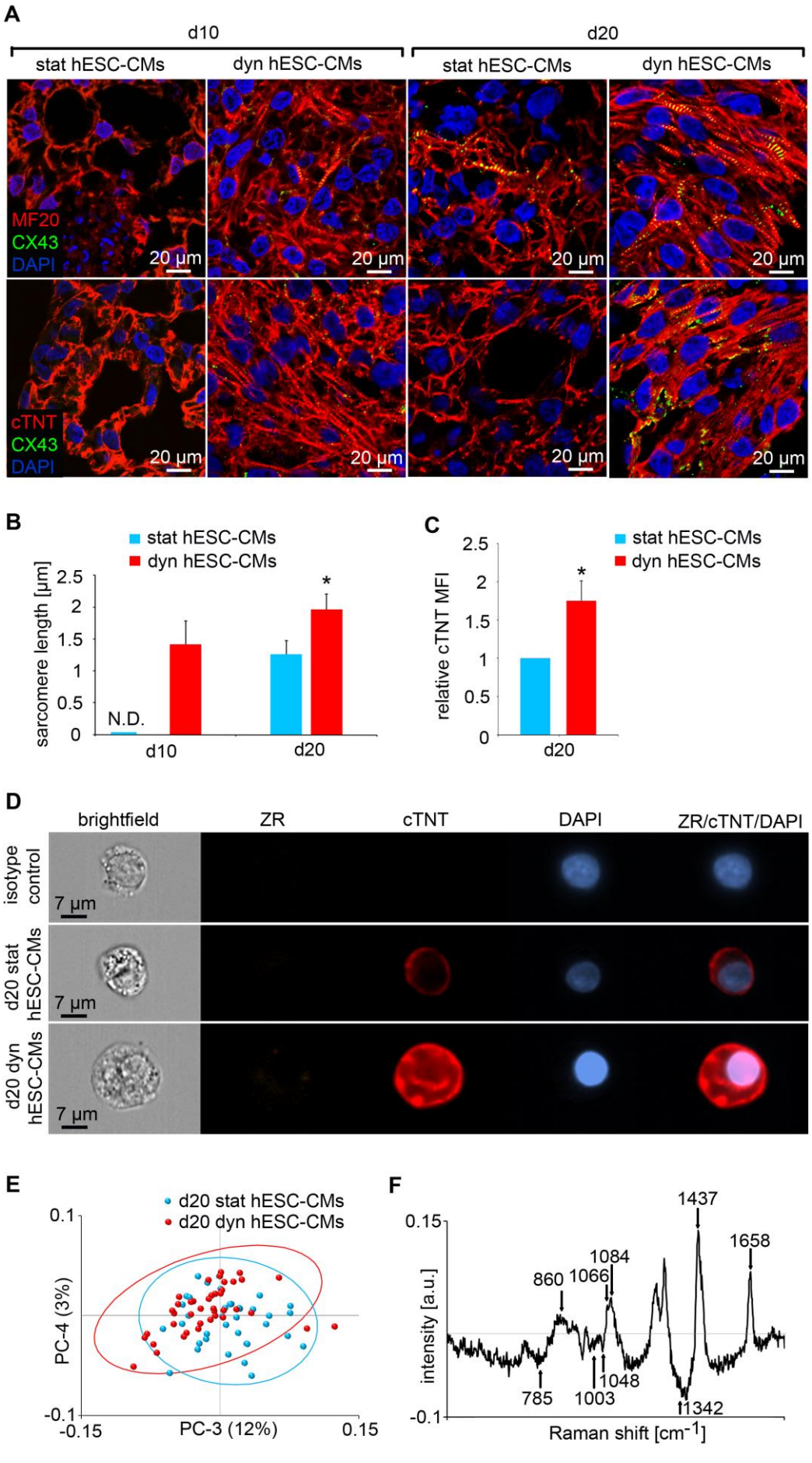
A
d10
d20
stat hESC-CMs
dyn hESC-CMs
stat hESC-CMs
dyn hESC-CMs
MF20
CX43
DAPI
20 µm
cTNT
CX43
DAPI
20 µm
B
stat hESC-CMs
dyn hESC-CMs
sarcomere length [µm]
2.5
2
1.5
1
0.5
0
N.D.
*
d10
d20
C
stat hESC-CMs
dyn hESC-CMs
relative cTNT MFI
2.5
2
1.5
1
0.5
0
*
d20
D
brightfield
ZR
cTNT
DAPI
ZR/cTNT/DAPI
isotype control
d20 stat hESC-CMs
d20 dyn hESC-CMs
7 µm
E
d20 stat hESC-CMs
d20 dyn hESC-CMs
0.1
PC-4 (3%)
-0.1
-0.15
PC-3 (12%)
0.15
F
0.15
intensity [a.u.]
-0.1
1437
1658
1084
860
1066
1048
785
1003
1342
Raman shift [cm-1]

Figure 5. Mechanical stimuli induced an enhanced cardiac protein expression pattern in hESC-CMs. (A) IF images show expression of MF20 (red), CX43 (green), cTNT (red) and DAPI (blue) in d10 stat and dyn, d20 stat and dyn hESC-CMs. (B) Quantification of sarcomere length in d10 and d20 hESC-CMs (n=20 cells from 3 independent cultures each). N.D. represents not detectable. * $p < 0.01$ versus stat hESC-CMs at the same time point. (C) Relative MFI of cTNT expression in d20 stat and dyn hESC-CMs (n=4). *p=0.0014. (D) Representative images of d20 stat and dyn hESC-CMs stained with ZR (orange), cTNT (red), and DAPI (blue). ZR/cTNT/DAPI represents an overlay. (E) Scores of PC-3 and PC-4 of Raman spectra from d20 stat hESC-CMs (n=30 measurements from 3 independent cultures) and d20 dyn hESC-CMs (n=45 measurements from 3 independent cultures). (F) PC-4 loadings represent Raman peaks that changed significantly in d20 dyn hESC-CMs when compared with static d20 stat hESC-CMs. (See also Figures S4-S6).

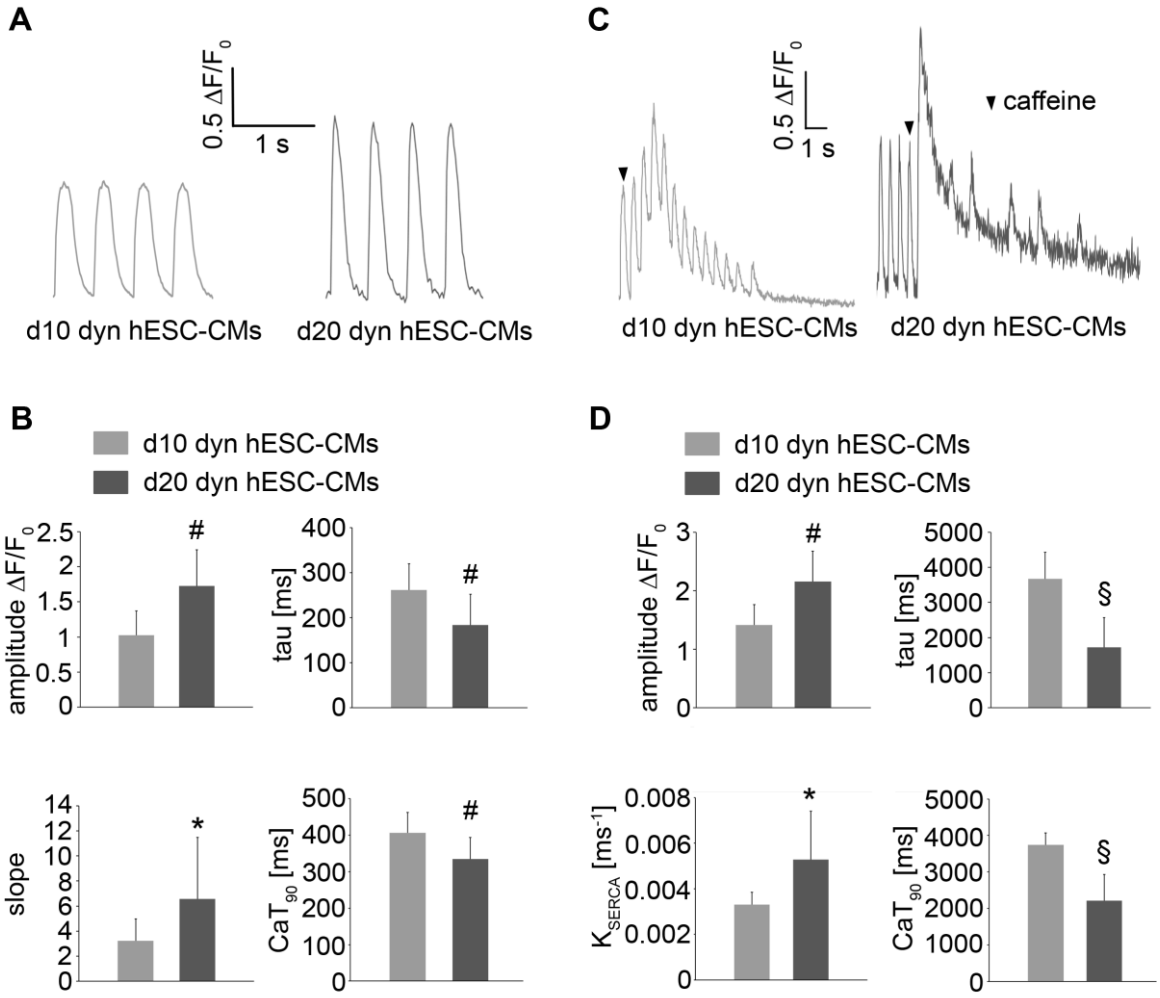

Figure 6. Assessment of calcium transient properties in dynamically-cultured hESC-CMs. (A) Typical systolic Ca^{2+} transient traces of d10 and d20 dyn hESC-CMs stimulated at the frequency of 2 Hz. (B) Average amplitude, time constant of decay (tau), slope and Ca^{2+} transient duration (CaT_{90}) in d10 (n=8) and d20 (n=12) dyn hESC-CMs. (C) Recording of caffeine-induced Ca^{2+} transient in d10 and d20 dyn hESC-CMs. (D) Average caffeine-induced amplitude, time constant of decay (tau), SERCA activity and Ca^{2+} transient duration (CaT_{90}) in d10 (n=8) and d20 dyn (n=12) hESC-CMs. * $p < 0.05$, # $p < 0.05$, § $p < 0.001$. (See also Figure S7).

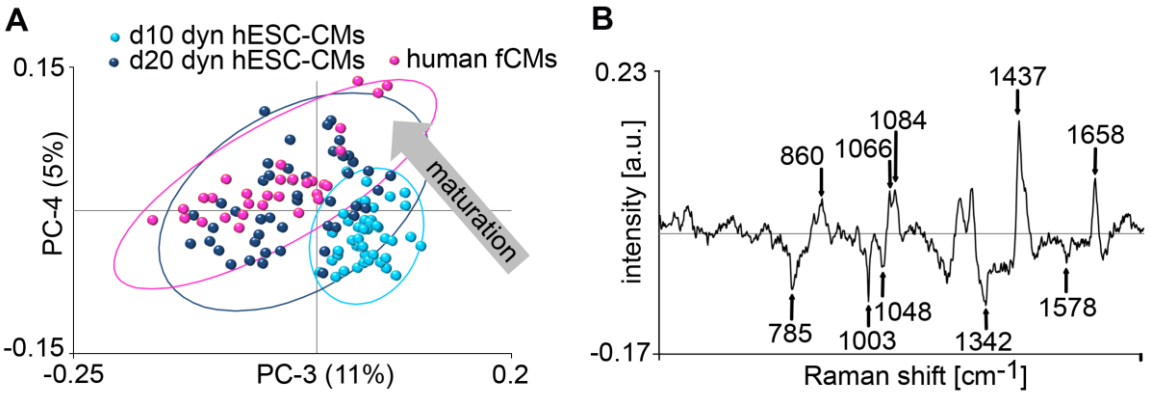

Figure 7. Raman microspectroscopic analysis of dynamically-cultured hESC-CMs. (A) Scores plot of human fCMs (n=30 measurements from 3 independent cultures), d10 dyn (n=30 measurements from 3 independent cultures) and d20 dyn hESC-CMs (n=45 measurements from 3 independent cultures). (B) Corresponding PC-4 loading spectrum describes the differences between the CM phenotypes. (C) Scores plot of human fCMs (n=30 measurements from 3 independent cultures) and d20 dyn hESC-CMs (n=45 measurements from 3 independent cultures). (D) Corresponding loading spectrum describes the differences between the CM phenotypes.

Supplemental Experimental Procedures

Bioreactor experimental set-up

The air chamber of the designed bioreactor was connected to an air pump and controlling system for amplitude and frequency. During the experiments, the cell-seeded membrane was placed on the top of silicone membrane. The vacuum- and pressure-driven air chamber generated a pressure gradient, which transferred strain from the silicone membrane to the cell-seeded membrane and the cells, resulting in a physiological stretch profile. The frequency of the cyclic strain was set by a controller**.** The fluidic chamber (1.5 × 1 × 0.7 cm) has one inlet- and outlet valve for laminar flow. The fluidic chamber was connected to a closed tubing system (Ismatec, Wertheim-Mondfeld, Germany) containing a 30-ml medium reservoir (Schott AG, Mainz, Germany) and a filter (Whatman GmbH, Dassel, Germany). The medium was pumped from the reservoir through the system using a peristaltic pump with a CA8 pump head and cassette (Ismatec). All in vitro experiments were performed at 37 °C, 5% CO_2.

mESC maintenance and in vitro differentiation

Except stated otherwise, all cell culture products were purchased from Life Technologies (Darmstadt, Germany). The mESC line CCE (ATCC, USA) was maintained mouse embryonic fibroblast (MEF)-free on 0.1% gelatin in knockout Dulbecco´s modified Eagle´s medium supplemented with 15% (v/v) ES-qualified FBS, 1% (v/v) non-essential amino acids (NNEA), 1% (v/v) penicillin/streptomycin (PenStrep), 2 mM L-Glutamin, 10 mM HEPES, 0.8 mM β -mercaptoethanol (β-ME; Sigma-Aldrich, Taufkirchen, Germany) and 1,000 U/ml leukemia inhibitory factor (Millipore, Schwalbach, Germany). The medium was changed daily. Cells were passaged every second day using 0.25 % trypsin-EDTA. The Thincert™ six-well culture inserts (Greiner Bio-One, Frickenhausen, Germany) were coated with 5 ng/ml fibronectin (Sigma-Aldrich) 24 hours prior to cell seeding. 1.18 x 10^6 cells/ 9.5 cm^2 were seeded on the center area of the Thincert™ inserts in MEM-alpha supplemented with 10 % FBS (v/v), 1% NNEA (v/v), 2 mM L-Glutamine, 1% (v/v) PenStrep, 10 mM HEPES and 0.8 mM β-ME. 24 hours after cell seeding, the cell-seeded membranes were cut out from Thincert™ inserts. Subsequently, half of the membranes were transferred into the bioreactor system and exposed to pulsatile flow-induced shear stress or/and strain for 12 or 18 days. The remaining membranes were cultured without stimulation and served as static controls. Afterwards, the cells were harvested for further analysis.

hESC maintenance and in vitro differentiation

H9 human ESCs, obtained from the WiCell Research Institute (Madison, WI, USA), were expanded on irradiated mouse embryonic feeder cells in human ESCs medium comprised of DMEM/F12 (1:1), supplemented with 20% knock-out serum replacement, 1% (v/v) NEAA, 1% (v/v) GlutaMAX™-I, 100 µg/ml β-ME and 10 ng/ml FGF-b (Miltenyi Biotec GmbH, Bergisch Gladbach, Germany) in six-well cell culture plates. Cells were passaged after three or four days and transferred to new feeder cells following dissociation with collagenase IV in DMEM/F12. The differentiation of hESCs was performed based on a protocol that was previously reported (Brauchle, Knopf et al. 2016) utilizing STEMPRO 34-medium, containing 2.6% supplements (10 ng/ml BMP4, 5 ng/ml FGF-b and 3 ng/ml Activin A (all R&D Systems). The medium was changed every day. The Thincert™ six-well culture inserts were coated with 0.1% gelatin for 24 hours prior cell seeding. On day four of differentiation, approximately 200 EBs/ 9.5 cm^2 were seeded on the center of Thincert™ inserts in medium that was supplemented with 5 µM IWR-1 (Sigma-Aldrich). On day five, the cell-seeded membranes were cut out from the Thincert™ inserts. Subsequently, half of the membranes were transferred into the bioreactor and exposed to pulsatile flow-induced shear stress and strain for 5 or 15 days (in total d10 and d20 of culture, counted from the undifferentiated cell stage) with a medium change every other day. The remaining membranes were cultured as static controls. Afterwards, the cells were harvested for further analysis.

Immunofluorescence staining

All samples were processed for immunofluorescence staining as previously described (Hinderer, Shen et al. 2015; Votteler, Berrio et al. 2013). DAPI was used to visualize cell nuclei. Images were acquired using identical parameters and were processed with Photoshop CS5 (Adobe Systems, San Jose, CA, USA). For semi-quantification of the MF20 expression, we compared gray value intensities (GVI) of antibody-stained samples as previously described (Votteler, Berrio et al. 2013).

Antibodies

The following primary antibodies were used: rabbit IgG anti–Nanog (1:100; abcam; ab80892), rabbit IgG1 anti–Oct4 (1:200; abcam; ab19857), mouse IgG2b anti-sarcomeric myosin (MF20; 1:50; DSHB), mouse-IgG1 cardiac troponin T (cTNT; 1:200; abcam; ab8295), rabbit-IgG connexin 43 (CX43; 1:200; Santa Cruz; sc-6560-R), mouse IgG1 anti-β-catenin (1:50, Santa Cruz; sc7963), and rabbit IgG anti-cTNT (1:3000, Sigma-Aldrich; HPA015774).

The following secondary antibodies were used in this study: anti-rabbit-IgG-Alexa Fluor 488 (1:250; Life Technologies; A-11034), anti-mouse-IgG2b-Alexa Fluor 594 (1:250; Life Technologies; A-21145), anti-mouse-IgG1-Alexa Fluor 594 (1:250; Life Technologies; A-21125), anti-mouse-IgG1 Alexa Fluor 488 (1:250; Life Technologies; A-21121) and anti-rabbit-IgG Alexa Fluor 594 (1:250; Life Technologies; A-11037).

Imaging flow cytometry

All cells were detached using TrypLE™ and stained with Zombie Red™ dye (Biolegend, Fell, Germany) according to the manufactures instruction to exclude dead cells. Afterwards, cells were fixed and permeabilized with FOXP3 Fix/Perm Buffer Set (Biolegend) and incubated with the primary monoclonal mouse IgG anti-cTNT antibody (1:200; abcam) for 35 minutes at 4°C, followed by Alexa Fluor 647-conjugated goat anti-mouse IgG1 secondary antibody (1:500; Life Technologies) staining for 25 minutes at 4°C in the dark. To visualize the cell nucleus, cells were incubated with DAPI (0.5 µg/ml) solution for 15 minutes at room temperature in the dark. Per sample, 2 x 10^4 events were acquired with the ImageStream X Mark II (Merck KGaA, Darmstadt, Germany) utilizing a 60x objective. The analysis was performed using the IDEAS® image analysis software 6.1.

RNA isolation and quantitative PCR analysis

RNA was extracted from all samples using TRIzol (Sigma-Aldrich) as previously described (Hinderer, Shen et al. 2015). An RNA quality indicator (RQI) > 8 was used for cDNA synthesis and qPCR. A total amount of 1 µg RNA was used to synthesize cDNA utilizing the transcriptor first strand cDNA synthesis kit (Roche, Mannheim, Germany). qPCR was carried out using a QuantiTect SYBR Green PCR kit for mESCs and a QuantiFast SYBR Green PCR kit for hESCs (both Qiagen, Hilden, Germany). All procedures were performed as instructed by the manufacturer. The samples were normalized to the housekeeping gene *Gapdh* (mouse) or *Rplp0* (mouse) / *GAPDH* (human) or *RPLP0* (human). After normalization to the housekeeping gene, the samples were additionally normalized to CMs yield assessed via flow cytometry (FACS). For the quantification of the qPCR data, the $2^{-\Delta\Delta Ct}$ (2 to the power of minus Delta Delta CT) method was applied (Livak and Schmittgen 2001).

Calcium transient recordings

mESC-CMs and hESC-CMs were transferred to plastic bottom petri dishes (Ibidi, Martinsried, Germany) that were coated with 5 ng/ml fibronectin. The cells were allowed to attach and

then incubated with 1 µM of Ca520-AM dye (Biomol GmbH) and 0.02% Pluronic F-127 (Life Technologies) in MEM-alpha medium or STEMPRO 34-medium for 30 minutes at 37 ºC. Subsequently, cells were washed once, and dye-free MEM-alpha medium or STEMPRO 34-medium was added to mESC-CMs or hESC-CMs. The fluorescence intensity of Ca520-AM dye was measured using the Confocal LSM710 microscope with controlled temperature 37 ºC and 5% CO_2. Electrical field stimulation was applied to evoke Ca^{2+} transients at the stimulation frequencies of 3 Hz (hESC-CMs) or 2 Hz (hESC-CMs) using bipolar electrodes attached to an STG-2004 stimulator (Multi Channel Systems MCS, Germany). The stimuli varied between +/- 3-4.5 V with pulse widths of 3 ms. Caffeine was added at a final concentration of 10 mM. Images and fluorescence data were acquired in frame mode with the Zeiss software (Zen2.1, Carl Zeiss GmbH) and analyzed with Image-Fiji software (Wayne Rasband, National Institutes of Health, USA). The fluorescence signals were normalized to baseline fluorescence. Systolic and caffeine-induced Ca^{2+} transient duration (from peak amplitude until 90% return to base level, CaT_{90}), decay, amplitude, and slope were determined based on a previously published method (Kosmidis, Bellin et al. 2015).

MEA measurements and data analysis

hESC-CMs were dissociated using the Embryoid Body Dissociation Kit (Miltenyi, Germany) according to the manufacturer´s protocol. 6-well (60-6wellMEA200/30iR-Ti-rcr) and 96-well (96W700/100F-288) MEAs (Multi Channel Systems, Germany) were coated using Geltrex® (Life Technologies) at 4°C overnight. The seeding density was 2.5 x 10^4 cells/ electrode array. Medium was changed every second day. Spontaneously beating mESC-CMs were measured on day 8 after seeding. One hour prior to the experiment, a full medium change was performed. During all measurements, cells were kept at 37 °C and exposed to 5% CO_2. A wash-in phase of 5 min following a substance application was applied before the recordings. Data were analyzed using MC_Rack (Multi Channel Systems, V 4.6.2) or the Multiwell Analyzer (Multi Channel Systems, V 1.2.9.0). 2-min-recordings were averaged to obtain the fAPd (displayed in ms). The fAPd was measured as the time from the maximal deflection of the depolarizing spike to the peak of the repolarizing wave. Electrodes were selected for analysis based on the stability of the fAP waveform over the entire duration of the experiments. 10 Hz highpass filtering was used in some cases for complete experiments to help to localize the repolarization component. All data were normalized to the control´s value. To show variations between replications the standard error of the mean was used.

Isolation of primary CMs

.

Hearts of adult mice (8 months; strain: CD1) and E15.5 embryos (CD1) were provided by the Institute of Cellular Biology and Immunology at University of Stuttgart, Germany. In accordance with the institutional guidelines of animal ethics and care of the University of Stuttgart, appropriate surgeries were performed, and the hearts were kept in a Hank's Balanced Salt Solution (HBSS, Biochrome, Berlin Germany) prior further analyses. First trimester hearts from 8-10-week-old embryos were used in accordance with institutional guidelines and approved by the local research ethics committee at the University Hospital of the Eberhard Karls University Tübingen (IRB #356/2008BO2 and #406/2011BO1). The isolation of primary CMs from mouse and human tissues was performed as previously described (Brauchle, Knopf et al. 2016).

Raman microspectroscopy and analysis of Raman spectra

A custom-built Raman microspectroscope was used to acquire Raman spectra of the cells as previously described (Brauchle, Knopf et al. 2016). The medium was removed before the measurements and cells were maintained in DPBS. The cells were placed under the Raman microspectroscopy and visualized in the bright field using an F-View camera and Cell^B 2.4 software (both Olympus). To measure the mESC-CMs and hESC-CMs, spontaneously contracting cells were targeted to discriminate CMs from other cell phenotypes. Once a cell of interest was located, the laser beam was focused on the center of the cell and a Raman spectrum was recorded. Each measurement had an acquisition time of 100 seconds using 85 mW laser powers. For every 3-5 cells measured, a corresponding background spectrum was acquired in a cell-free area at the same focal plane. 30-60 spectra were measured for each sample.

Spectral processing and principal component analysis

The raw Raman spectra were loaded into OPUS (OPUS® 4.2 Bruker Optics, Billerica, MA, USA) to remove cosmic ray interferences manually and to subtract the background from each sample spectrum. A baseline correction (128-baseline point rubberband method, OPUS) was also performed to correct background shifts throughout the spectra. The background-corrected spectra were further smoothed to increase the signal-to-noise ratio (5-smoothing point Savitzky-Golay method, OPUS). The spectra were then imported to Unscrambler®X (Unscrambler®X 10.2, CAMO, Oslo, Norway). All Raman spectra were normalized using vector normalization (Unscrambler®) to correct system-induced intensity variations between spectra. Additional details on these pre-processing steps were previously described in detail (Brauchle, Knopf et al. 2016). As vector-normalized spectra have

comparable total intensities, different samples can be objectively compared without acquisition variations. The background-corrected, vector-normalized Raman spectra were analyzed using PCA. Seven successive PCAs were calculated as described previously to visualize the differences between phenotypes (Brauchle, Knopf et al. 2016).

Supplemental Figures

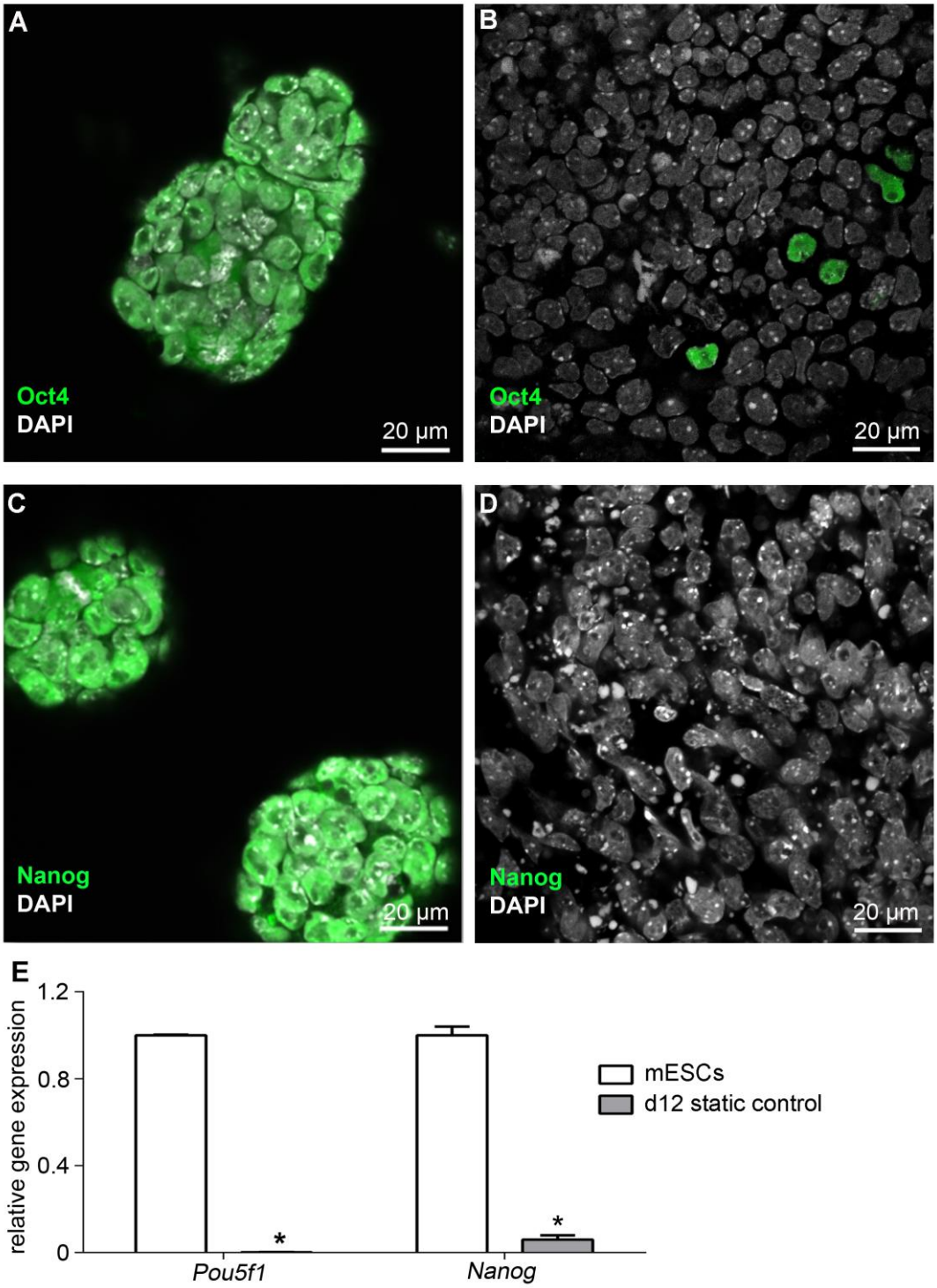

Figure S1. Characteristics of pluripotency in mESCs, and loss of the pluripotency markers after 12 days in culture. Nanog (green) and DAPI (white) images of (A) undifferentiated mESCs and (B) cells after exposure to d12 static conditions. Oct4 (green) and DAPI (white) images of (C) undifferentiated mESCs and (D) cells after exposure to d12

.

static conditions. (E) Expression of pluripotency-associate genes (*Pou5f1* and *Nanog*) encoding in mESCs and cells after exposure to d12 static conditions. * $p < 0.05$ versus mESCs. All gene expression data was normalized to *Gapdh* and undifferentiated mESCs. n=3 for all the experiments in this figure. Error bars show standard deviation.

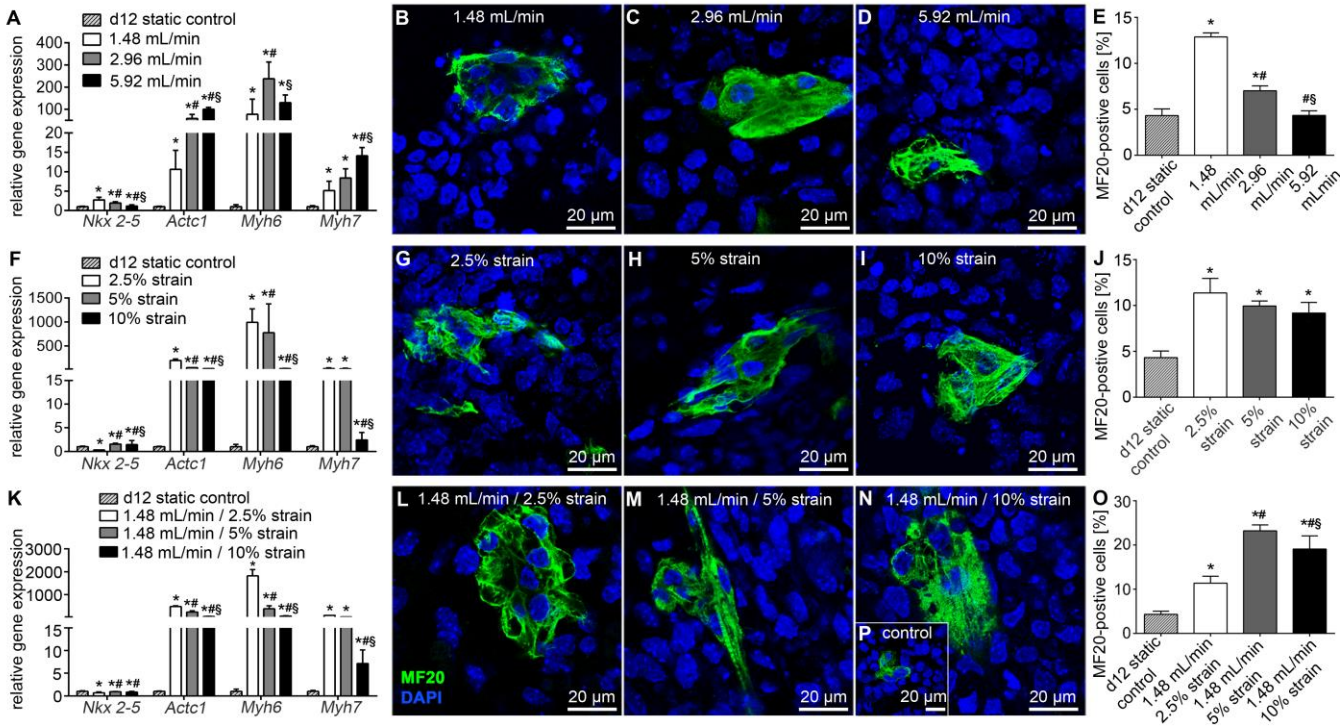

Figure S2. Mechanical stimuli induce cardiac differentiation and maturation in mESC-derived cells after 12 days of culture. ***Related to Figure 2.*** (A) Expression of cardiac genes (*Nkx2-5, Actc1, Myh6* and *Myh7*) in mESC-derived cells cultured under flow or static conditions. * $p < 0.05$ versus d12 static conditions, # $p < 0.05$ versus 1.48 mL/min, § $p < 0.05$ versus 2.96 mL/min. MF20 (green) and DAPI (blue) staining of d12 mESC-derived cells cultured under different medium flow rates: (B) 1.48 mL/min, (C) 2.96 mL/min and (D) 5.92 mL/min. (E) Percentage of $MF20^+$ cells in flow or static conditions. * $p < 0.05$ versus d12 static conditions, # $p < 0.05$ versus 1.48 mL/min, § $p < 0.05$ versus 2.96 mL/min. (F) Expression of cardiac genes in mESC-derived cells that were cultured under strain or static conditions. * $p < 0.05$ versus d12 static conditions, # $p < 0.05$ versus 2.5% strain, § $p < 0.05$ versus 5% strain. MF20 (green) and DAPI (blue) staining of mESC-derived cells cultured under exposure to different strains: (G) 2.5 %, (H) 5 % and (I) 10 %. (J) Percentage of $MF20^+$ cells cultured under strain or static conditions. * $p < 0.05$ versus d12 static conditions, # $p < 0.05$ versus 2.5% strain, § $p < 0.05$ versus 5% strain. (K) Expression of cardiac genes in mESC-derived cells that were cultured under the combination of flow and strain or static conditions. * $p < 0.05$ versus d12 static conditions. MF20 (green) and DAPI (blue) staining of mESC-derived cells cultured with exposure to 1.48 mL/min flow and (L) 2.5 % strain, (M) 5 % strain and (N) 10 % strain. (O) Percentage of $MF20^+$ cells cultured combining flow and strain conditions or static conditions. * $p < 0.05$ versus d12 static conditions, # $p < 0.05$ versus 1.48 mL/min/ 2.5 % strain, § $p < 0.05$ versus 1.48 mL/min/ 5 % strain. (P) MF20 (green) and

DAPI (blue) staining of d12 static controls. Gene expression data were normalized to *Gapdh* and the static controls. n=3 for all the experiments in this figure. All error bars displayed in this figure represent the standard deviation.

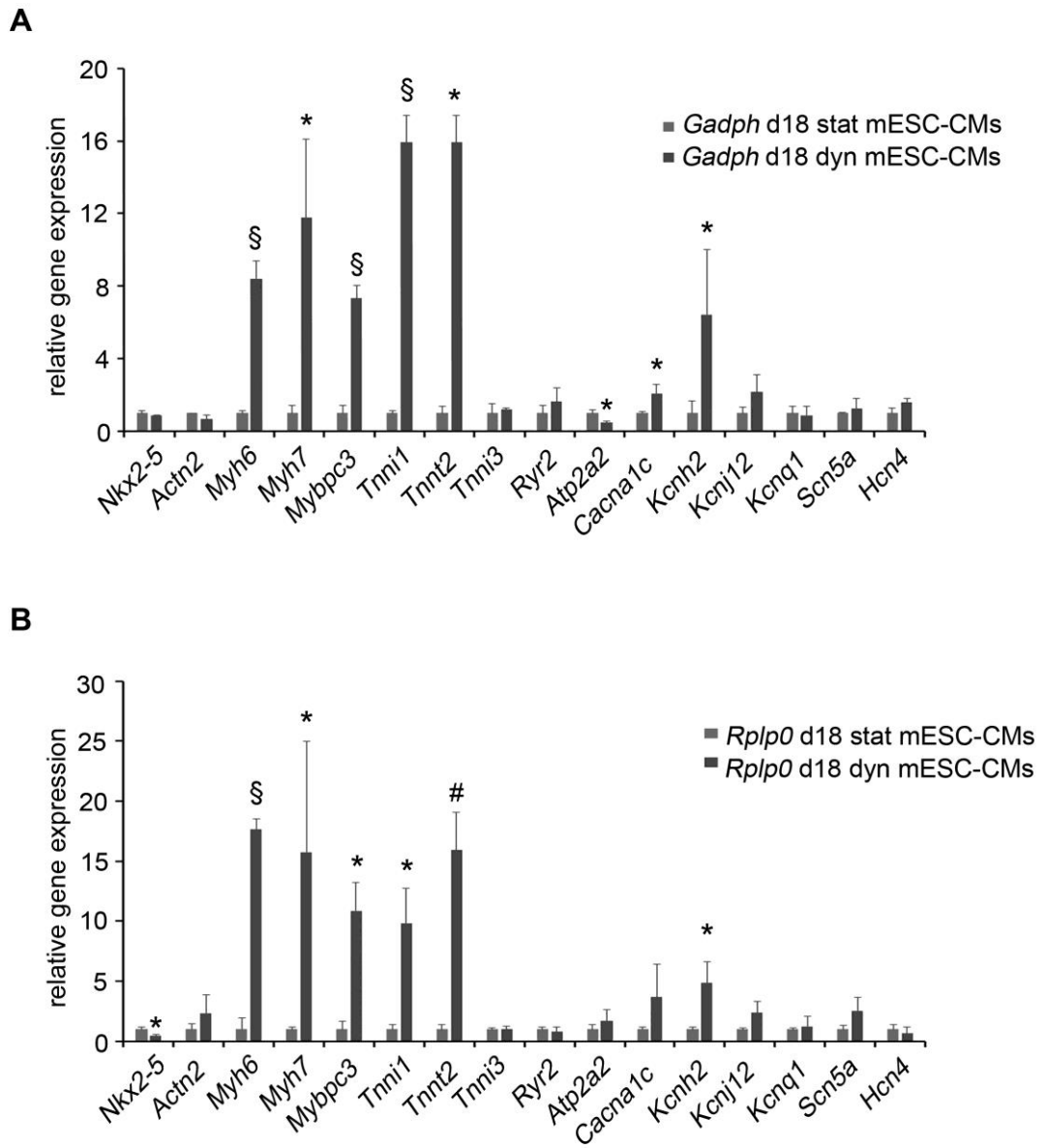

Figure S3. Quantification of the relative gene expression in d18 stat mESC-CMs and d18 dyn mESC-CMs. ***Related to Figure 2.*** Expression of cardiac-associated markers (*Nkx2-5, Actn2, Myh6, Myh7, Mybpc3, Tnni1, Tnnt2, and Tnni3*), calcium handling channels (*Ryr2, Atp2a2, Cacna1c*), and membrane ion channels (*Kcnh2, Kcnj12, Kcnq1, Scn5a,* and *Hcn4*) normalized to housekeeping gene *Gapdh* (A) and *Rplp0* (B), and average percentage of mESC-CMs assessed via FACS. * $p < 0.05$, # $p < 0.01$, and § $p < 0.001$ versus d18 stat mESC-CMs. n=3 for all the experiments in this figure. All error bars displayed in this figure represent the standard deviation.

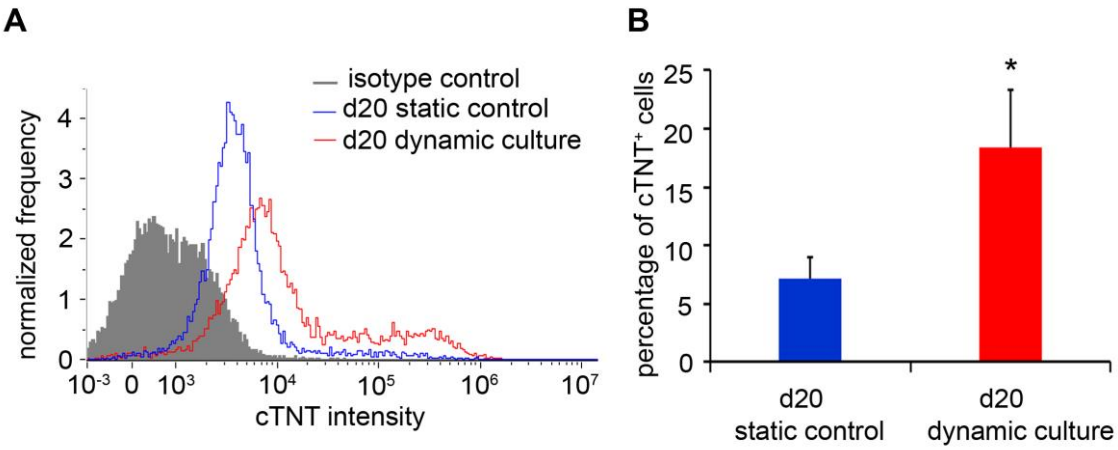

Figure S4. Assessment of hESC cardiac differentiation efficiency after 20 days. ***Related to Figure 5.*** (A) Histogram of cTNT$^+$ cells in d20 static controls (blue; n=8,479 cells) and d20 dynamic cultures (red; n=7,562 cells). Isotype control is shown in grey (n=7,727 cells). (B) The average percentage of cTNT$^+$ cells in d20 static controls and dynamic cultures. * $p < 0.05$ versus d20 static control, n=3. Error bars show the standard deviation.

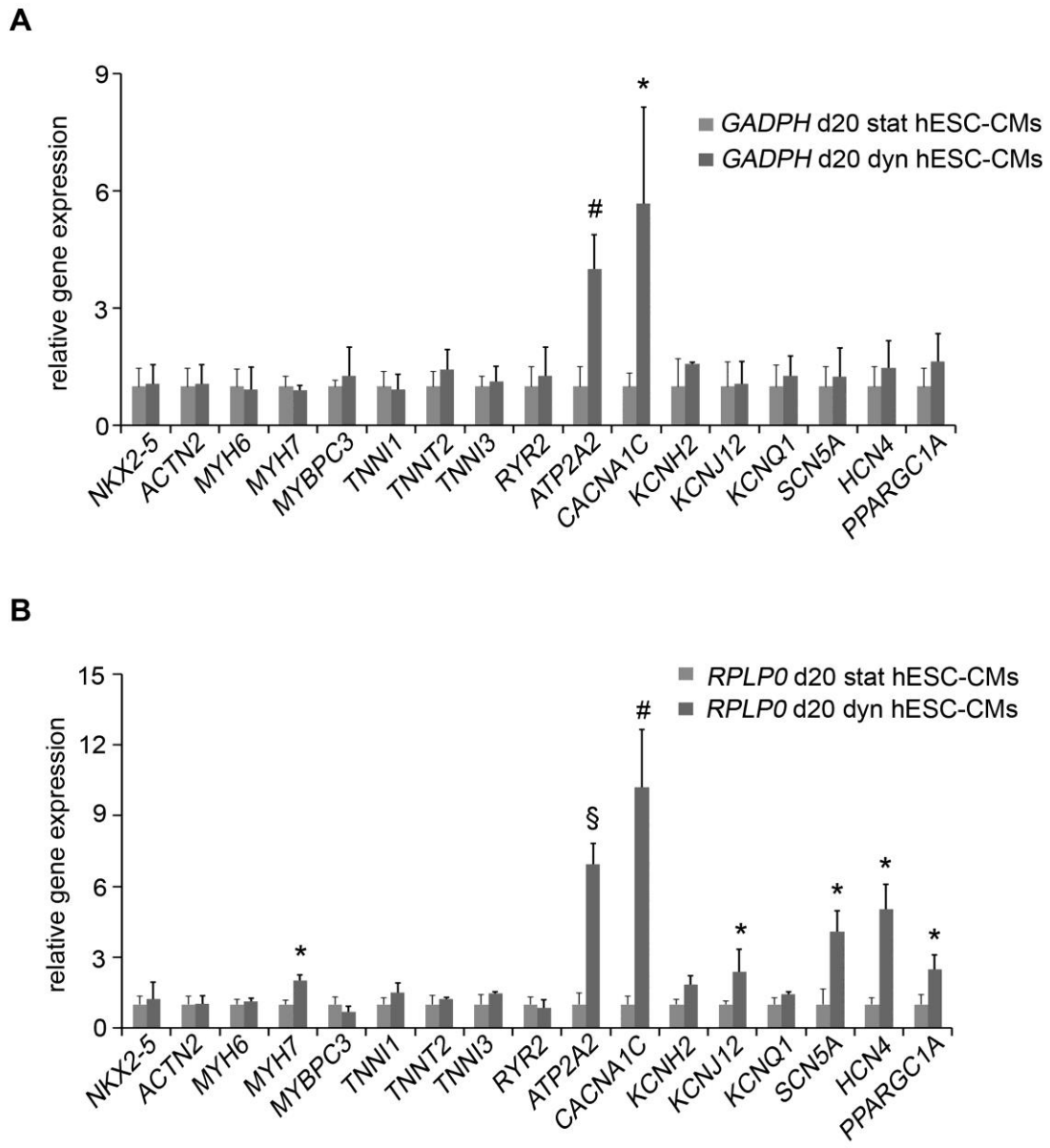

Figure S5. Quantification of the relative gene expression in d20 stat hESC-CMs and d20 dyn hESC-CMs. ***Related to Figure 5.*** Expression of cardiac-associated markers (*NKX2-5, ACTN2, MYH6, MYH7, MYBPC3, TNNI1, TNNT2, TNNI3*), calcium handling channels (*RYR2, ATP2A2, CACNA1C*), membrane ion channels (*KCNH2, KCNJ12, KCNQ1, SCN5a,* and *HCN4*) and the mitochondrial master regulator (*PPARGC1A*) normalized to housekeeping gene (A) *GAPDH* and (B) *RPLP0*, and average percentage of hESC-CMs assessed via FACS (n = 3). * $p < 0.05$, # $p < 0.01$, and § $p < 0.001$ versus d20 stat hESC-CMs. n=3 for all the experiments in this figure. All error bars displayed in this figure represent the standard deviation.

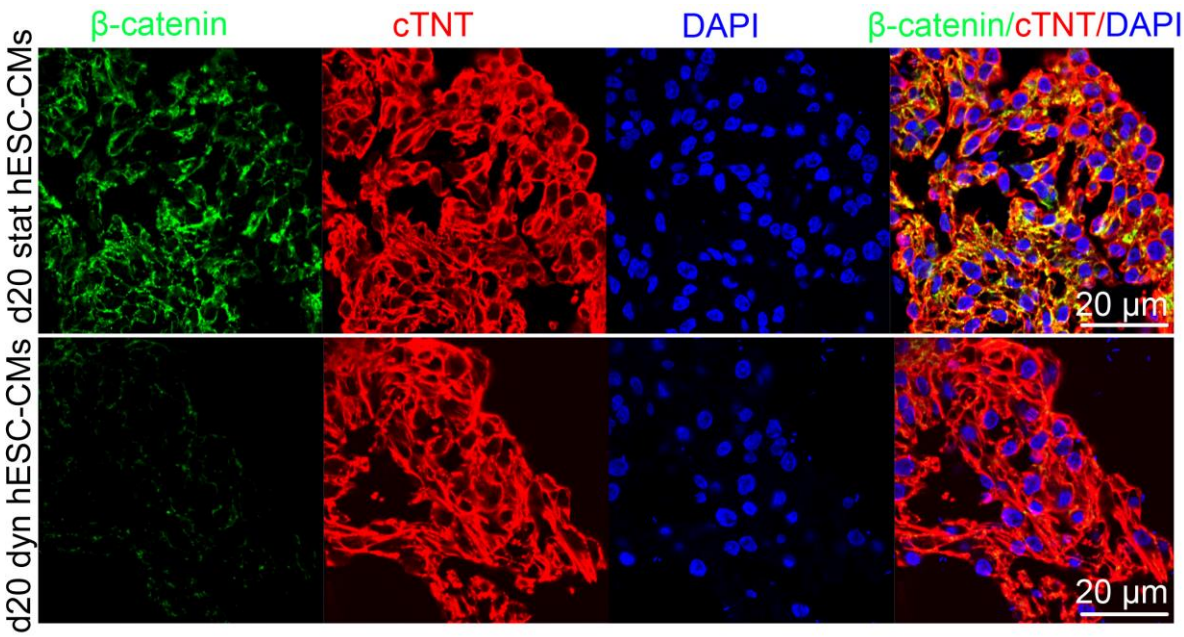

Figure S6. Expression of β-catenin in hESC-CMs. ***Related to Figure 5.*** β-catenin (green), cTNT (red), and DAPI (blue) in d20 stat hESC-CMs and d20 dyn hESC-CMs. β-catenin/cTNT/DAPI represents an overlay. Scale bars equal 20 μm.

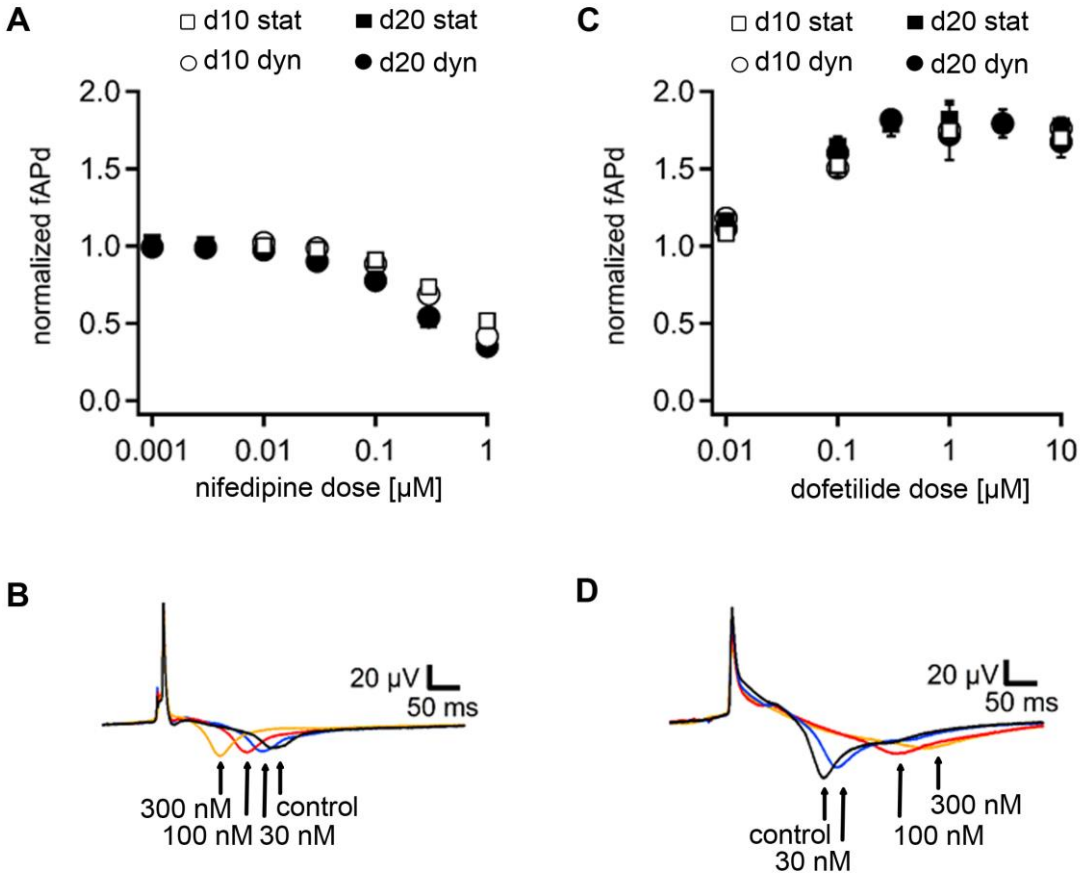

Figure S7. Pharmacological profiling of hESC-CMs. ***Related to Figure 6.*** (A) Concentration-response relationship for the specific L-type Ca^{2+} channel inhibitor nifedipine. n=10. (B) Superposition of exemplary traces for fAPds of hESC-CMs exposed to cumulative concentrations of nifedipine obtained from one recording. fAPd decreases with increasing channel inhibition. Control (black), 30 nM (blue), 100 nM (red) and 300 nM (yellow) nifedipine. Depolarizing voltage deflection is cut for displaying reasons. (C) Concentration-response relationship for the potent hERG channel inhibitor dofetilide. n=12. (D) Superposition of exemplary traces for fAPds of hESC-CMs exposed to dofetilide. fAPd prolongs with increasing exposition to dofetilide. Control (black), 30 nM (blue), 100 nM (red) and 300 nM (yellow) dofetilide. Arrows indicate the repolarization phase. Error bars are not visible if smaller than the data point symbol. All error bars displayed in this figure represent the standard error of the mean.

Supplemental Table

Table S1: RT-qPCR primers used in this study. *Related to Figures 2 and 5.*

Primers	Gene names
Mm_Nanog_2_SG QuantiTect Primer Assay. Cat.N./ID: QT01076334	*Nanog*
Mm_Pou5f1_1_SG QuantiTect Primer Assay. Cat.N./ID: QT00109186	*Pou5f1*
Mm_Nkx2-5_1_SG QuantiTect Primer Assay. Cat.N./ID: QT00124810	*Nkx2-5*
Mm_Actc1_1_SG QuantiTect Primer Assay. Cat.N./ID: QT00322434	*Actc1*
Mm_Myh6_SG QuantiTect Primer Assay. Cat.N./ID: QT00160902	*Myh6*
Mm_Myh7_1_SG QuantiTect Primer Assay. Cat.N./ID: QT01051813	*Myh7*
Mm_Actn2_1_SG QuantiTect Primer Assay. Cat.N./ID: QT00122157	*Actn2*
Mm_Mybpc3_1_SG QuantiTect Primer Assay. Cat.N./ID: QT00105693	*Mybpc3*
Mm_Tnni1_1_SG QuantiTect Primer Assay. Cat.N./ID: QT00124012	*Tnni1*
Mm_TNNT2_1_SG QuantiTect Primer Assay. Cat.N./ID: QT01052982	*Tnnt2*
Mm_Tnni3_1_SG QuantiTect Primer Assay. Cat.N./ID: QT01077657	*Tnni3*
Mm_Ryr2_1_SG QuantiTect Primer Assay. Cat.N./ID: QT00149121	*Ryr2*
Mm_Atp2a2_1_SG QuantiTect Primer Assay. Cat.N./ID: QT00077231	*Atp2a2*
Mm_Cacna1c_1_SG QuantiTect Primer Assay. Cat.N./ID: QT00150752	*Cacna1c*
Mm_Kcnh2_1_SG QuantiTect Primer Assay. Cat.N./ID: QT00105574	*Kcnh2*
Mm_Kcnj12_1_SG QuantiTect Primer Assay. Cat.N./ID: QT00101451	*Kcnji2*
Mm_Kcnq1_1_SG QuantiTect Primer Assay. Cat.N./ID: QT00171115	*Kcnq1*
Mm_Scn5a_1_SG QuantiTect Primer Assay. Cat.N./ID: QT00126714	*Scn5a*
Mm_Hcn4_1_SG QuantiTect Primer Assay. Cat.N./ID: QT00268660	*Hcn4*
Mm_Gapdh_3_SG QuantiTect Primer Assay. Cat.N./ID: QT01658692	*Gapdh*
Mm_Rplp0_1_SG QuantiTect Primer Assay. Cat.N./ID: QT00249375	*Rplp0*
Hs_NKX2-5_1_SG QuantiTect Primer Assay. Cat.N./ID: QT00010619	*NKX2-5*
Hs_ACTN2_1_SG QuantiTect Primer Assay. Cat.N./ID: QT00082131	*ACTN2*
Hs_MYH6_1_SG QuantiTect Primer Assay. Cat.N./ID: QT00030807	*MYH6*
Hs_MYH7_1_SG QuantiTect Primer Assay. Cat.N./ID: QT00000602	*MYH7*
Hs_MYBPC3_1_SG QuantiTect Primer Assay. Cat.N./ID: QT00093919	*MYBPC3*
Hs_TNNI1_1_SG QuantiTect Primer Assay. Cat.N./ID: QT00043890	*TNNI1*
Hs_TNNT2_1_SG QuantiTect Primer Assay. Cat.N./ID: QT00089782	*TNNT2*
Hs_TNNI3_1_SG QuantiTect Primer Assay. Cat.N./ID: QT00084917	*TNNI3*
Hs_RYR2_1_SG QuantiTect Primer Assay. Cat.N./ID: QT00018368	*RYR2*
Hs_ATP2A2_1_SG QuantiTect Primer Assay. Cat.N./ID: QT00077231	*ATP2A2*
Hs_CACNA1C_1_SG QuantiTect Primer Assay. Cat.N./ID: QT00053480	*CACNA1C*

Hs_KCNH2_2_SG QuantiTect Primer Assay. Cat.N./ID: QT01003254	*KCNH2*
Hs_KCNJ12_1_SG QuantiTect Primer Assay. Cat.N./ID: QT01003296	*KCNJ12*
Hs_KCNQ1_1_SG QuantiTect Primer Assay. Cat.N./ID: QT00016065	*KCNQ1*
Hs_SCN5A_1_SG QuantiTect Primer Assay. Cat.N./ID: QT00091812	*SCN5A*
Hs_HCN4_1_SG QuantiTect Primer Assay. Cat.N./ID: QT00038108	*HCN4*
Hs_PPARGC1A_1_SG QuantiTect Primer Assay. Cat.N./ID: QT00095578	*PPARGC1A*
Hs_GAPDH_2_SG QuantiTect Primer Assay. Cat.N./ID: QT01192646	*GAPDH*
Hs_RPLP0_2_SG QuantiTect Primer Assay. Cat.N./ID: QT01839887	*RPLP0*

Supplemental References

Brauchle, E., Knopf, A., Bauer, H., Shen, N., Linder, S., Monaghan, M. G., Ellwanger, K., Layland, S. L., Brucker, S. Y., Nsair, A., et al. (2016). Novel non-invasive identification of chamber specific cardiomyocytes in differentiating pluripotent stem cells. Stem Cell Reports *6*, 188-199.

Hinderer, S., Shen, N., Ringuette, L. J., Hansmann, J., Reinhardt, D. P., Brucker, S. Y., Davis, E. C., and Schenke-Layland, K. (2015). In vitro elastogenesis: instructing human vascular smooth muscle cells to generate an elastic fiber-containing extracellular matrix scaffold. Biomed Mater *4,* 2326-2341.

Kosmidis, G., Bellin, M., Ribeiro, M. C., van Meer, B., Ward-van Oostwaard, D., Passier, R., Tertoolen, L. G. J., Mummery, C. L., and Casini, S. (2015). Altered calcium handling and increased contraction force in human embryonic stem cell derived cardiomyocytes following short term dexamethasone exposure. Biochem Biophys Res Commun *467*, 998-1005.

Livak, K.J., and Schmittgen, T.D. (2001). Analysis of relative gene expression data using real-time quantitative PCR and the 2(-Delta Delta C(T)) Method. Methods *25*, 402-408.

Votteler, M., Berrio, D. A. C., Horke, A., Sabatier, L., Reinhardt, D. P., Nsair, A., Aikawa, E., and Schenke-Layland, K. (2013). Elastogenesis at the onset of human cardiac valve development. Development *140*, 2345-2353.

Appendix II: Shen et al. 2016

CHAPTER 5

Scaffold and Biomechanical Transductive Approaches to Elastic Tissue Engineering

Nian Shen, Svenja Hinderer, and
Katja Schenke-Layland

CONTENTS

5.1 INTRODUCTION

Elastin-containing elastic fibers are one of the main components of the extracellular matrix (ECM), endowing dynamic tissues such as lungs, skin, blood vessels, heart valve leaflets, and ligaments with flexibility and elasticity. Previous research efforts suggest that poor recruitment and cross-linking of elastin precursors as well as the need to organize the matrix into functional structures are the main limitations when aiming to develop a tissue-engineered elastic matrix. Scaffolds that mimic the cellular microenvironment in vitro can either be designed to recapitulate the elastic properties of the native ECM or they can be used to induce cell-mediated elastic fiber assembly. Applying defined biophysical signals to further mimic physiological parameters is another potential solution to induce elastic fiber formation and maturation. This chapter provides an overview of scaffolds and biomechanical approaches in elastic matrix engineering and discusses recent advances and prospects for the application of these two strategies.

5.2 SCAFFOLDS IN TISSUE ENGINEERING

Tissue-engineered constructs are generated using cells, biomolecules, and biomaterial scaffolds and aim to support, replace, or regenerate damaged tissues and organs. The scaffolds are designed to provide a three-dimensional (3D), ECM mimicking microenvironment, where cells can attach, migrate, proliferate, and differentiate (Schenke-Layland et al. 2011). Rat aortic smooth muscle cells for example showed an increased proliferation on 3D electrospun scaffolds when compared with two-dimensional (2D) controls (Bashur and Ramamurthi 2011a). It has previously been demonstrated that mechanical properties such as strength, stiffness, and elasticity also significantly impact cell behavior (Kim et al. 2012, Hopkins et al. 2013). Mesenchymal stem cells are able to differentiate into neural, myogenic, or osteogenic tissue when cultured on 3D hydrogels with a stiffness of 0.1, 11, or 34 kPa, respectively (Kim et al. 2012). Therefore, the choices of material as well as the selection of an adequate fabrication method are important parameters in scaffold design.

5.2.1 Scaffolds with Elastic Properties

Scaffolds used for in vivo applications need to resist mechanical forces including high pressure, tension, and compression. Especially in the field of cardiovascular or skin tissue engineering, resilient and highly

elastic scaffolds are desired. Therefore, various synthetic and natural polymers have been used in order to generate scaffolds with elastic properties. The degradable elastomer poly(glycerol sebacate) (PGS) has been intensively studied for tissue engineering applications (Chen et al. 2008, Masoumi et al. 2014, Jeffries et al. 2015). To generate 3D PGS scaffolds, processing methods such as electrospinning, foaming, and sheet-forming techniques have been investigated. Interestingly, it has been described that electrospun fibrous PGS shows a higher tensile strength compared to porous PGS foams (Jeffries et al. 2015). Masoumi et al. identified microfabricated PGS in combination with electrospun poly-ε-caprolactone (PCL) as a suitable scaffold to replace heart valves (Masoumi et al. 2014).

Because elastin is a major component of elastic fibers, many studies focus on elastin- or tropoelastin-containing scaffolds. Electrospinning of recombinant tropoelastin with PCL results in a scaffold that matches the mechanical properties of the internal mammary artery (Wise et al. 2011). Other technologies to generate elastic scaffolds with elastin are freeze-drying (Chen et al. 2013) or hydrogel formation (Tu et al. 2010). Tu et al. described an elegant hydrogel-forming method where tropoelastin monomers coalesce and form a porous elastic hydrogel after further chemical cross-linking (Tu et al. 2010).

Elastin is an interesting natural biomaterial, because it exhibits non-thrombogenic properties (Waterhouse et al. 2011). Accordingly, an elastin coating of synthetic scaffolds is highly attractive in order to increase cell adhesion and proliferation (Barenghi et al. 2014). Another material investigated for tissue engineering applications are elastin-like peptides (ELPs). ELPs are engineered biopolymers that contain elastin-based repeat motifs. For tissue engineering applications, they are commonly used in combination with other biomaterials (Yeo et al. 2015). For example, reduced platelet adhesion has been determined in vascular grafts composed of ELPs and collagen (Kumar et al. 2013). In another study, the addition of ELPs to collagen hydrogels significantly increased the tensile strength and the elastic modulus of these hydrogels (Boccafoschi et al. 2015). So far, promising results were obtained by using elastic natural and synthetic 3D scaffolds for tissue engineering. Although it is possible to adjust material properties using different materials and different scaffold fabrication techniques, much more research is necessary in order to completely recapitulate the mechanical and biochemical properties of the native ECM.

5.2.2 Elastic Fibers in Tissue-Engineered Constructs

Recombinant elastin and ELPs were successfully used to generate elastic scaffolds; however, due to the absence of microfibrillar components and elastic fiber-associated proteins, these scaffolds are not able to provide biological stimuli like the native ECM (Bashur et al. 2012). Thus, there is a high interest in developing scaffolds and scaffold fabrication methods that enable elastin synthesis and cell-mediated matrix assembly in tissue-engineered constructs (Bashur et al. 2012). Elastic fibers play a major role in normal tissue development (Votteler et al. 2013) and contribute to approximately 30%–50% of the ECM dry weight of vascular tissues (Bashur et al. 2012). In vitro elastin deposition has been described in 2D cell cultures using neonatal or adult rat vascular smooth muscle cells (SMCs) or human neonatal fibroblasts (Hirai et al. 2007, Kothapalli et al. 2009, Noda et al. 2013). There are also strategies to generate elastic fibers in 3D tissue-engineered constructs, such as decellularized scaffolds or synthetic and natural hydrogel. For example, Keire et al. generated scaffolds using rat arterial SMCs in combination with the cell-sheet technology. Interestingly, not only tropoelastin and elastin-associated protein and gene expression were observed, but also desmosine cross-links, indicating maturation of elastic fibers (Keire et al. 2009). Furthermore, hyaluronic acid (HA)-based scaffolds have been prepared and cultured with rat aortic SMCs in order to induce elastogenesis. A significant upregulation of elastin-stabilizing desmosine cross-links was determined in this study (Joddar and Ramamurthi 2006b). HA seems to be an interesting biomaterial or biomaterial modification agent when aiming for robust cell-mediated elastic matrix deposition. High molecular weight HA stimulates and enhances elastin precursor recruitment and deposition as a matrix through largely electrostatic interactions, whereas the introduction of smaller HA molecules leads to an increased tropoelastin synthesis (Joddar and Ramamurthi 2006a, Joddar et al. 2007). Although there are some approaches using animal-derived cells to generate mature elastic fibers in 3D tissue-engineered constructs, the generation of human-based elastic matrix still remains challenging. Various human studies show (tropo-)elastin upregulation on both, the RNA and protein level (Sommer et al. 2013); however, detailed information on elastic fiber assembly, cross-linking, or maturation is commonly missing. Hinderer et al. used a fibrous and porous polymeric HA-coated scaffold composed of poly(L-lactide) (PLA) and

poly(ethylene glycol) dimethacrylate (PEGdma) and seeded human vascular SMCs to induce elastic matrix assembly. Ultrastructural analysis after a dynamic culture revealed microfibril formation as well as elastin deposition (Hinderer et al. 2015). Despite these promising results, developing a tissue-engineered elastic fiber-containing matrix with an appropriate size for clinical use is still an unmet challenge in the field (Bashur et al. 2012).

5.3 BIOMECHANICAL TRANSDUCTION STRATEGIES TOWARD ELASTIC TISSUE ENGINEERING

Previous research efforts suggest that the main limitations to growing elastic tissues in vitro are poor recruitment and cross-linking of elastin precursors and the need to organize the matrix into functional structures (Opitz et al. 2004, Zhang et al. 2009, Bashur and Ramamurthi 2011b, Bashur et al. 2012). These challenges have been addressed via multiple approaches (Kim et al. 1999, Iwasaki et al. 2008, Lee et al. 2011, Lin et al. 2011, Bashur et al. 2012). As discussed before, the scaffold, which provides a 3D microenvironment to the cells, is one potential solution to induce mature elastic fiber formation while at the same time serving to direct the orientation of elastic matrix structures (Patel et al. 2006, Lin et al. 2011). Biomechanical transduction of SMCs and fibroblasts via the application of mechanical stimuli has been shown to modulate the synthesis of almost all major components of the ECM, including elastin, collagen, glycosaminoglycans, proteoglycans, glycoproteins, and various soluble proteins such as growth factors during development and disease (Choe et al. 2006, Gupta and Grande-Allen 2006, Boccafoschi et al. 2013). This section will focus on induction of elastogenesis using biomechanical cues.

5.3.1 Signaling Pathways Activated by Mechanotransduction in Cells

Several biological components, such as ion channels, intergrins, and cell surface receptors, have been proposed to act as cellular mechanosensors and are depicted schematically in Figure 5.1. Such mechanosensors activate signaling pathways, which in turn activate transcription factors and modulate the expression of mechanosensitive genes (Brosig 2011). Many cells and organs are exposed to at least one of these mechanical stimuli: shear stress, stretch, compression, or tension. In general, external stimuli can impact cellular behavior (Brosig 2011, Huang et al. 2004). For example, cardiac cells adapt to high strain by increasing

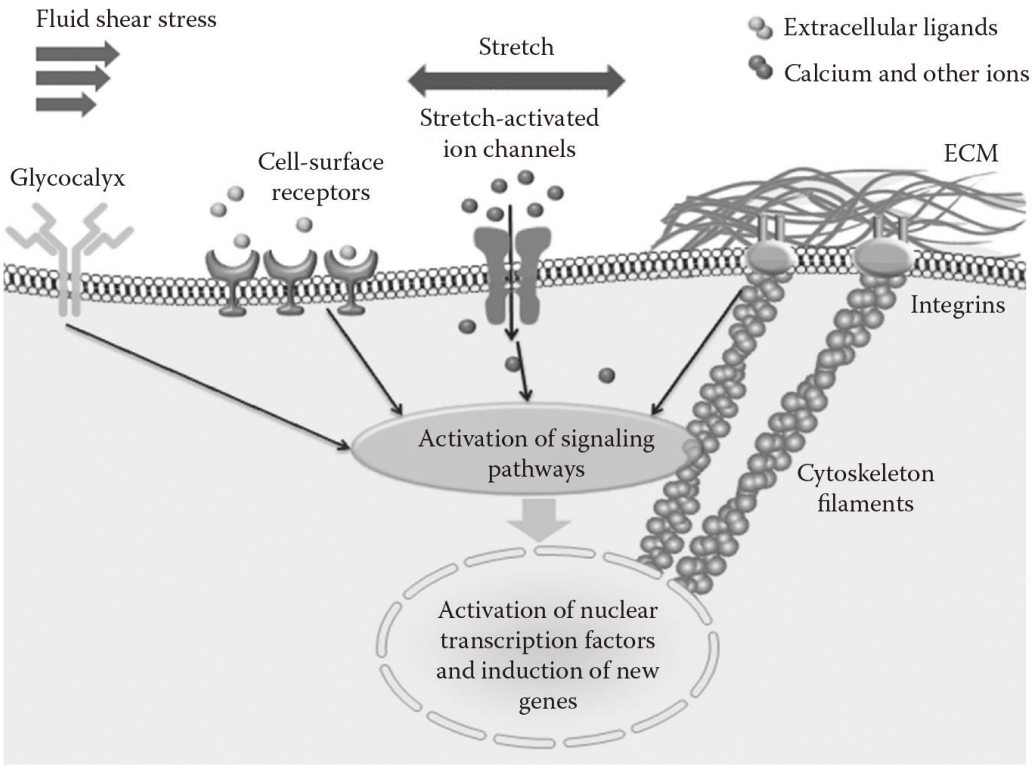

FIGURE 5.1 Schematic depiction of how cells are exposed to various types of mechanical stimuli by their local environment.

their cell size and modifying their surrounding ECM (Huang et al. 2004, Jaalouk and Lammerding 2009). Mechanotransduction is the transduction of mechanical stimuli into biochemical signals, which is crucial for normal organ development and the maintenance of tissues that are under permanent mechanical stress (Jaalouk and Lammerding 2009). As depicted in Figure 5.1, several components such as ion channels, cell surface receptors, and cell adhesion molecules can act as mechanosensors that transmit mechanical changes of the environment to the cell (Haga et al. 2007, Jaalouk and Lammerding 2009, Brosig 2011, Shi and Tarbell 2011). Cells, including SMCs and fibroblasts, respond directly to stretch by opening stretch-activated ion channels in the membranes and allowing the transport of calcium and other ions (Jaalouk and Lammerding 2009). Stretching of cells activates a nonselective cation channel, which is permeable to K^+, Na^+, and Ca^{2+} (Davis et al. 1992). It leads to the activation of the phosphatidylinositol 3 kinase (PI3K)–protein kinase B (Akt) signal transduction pathway (Haga et al. 2003) and p21 (Ras)/extracellular signal regulated kinases

1/2 (ERK1/2) signaling pathway (Iwasaki et al. 2000). Activating these signaling pathways further regulates cell proliferation and apoptosis (Iwasaki et al. 2003). In addition to ion channels, integrins and integrin-associated proteins as well as cell-surface receptors play a significant role in response to mechanotransduction mediated by stretch (Haga et al. 2007, Jaalouk and Lammerding 2009, Qiu et al. 2013). Integrins interact with specific ECM proteins with a variety of focal adhesion kinase (FAK) and tyrosine-protein kinase (c-Src) proteins, which regulate the cell functions via Ras homolog gene family, member A (RhoA)/Rho-associated protein kinase (ROCK) signaling pathway (Gambillara et al. 2008). Additionaly, activated integrins can lead to the initiation of mitogen-activated kinase pathway (MAPK) via FAK and activate nuclear factor-kappaB (NF-κB) and p53 (Wernig et al. 2003, Zampetaki et al. 2005, Qiu et al. 2013). The receptor tyrosine kinase is also involved in mechanotransduction (Katsumi et al. 2004). Stretching of cells induces a rapid phosphorylation of platelet-derived growth factor (PDGF) receptor alpha and epidermal growth factor (EGF) receptor (Hu et al. 1998, Balestreire and Apodaca 2007, Qiu et al. 2013). As a direct response, intracellular ERK1/2 signaling pathway is triggered to regulate ECM synthesis and cell proliferation (Lehoux et al. 2006, Qiu et al. 2013). Nevertheless, it has to be noticed that mechanical stimuli often activate multiple signaling pathways at once. It is rather difficult to perform research on one specific pathway, because signaling pathways can have significant overlap and crosstalk (Jaalouk and Lammerding 2009).

Similar to stretch, ion channels (Ca^{2+} and other ion channels), cell surface receptors, and cell adhesion molecules act as cell mechanosensors when the cells are exposed to fluid shear stress (Chen et al. 1999, Haga et al. 2007, Jaalouk and Lammerding 2009, Shi and Tarbell 2011). It has been reported that exposure to shear stress activates multiple cellular signaling pathways including MAPK, calcium, and Ras/Rho and Akt signaling (Zampetaki et al. 2005, Ingber 2006, Shi and Tarbell 2011). The activation of these pathways controls cell proliferation, migration, apoptosis, and ECM synthesis (Huang et al. 2004, Jaalouk and Lammerding 2009, Shi and Tarbell 2011). Specifically the surface protein glycocalyx can sense fluid shear stress (Kang et al. 2011). The glycocalyx plays a dominant role in controling SMC contraction in vitro and modulating the SMC phenotype by amplifying interstitial flow-mediated mechanotransduction (Kang et al. 2011, Shi and Tarbell 2011).

5.3.2 Impact of Mechanical Signals on Elastogenesis Using Vascular SMCs

Bioreactors have been employed to expose cells to defined mechanical signals in vitro that can mimic the biophysical in vivo environment. There has been an increasing interest in using bioreactor systems to promote elastogenesis in vascular SMC cultures due to its importance for vascular tissue engineering (Patel et al. 2006). Table 5.1 summarizes studies that have been performed utilizing SMCs for elastic fiber formation. In general, applying mechanical forces to SMCs leads to an increased collagen and elastin synthesis (Howard et al. 1998, Gupta and Grande-Allen 2006, Gao et al. 2008, Venkataraman et al. 2014). These responses are highly dependent on parameters such as flow rate, strain magnitude, frequency, and duration (Gupta and Grande-Allen 2006, Gao et al. 2008, Venkataraman et al. 2014). Sumpio et al. seeded porcine SMCs in a flexible culture well and exposed them to high strains (25%) at 0.05 Hz. As a result, a significant increase in total protein and collagen synthesis was detected after 5 days (Sumpio et al. 1988). Another study showed an increased elastin and collagen synthesis by applying 20% strain for 4 to 14 days on rat aortic SMCs (Kim et al. 1999). Additionally, long-term application (4–20 weeks) of cyclic strains upregulated elastin and collagen gene expression. However, it has to be noticed that an extremely high strain can also lead to vascular SMC apoptosis via the endothelin B receptor, which is located in the cell membrane (Cattaruzza et al. 2000). Venkataraman et al. applied a low cyclic strain (2.5%) between 0.5, 1.5, and 3 Hz to human vascular SMCs. The authors determined a significant increase in elastin mRNA expression and total matrix secretion after 21 days of culture when using a frequency of 1.5 Hz (Venkataraman et al. 2014). Although strain was used as one of the important parameters to induce elastin synthesis, many groups did not consider the effect of shear stress due to the fact that vascular SMCs are not directly exposed to the blood flow in vivo. However, Shi and Tarbell demonstrated that shear forces experienced by endothelial cells (ECs) in blood vessels can be transferred to the underlying SMCs (Shi and Tarbell 2011). Furthermore, SMCs are exposed to interstitial flow, which is driven by the transvascular pressure (Figure 5.2). It was estimated that the transmural interstitial shear stress on SMCs is approximately 1 dyne/cm^2, even though the superficial interstitial flow velocity is extremely low (~10^{-6} cm/s) (Shi and Tarbell 2011). According to Qiu et al., high shear stress leads to SMC apoptosis, whereas low shear stress results in the induction of matrix

TABLE 5.1 Summary of Mechanical Stimulation Regimens Used to Regulate Elastin Synthesis

Construct	Cell Type	Mechanical Stimuli Conditions	Duration	Elastogenic Results
Flexible culture plates	Porcine SMCs	25% strain at 0.05 Hz	5d	In total protein ↑ Collagen ↑ (Sumpio et al. 1988)
Collagen I or PLA scaffold	Rat aortic SMCs	0–20% cyclic strain at 0.05–0.25Hz	4–14d 5–20w	Elastin and collagen expression ↑ ELN and COL1;↑ Elastin protein expression ↑ (Kim et al. 1999)
Collagen I	Human vascular SMCs from aorta and FB	10% cyclic strain	4–8d	ELN ↑ (Seliktar et al. 2003)
3D tubular collagen gel	Human vascular SMCs	2.5% cyclic strain at 0.5, 1.5, and 3 Hz	21d	ELN and total matrix elastin↑(Venkataraman et al. 2014)
PGA scaffold	Bovine SMCs and ECs	Pulsatile culture, flow rate: 0.2 to 0.6 l/min	30d static then 2w dynamic	Matrix elastin around regions of high cell densities (Iwasaki et al. 2008)
Electrospun silk fibroin scaffolds	Human coronary artery SMCs and human aortic ECs	Physiological pulsatile flow	15d	ELN ↑ No elastic fiber (Zhang et al. 2009)
PGS tubular scaffold	Baboon arterial SMCs and endothelial progenitor cells	Pulsatile flow from 1 ml/min to 12 dynes/cm^2	7d SMCs and 2w coculture	Circumferentially aligned elastin (Gao et al. 2008)
		Pulsatile flow from 2 ml/min to 14 ml/min	7w SMCs and 2w coculture	

(*Continued*)

TABLE 5.1 (*Continued*) Summary of Mechanical Stimulation Regimens Used to Regulate Elastin Synthesis

Construct	Cell Type	Mechanical Stimuli Conditions	Duration	Elastogenic Results
PGS scaffold	Baboon SMCs	Pulsatile flow	3w	Mature elastin equivalent to 19% of the native arteries (Lee et al. 2011)
PEG and PLA electrospun scaffold	Human vascular SMCs	Laminar flow 0.74 ml/min first day, then 1.48 ml/min	3d and 6d	Elastin gene and protein expression; ↑ elastic fiber-associated proteins, maturing elastic fibers (Hinderer et al. 2015)

SMC, smooth muscle cells ; d, day; w, week.

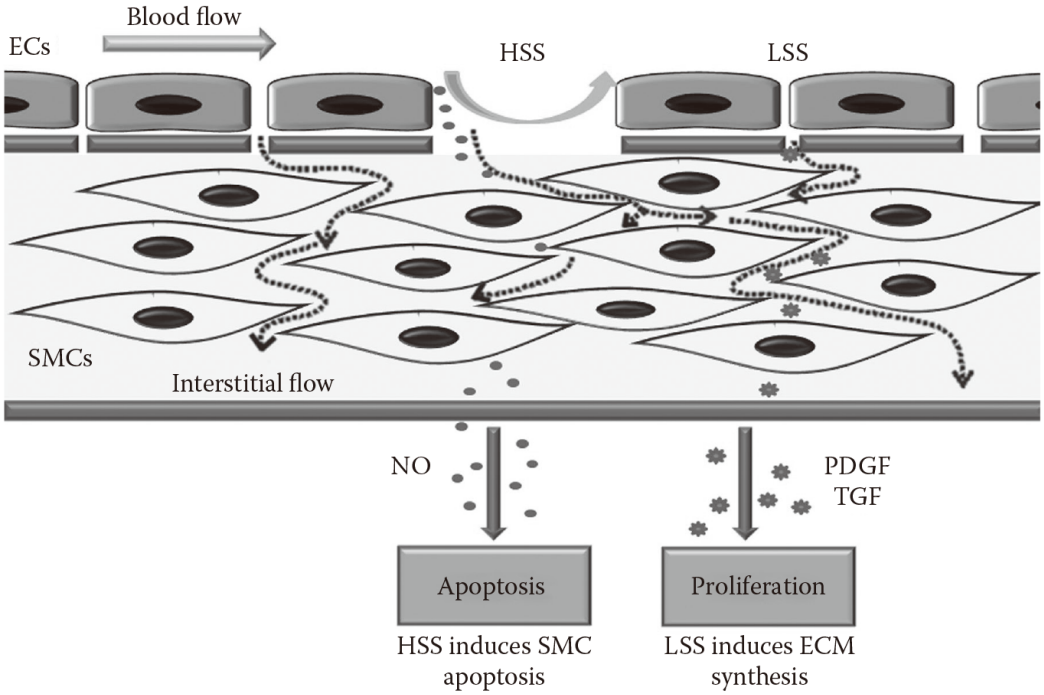

FIGURE 5.2 Schematic depiction of how shear stress regulates vascular SMC activity. In the vasculature, SMCs are exposed to low transmural interstitial flow indicated by the dashed lines. Low shear stress (LSS) upregulates vascular SMC proliferation, migration, and ECM synthesis through the release of platelet-derived growth factor (PDGF) and transforming growth factor (TGF-β) by endothelial cells (ECs). When the endothelium is damaged or injured, the superficial SMCs are exposed to the blood flow. High shear stress (HSS) induces SMC apoptosis through the release of nitric oxide (NO) by ECs. (Adapted from Shi and Tarbell 2011, Qiu et al. 2013, with permission.)

synthesis, including collagen and elastin synthesis (Qiu et al. 2013). Other groups have confirmed that application of low shear stress leads to elastin synthesis (Gao et al. 2008, Iwasaki et al. 2008, Zhang et al. 2009).

Iwasaki et al. seeded bovine aortic SMCs on PGA and PCL sheets, and bovine aortic fibroblasts on PGA sheets. The SMC sheets were then wrapped around a 6 mm silicone tube, cultured for 30 days, subsequently seeded with bovine aortic ECs, and finally exposed to a regulated gradual increased flow and pressure from 0.2 L/min and 20 mm Hg to 0.6 L/min and 100 mm Hg for another 2 weeks. As a result, the engineered vessels showed equivalent elastic characteristics to native arteries in tensile tests (Iwasaki et al. 2008). To stimulate ECM generation, tubular electrospun silk fibroin scaffolds that were seeded with human coronary artery SMCs, and human aortic ECs were exposed to physiological pulsatile flow (Zhang et al. 2009). In this study, an increased elastin gene expression

was observed, although no elastic fibers were visualizable using Verhoeff's elastic stain. Lee et al. reported to induce elastin production, which was equivalent to 19% of the native arteries, by using baboon SMCs and a pulsatile flow (Lee et al. 2011). However, despite this success, the generation of elastic fibers in a tissue-engineered construct with human cells still proves challenging. Hinderer et al. have first reported the successful generation of maturing elastic fibers, utilizing human primary isolated vascular SMCs with a combination of a customized fluid-flow bioreactor system and a hybrid fibrous 3D polymeric scaffold (Hinderer et al. 2015). In this study, shear stress between 6×10^{-4} and 11×10^{-4} dyne/cm^2 (equals $6–11 \times 10^{-5}$ Pa) was applied to the human SMCs. This shear stress differs from the physiological blood luminal flow, but as discussed previously, it corresponds to the in vivo condition, where SMCs are exposed to an extremely low transmural interstitial flow (Hinderer et al. 2015).

5.3.3 Effect of Mechanical Cues on Fibroblasts

Fibroblasts are the most abundant cells in the human body and have been widely used for producing tissue-engineered skin substitutes (Wong et al. 2007). Over the past two decades, various research efforts have focused on the incorporation of elastic fibers into tissue-engineered skin substitutes. Fibroblasts, specifically cardiac, lung, and tendon fibroblasts, were exposed to tension, compression, and shear stress (Chiquet et al. 2009, Shi and Tarbell 2011). Mechanical stimulation of fibroblasts in vitro has been reported to significantly increase proliferation (Yang et al. 2004), modulate cell morphology to an elongated, spindle-like shape (Lee et al. 2005, Wang et al. 2004), and alter ECM deposition (MacKenna et al. 2000, Lee et al. 2005). Exposing human dermal fibroblasts to biophysical signals resulted in an increased expression of 57 genes related to ECM proteins that included collagen types I and VI, fibronectin, as well as elastin (Kessler et al. 2001). In addition, there are reports about an increased elastin protein expression due to mechanical stimulation. For example, Bing et al. subjected rat pelvic ligament fibroblasts to 10% strain (1 Hz and 2 Hz) for 12 hours, followed by a co-culture with bone marrow stromal cells under stretch for an additional 6 to 12 days, after which a significant increase of elastin, LOX, and fibulin-5 was reported (Bing et al. 2012). In contrast, Howard et al. applied biaxial stretch (5%, 0.5Hz, 14 hours) to ligament fibroblasts (Howard et al. 1998). The authors observed that although collagen type I and fibronectin synthesis were increased, tropoelastin production was decreased compared to the static controls. One of

the possible reasons for these opposing results is that the parameters of the mechanical stimulation varied between the studies. Fibroblasts are highly sensitive to the flow rate, strain magnitude, frequency, and duration; therefore, different stimuli parameters potentially lead to completely different results and cannot be objectively compared with each other. Another possible reason might be that the fibroblast and bone marrow stromal cell co-culture system in the study performed by Bing et al. led to the increase of elastin. Despite the great promise of such studies, only a few reports have focused on the induction of elastogenesis by fibroblasts utilizing biomechanical cues. Further studies are required to address this complex problem. Our previous study using human vascular SMCs showed the successful generation of maturing elastic fibers in vitro (Hinderer et al. 2015). Therefore, we aimed to identify if the same experimental approach would lead to the production of maturing elastic fibers employing human dermal fibroblasts. For this purpose, foreskin fibroblasts were isolated from patients between 2 and 7 years, and normal adult skin fibroblasts were isolated from patients ranging between 20 and 40 years. All cells were used between passages 3 and 4. To produce the 3D fibrous hybrid scaffolds, we electrospun poly(L-lactide) (PLA) and poly(ethylene glycol) dimethacrylate (PEGdma) as previously described (Hinderer et al. 2015). A fluid flow bioreactor capable of providing laminar shear stress was used in this study. Scaffolds were coated with 1:5 mixture of 1% w/v HA in Dulbecco's phosphate-buffered saline (PBS) 2 hours prior to cell seeding. HA of a molecular weight of ~750,000 Da was used in this study due to its ability to support tropoelastin cross-linking (Joddar and Ramamurthi 2006b, Hinderer et al. 2015). Approximately 3×10^5 cells were seeded onto each scaffold. After 24 hours of preculture, the scaffolds were transferred into the bioreactor system with Dulbecco's modified eagle medium (DMEM) supplemented with 10% v/v fetal bovine serum (FBS) and 1% v/v penicillin/streptomycin as well as 3.2 ng/ml transforming growth factor beta 1 (TGFβ1). TGFβ1 had been reported to play a crucial role in protein binding and elastic fiber assembly (Kothapalli et al. 2009, Hinderer et al. 2015). Furthermore, the combination of TGFβ1 and HA induced much greater assembly of mature elastin fibers (Kothapalli et al. 2009, Hinderer et al. 2015). In order to provide constant medium change without shearing the cells off, the flow rate was initially set at 0.74 ml/min and then adjusted to 1.48 ml/min from the second day on. As a control, cell-seeded scaffolds were statically cultured without applying shear stress. After 6 days of dynamic culture, the scaffolds from the bioreactor and the static controls

were harvested and further analyzed. Quantitative real-time polymerase chain reaction (qPCR) was performed as previously described (Hinderer et al. 2015) using elastin (ELN), fibulin-5 (FBLN5), fibrillin-1 (FBN1), fibronectin (FN1), EMILIN1, and glyceraldehyde 3-phosphate dehydrogenase (GAPDH) primers from Qiagen. Immunofluorescence staining (IF staining) was performed according to the previously published protocol in order to detect the secreted proteins (Hinderer et al. 2015). As shown in Figure 5.3, shear stress induced a fivefold upregulation of ELN

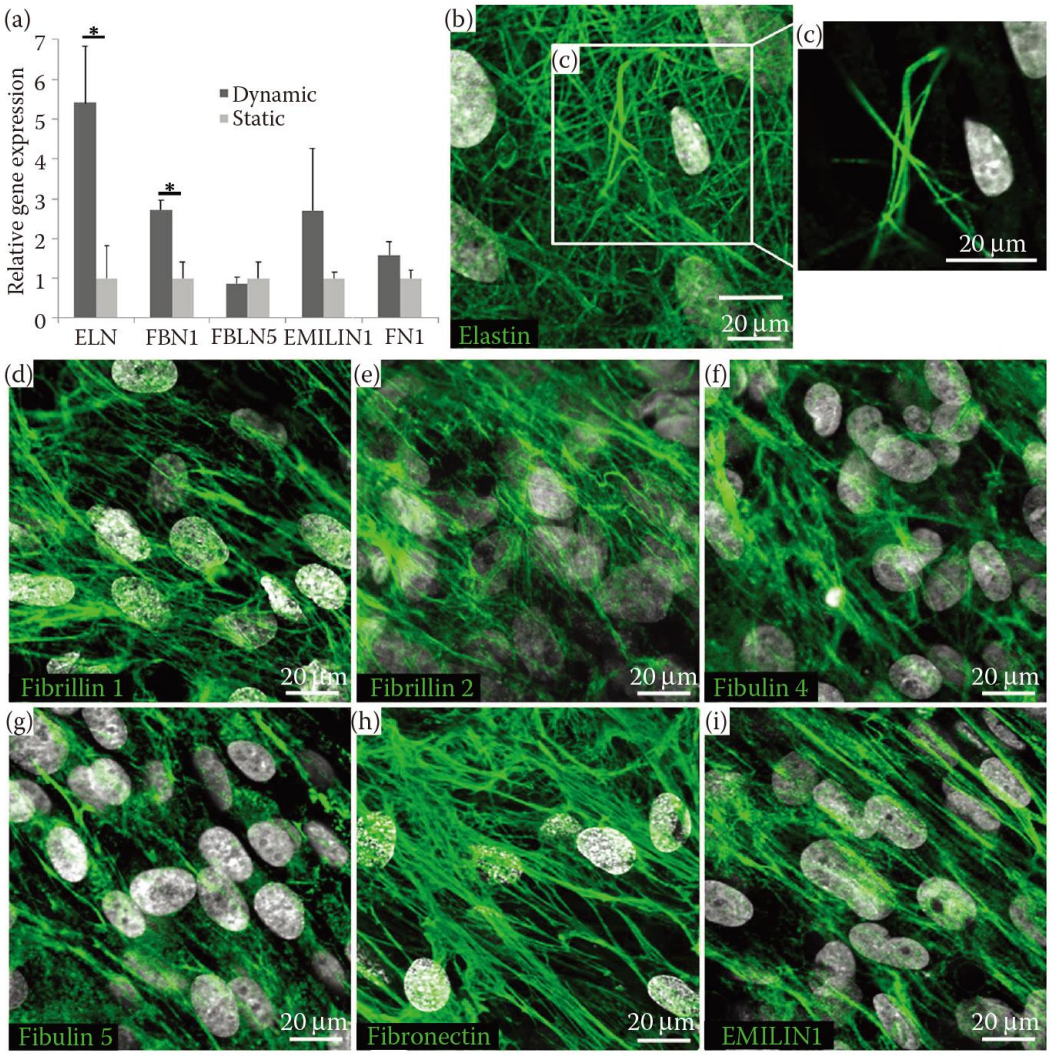

FIGURE 5.3 Impact of shear stress on cultured foreskin fibroblasts. (a) Gene expression of ELN (elastin), FBN1 (fibrillin-1), FBLN5 (fibulin-5), EMILIN-1, and FN1 (fibronectin). (b–i) IF staining of elastin and elastogenesis-associated proteins after a 6-day dynamic culture on 3D HA-coated scaffolds with TGFβ1. Cell nuclei are depicted in white (DAPI). *$p \leq .05$ static versus dynamic (Student's *t*-test was used for statistics analysis).

and threefold upregulation of FBN1 when compared to the static controls (ELN: 5.41 ± 1.43 (dynamic) vs. 1 ± 0.82 (static), $p = .021$; FBN1: 2.72 ± 0.23 (dynamic) vs. 1 ± 0.41 (static), $p = .01$). An increase in FBLN5, FN1, and EMILIN1 expression was also noticed, although this increase was not statistically significant. IF staining of the six-day dynamically cultured foreskin fibroblasts revealed the presence of elastic fibers (Figure 5.3b,c). In addition, the elastogenesis-associated proteins fibrillin 1 and 2, fibulin 4 and 5, as well as fibronectin and EMILIN-1, which have been proven to be critical for proper matrix assembly and cross-linking (Zanetti et al. 2004, Votteler et al. 2013), were highly expressed (Figure 5.3d–i).

Similar results were seen using normal adult skin fibroblasts. As shown in Figure 5.4a, approximately fourfold upregulation of ELN and twofold upregulation of FBN1 were determined when comparing dynamic versus static cultures (ELN 3.75 ± 0.29 (dynamic) vs. 1 ± 0.49 (static), $p = .0028$; FBN1 1.94 ± 0.38 (dynamic) vs. 1 ± 0.41 (static), $p = .042$). Elastin and elastogenesis-associated protein expression profiles were also similar to those seen in the 6-day dynamic foreskin fibroblast cultures (Figure 5.4b–i).

It is well established that IF staining utilizing commercially available elastin antibodies cannot discriminate between tropoelastin and cross-linked elastin. For the detection of cross-links, we thus employed Raman microspectroscopy. Raman microspectroscopy is a laser-based technology that is increasingly employed in the field of tissue engineering and regenerative medicine (Movasaghi et al. 2007, Brauchle and Schenke-Layland 2013). With this technology, it is possible to generate individual biochemical fingerprints by detecting molecular vibrations from proteins, lipids, nucleic acids, as well as macromolecular conformations (Chan et al. 2006, Brauchle and Schenke-Layland 2013). Raman spectroscopy has been used to characterize ECM proteins, such as collagen (Gullekson et al. 2011, Nguyen et al. 2012, Votteler et al. 2012b), elastin (Frushour and Koenig 1975, Debelle et al. 1995, Votteler et al. 2012a), and proteoglycans (Pudlas et al. 2013, Gamsjaeger et al. 2014). Frushour and Koenig have investigated the Raman spectra of collagen, gelatin, and elastin. They identified three Raman bands, 529, 966, and 1108 cm^{-1} that can be assigned to desmosine and isodesmosine (Frushour and Koenig 1975). Desmosine and isodesmosine are two elastic fiber-specific amino acids that are involved in cross-linking of elastic fibers (Kielty et al. 2002). In our study, the dynamically cultured dermal fibroblasts were harvested from the bioreactor cultures and placed in glass bottom dishes filled with PBS. Thirty spectra from

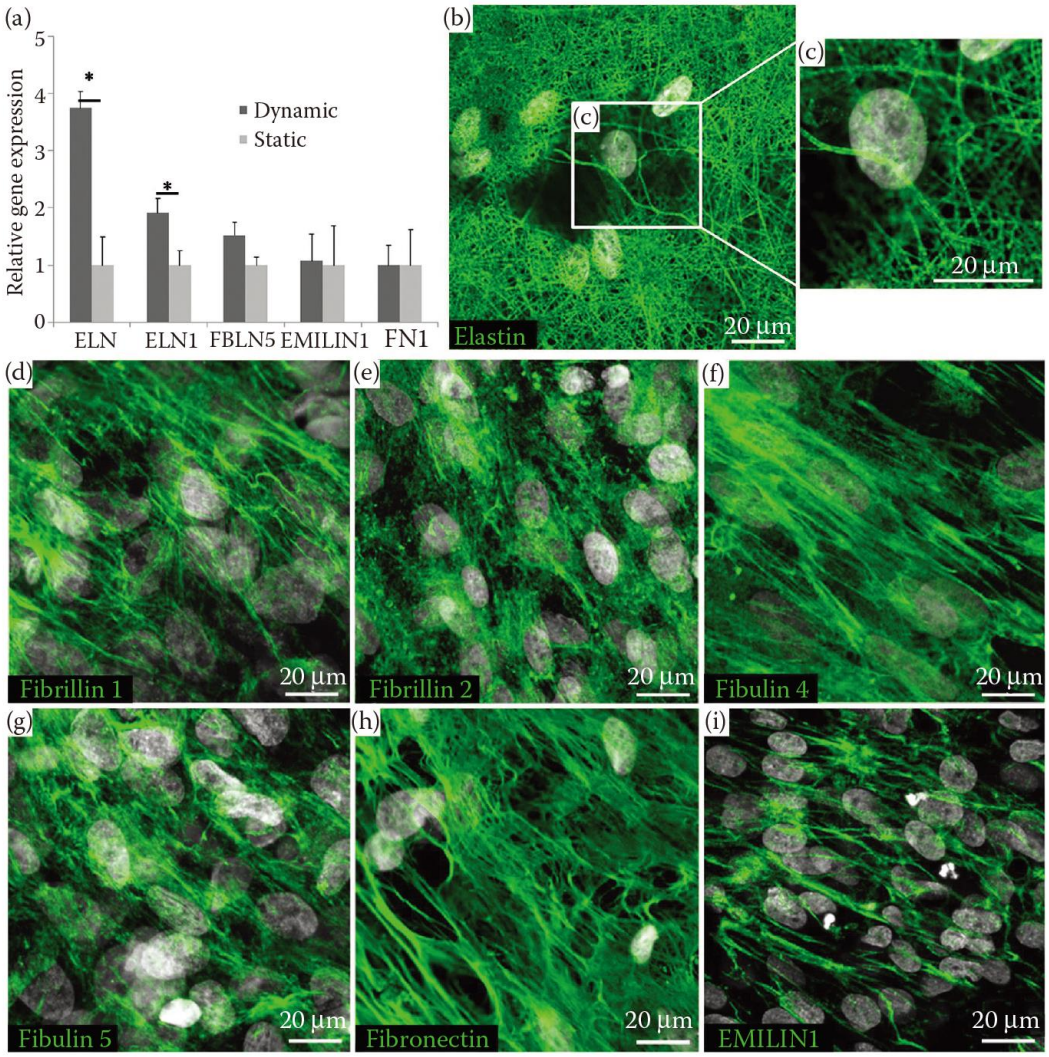

FIGURE 5.4 Impact of shear stress on adult skin fibroblasts. (a) Gene expression of ELN (elastin), FBN1 (fibrillin-1), FBLN5 (fibulin-5), EMILIN-1, and FN1 (fibronectin). (b–i) IF staining of elastin and elastogenesis-associated proteins after a 6-day dynamic culture on 3D HA-coated scaffolds with TGFβ1. Cell nuclei are stained with DAPI (white). *$p \leq .05$ static versus dynamic (student's *t*-test was used for statistics analysis).

three samples were measured with a custom-built Raman microspectrometer (Pudlas et al. 2011). In order to exclude background signals from the scaffold, 30 spectra from three different PEGdma and PLA scaffolds were measured as control. All Raman spectra were reduced to the spectral region between 400 and 1800 cm^{-1} and processed as previously described (Pudlas et al. 2011). Figure 5.5 shows the average Raman spectra of the six-day dynamically cultured dermal fibroblasts and the static controls. These two sample groups revealed clearly distinguishable Raman spectra

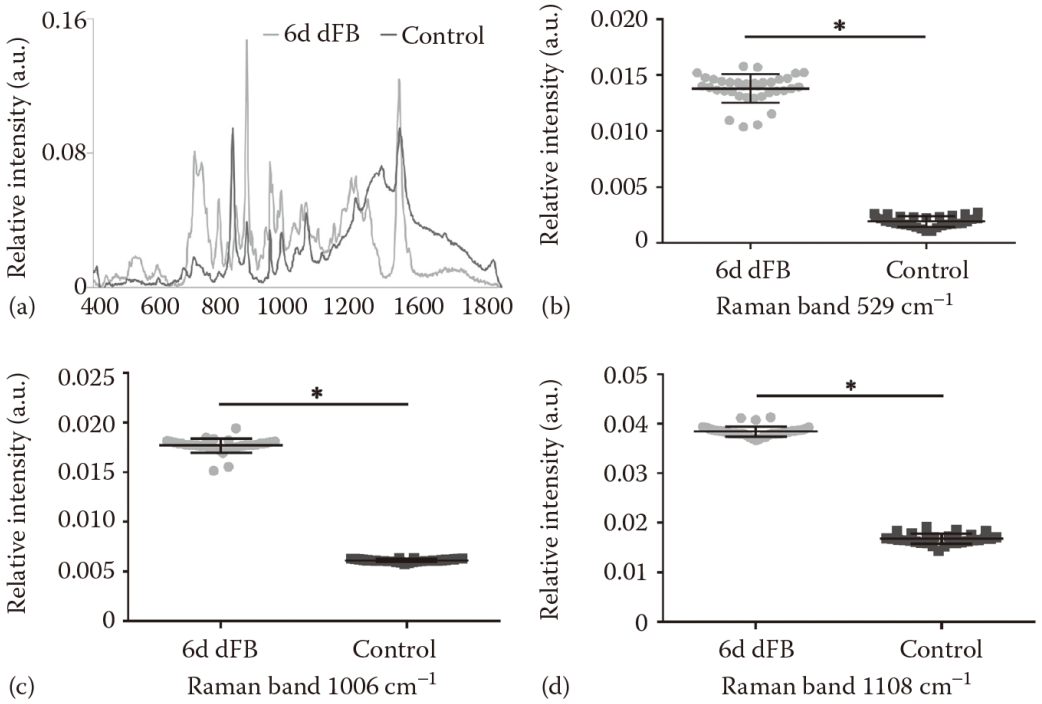

FIGURE 5.5 Raman spectra analysis of human dermal fibroblasts after 6-day dynamic culture on 3D HA-coated scaffolds with TGFβ1. (a) Mean Raman spectra of dynamically cultured dermal fibroblasts and the corresponding static controls. Raman bands at (b) 529 cm^{-1} (c) 966 cm^{-1}, and (d) 1108 cm^{-1} indicate maturation of elastic fibers. *$p \leq .001$.

patterns. When focusing on the previously identified Raman bands at 529, 966, and 1108 cm^{-1} (Frushour and Koenig 1975), significantly higher intensities were seen in the 6-day dynamic cultures when compared to the static controls (Raman band 529 cm^{-1}, $p = 4.22 \times 10^{-52}$; Raman band 966 cm^{-1}, $p = 4.12 \times 10^{-52}$; Raman band 1108 cm^{-1}, $p = 9.66 \times 10^{-39}$), indicating the presence of properly cross-linked, mature elastic fibers.

5.4 CONCLUSION

In order to provide an optimal environment for cells to synthesize elastin and to assemble it to a functional elastic matrix, several different factors need to be carefully considered. Here, we discussed two parameters in detail that are crucial for elastic tissue engineering: (a) three-dimensionality to mimic the ECM structure and (b) mechanical forces to mimic physiological parameters such as blood flow and the corresponding strains. It has been shown that either factor has a significant impact on cell behavior and elastic fiber maturation. In future studies, the interplay of such factors

must be further explored, especially when aiming for the engineering of implants for elastic fiber-rich tissues and organs.

ACKNOWLEDGMENTS

The authors thank Shannon L. Layland (Fraunhofer IGB Stuttgart, Germany) and Marsha W. Rolle (Worchester Polytechnic Institute, the United States) for their thoughtful suggestions. This work was financially supported by the Fraunhofer-Gesellschaft Internal programs (Attract to KSL, Talenta speed up to SH), the BMBF (0316059 to KSL), and the Ministry of Science, Research and the Arts of Baden-Württemberg (33-729.55-3/214 and SI-BW 01222-91 to KSL).

REFERENCES

Balestreire, E. M. and G. Apodaca. 2007. Apical epidermal growth factor receptor signaling: Regulation of stretch-dependent exocytosis in bladder umbrella cells. *Molecular Biology of the Cell* 18(4): 1312–1323.

Barenghi, R., S. Beke, I. Romano et al. 2014. Elastin-coated biodegradable photopolymer scaffolds for tissue engineering applications. *BioMed Research International* 2014: 624–645.

Bashur, C. A. and A. Ramamurthi. 2011a. Aligned electrospun scaffolds and elastogenic factors for vascular cell-mediated elastic matrix assembly. *Journal of Tissue Engineering and Regenerative Medicine* 6(9): 673–686.

Bashur, C. A. and A. Ramamurthi. 2011b. Perspectives on strategies to direct elastic matrix assembly. *Journal of Tissue Science & Engineering* 2: 106e.

Bashur, C. A., L. Venkataraman, and A. Ramamurthi. 2012. Tissue engineering and regenerative strategies to replicate biocomplexity of vascular elastic matrix assembly. *Tissue Engineering Part B Reviews* 18(3): 203–217.

Bing, Z., L. Linlin, Y. Jianguo et al. 2012. Effect of mechanical stretch on the expressions of elastin, LOX and Fibulin-5 in rat BMSCs with ligament fibroblasts co-culture. *Molecular Biology Reports* 39(5): 6077–6085.

Boccafoschi, F., C. Mosca, M. Ramella, G. Valente, and M. Cannas. 2013. The effect of mechanical strain on soft (cardiovascular) and hard (bone) tissues: Common pathways for different biological outcomes. *Cell Adhesion & Migration* 7(2): 165–173.

Boccafoschi, F., M. Ramella, T. Sibillano et al. 2015. Human elastin polypeptides improve the biomechanical properties of three-dimensional matrices through the regulation of elastogenesis. *Journal of Biomedical Materials Research Part A* 103(3): 1218–1230.

Brauchle, E. and K. Schenke-Layland. 2013. Raman spectroscopy in biomedicine–Non-invasive in vitro analysis of cells and extracellular matrix components in tissues. *Biotechnology Journal* 8(3): 288–297.

Brosig, M. 2011. Mechanotransduction in fibroblasts. PhD dissertation, Universität Basel.

Cattaruzza, M., C. Dimigen, H. Ehrenreich, and M. Hecker. 2000. Stretch-induced endothelin B receptor-mediated apoptosis in vascular smooth muscle cells. *FASEB Journal* 14(7): 991–998.

Chan, J. W., D. S. Taylor, T. Zwerdling et al. 2006. Micro-Raman spectroscopy detects individual neoplastic and normal hematopoietic cells. *Biophysical Journal* 90(2): 648–656.

Chen, K. D., Y. S. Li, M. Kim et al. 1999. Mechanotransduction in response to shear stress. Roles of receptor tyrosine kinases, integrins, and Shc. *Journal of Biological Chemistry* 274(26): 18393–18400.

Chen, Q., A. Bruyneel, C. Carr, and J. Czernuszka. 2013. Bio-mechanical properties of novel bi-layer collagen-elastin scaffolds for heart valve tissue engineering. *Procedia Engineering* 59: 247–254.

Chen, Q. Z., A. Bismarck, U. Hansen et al. 2008. Characterisation of a soft elastomer poly(glycerol sebacate) designed to match the mechanical properties of myocardial tissue. *Biomaterials* 29(1): 47–57.

Chiquet, M., L. Gelman, R. Lutz, and S. Maier. 2009. From mechanotransduction to extracellular matrix gene expression in fibroblasts. *Biochimica et Biophysica Acta (BBA)–Molecular Cell Research* 1793(5): 911–920.

Choe, M. M., P. H. Sporn, and M. A. Swartz. 2006. Extracellular matrix remodeling by dynamic strain in a three-dimensional tissue-engineered human airway wall model. *American Journal of Respiratory Cell and Molecular Biology* 35(3): 306–313.

Davis, M. J., G. A. Meininger, and D. C. Zawieja. 1992. Stretch-induced increases in intracellular calcium of isolated vascular smooth muscle cells. *American Journal of Physiology* 263(4 Pt 2): H1292–H1299.

Debelle, L., A. J. Alix, M. P. Jacob et al. 1995. Bovine elastin and κ-elastin secondary structure determination by optical spectroscopies. *Journal of Biological Chemistry* 270(44): 26099–26103.

Frushour, B. G. and J. L. Koenig. 1975. Raman scattering of collagen, gelatin, and elastin. *Biopolymers* 14(2): 379–391.

Gambillara, V., T. Thacher, P. Silacci, and N. Stergiopulos. 2008. Effects of reduced cyclic stretch on vascular smooth muscle cell function of pig carotids perfused ex vivo. *American Journal of Hypertension* 21(4): 425–431.

Gamsjaeger, S., K. Klaushofer, and E. P. Paschalis. 2014. Raman analysis of proteoglycans simultaneously in bone and cartilage. *Journal of Raman Spectroscopy* 45(9): 794–800.

Gao, J., P. Crapo, R. Nerem, and Y. Wang. 2008. Co-expression of elastin and collagen leads to highly compliant engineered blood vessels. *Journal of Biomedical Materials Research Part A* 85(4): 1120–1128.

Gullekson, C., L. Lucas, K. Hewitt, and L. Kreplak. 2011. Surface-sensitive Raman spectroscopy of collagen I fibrils. *Biophysical Journal* 100(7): 1837–1845.

Gupta, V. and K. J. Grande-Allen. 2006. Effects of static and cyclic loading in regulating extracellular matrix synthesis by cardiovascular cells. *Cardiovascular Research* 72(3): 375–383.

Haga, J. H., Y. S. Li, and S. Chien. 2007. Molecular basis of the effects of mechanical stretch on vascular smooth muscle cells. *Journal of Biomechanics* 40(5): 947–960.

Haga, M., A. Yamashita, J. Paszkowiak, B. E. Sumpio, and A. Dardik. 2003. Oscillatory shear stress increases smooth muscle cell proliferation and Akt phosphorylation. *Journal of Vascular Surgery* 37(6): 1277–1284.

Hinderer, S., N. Shen, L. J. Ringuette et al. 2015. In vitro elastogenesis – Instructing human vascular smooth muscle cells to generate an elastic fiber-containing extracellular matrix scaffold. *Biomedical Materials* 10(3): 034102.

Hirai, M., M. Horiguchi, T. Ohbayashi et al. 2007. Latent TGF-[beta]-binding protein 2 binds to DANCE/fibulin-5 and regulates elastic fiber assembly. *EMBO Journal* 26(14): 3283–3295.

Hopkins, A. M., L. De Laporte, F. Tortelli et al. 2013. Silk hydrogels as soft substrates for neural tissue engineering. *Advanced Functional Materials* 23(41): 5140–5149.

Howard, P. S., U. Kucich, R. Taliwal, and J. M. Korostoff. 1998. Mechanical forces alter extracellular matrix synthesis by human periodontal ligament fibroblasts. *Journal of Periodontal Research* 33(8): 500–508.

Hu, Y., G. Böck, G. Wick, and Q. Xu. 1998. Activation of PDGF receptor α in vascular smooth muscle cells by mechanical stress. *The FASEB Journal* 12(12): 1135–1142.

Huang, H., R. D. Kamm, and R. T. Lee. 2004. Cell mechanics and mechanotransduction: Pathways, probes, and physiology. *American Journal of Physiology* 287(1): C1–11.

Ingber, D. E. 2006. Cellular mechanotransduction: Putting all the pieces together again. *The FASEB Journal* 20(7): 811–827.

Iwasaki, H., S. Eguchi, H. Ueno, F. Marumo, and Y. Hirata. 2000. Mechanical stretch stimulates growth of vascular smooth muscle cells via epidermal growth factor receptor. *American Journal of Physiology* 278(2): H521–H529.

Iwasaki, H., T. Yoshimoto, T. Sugiyama, and Y. Hirata. 2003. Activation of cell adhesion kinase β by mechanical stretch in vascular smooth muscle cells. *Endocrinology* 144(6): 2304–2310.

Iwasaki, K., K. Kojima, S. Kodama et al. 2008. Bioengineered three-layered robust and elastic artery using hemodynamically-equivalent pulsatile bioreactor. *Circulation* 118(14 Suppl): S52–57.

Jaalouk, D. E. and J. Lammerding. 2009. Mechanotransduction gone awry. *Nature Reviews Molecular Cell Biology* 10(1): 63–73.

Jeffries, E. M., R. A. Allen, J. Gao, M. Pesce, and Y. Wang. 2015. Highly elastic and suturable electrospun poly(glycerol sebacate) fibrous scaffolds. *Acta Biomaterialia* 18: 30–39.

Joddar, B., S. Ibrahim, and A. Ramamurthi. 2007. Impact of delivery mode of hyaluronan oligomers on elastogenic responses of adult vascular smooth muscle cells. *Biomaterials* 28(27): 3918–3927.

Joddar, B. and A. Ramamurthi. 2006a. Elastogenic effects of exogenous hyaluronan oligosaccharides on vascular smooth muscle cells. *Biomaterials* 27(33): 5698–5707.

Joddar, B. and A. Ramamurthi. 2006b. Fragment size- and dose-specific effects of hyaluronan on matrix synthesis by vascular smooth muscle cells. *Biomaterials* 27(15): 2994–3004.

Kang, H., Y. Fan, and X. Deng. 2011. Vascular smooth muscle cell glycocalyx modulates shear-induced proliferation, migration, and NO production responses. *American Journal of Physiology* 300(1): H76–H83.

Katsumi, A., A. W. Orr, E. Tzima, and M. A. Schwartz. 2004. Integrins in mechanotransduction. *Journal of Biological Chemistry* 279(13): 12001–12004.

Keire, P. A., N. L'Heureux, R. B. Vernon et al. 2009. Expression of versican isoform V3 in the absence of ascorbate improves elastogenesis in engineered vascular constructs. *Tissue Engineering Part A* 16(2): 501–512.

Kessler, D., S. Dethlefsen, I. Haase et al. 2001. Fibroblasts in mechanically stressed collagen lattices assume a "synthetic" phenotype. *The Journal of Biological Chemistry* 276(39): 36575–36585.

Kielty, C. M., M. J. Sherratt, and C. A. Shuttleworth. 2002. Elastic fibres. *Journal of Cell Science* 115(Pt 14): 2817–2828.

Kim, B. S., J. Nikolovski, J. Bonadio, and D. J. Mooney. 1999. Cyclic mechanical strain regulates the development of engineered smooth muscle tissue. *Nature Biotechnology* 17(10): 979–983.

Kim, T. G., H. S. Shin, and D. W. Lim. 2012. Biomimetic scaffolds for tissue engineering. *Advanced Functional Materials* 22(12): 2446–2468.

Kothapalli, C. R., P. M. Taylor, R. T. Smolenski, M. H. Yacoub, and A. Ramamurthi. 2009. Transforming growth factor beta 1 and hyaluronan oligomers synergistically enhance elastin matrix regeneration by vascular smooth muscle cells. *Tissue Engineering Part A* 15(3): 501–511.

Kumar, V. A., J. M. Caves, C. A. Haller et al. 2013. Acellular vascular grafts generated from collagen and elastin analogs. *Acta Biomaterialia* 9(9): 8067–8074.

Lee, C. H., H. J. Shin, I. H. Cho et al. 2005. Nanofiber alignment and direction of mechanical strain affect the ECM production of human ACL fibroblast. *Biomaterials* 26(11): 1261–1270.

Lee, K. W., D. B Stolz, and Y. Wang. 2011. Substantial expression of mature elastin in arterial constructs. *Proceedings of the National Academy of Sciences* 108(7): 2705–2710.

Lehoux, S., Y. Castier, and A. Tedgui. 2006. Molecular mechanisms of the vascular responses to haemodynamic forces. *Journal of Internal Medicine* 259(4): 381–392.

Lin, S., M. Sandig, and K. Mequanint. 2011. Three-dimensional topography of synthetic scaffolds induces elastin synthesis by human coronary artery smooth muscle cells. *Tissue Engineering Part A* 17(11–12): 1561–1571.

MacKenna, D., S. R. Summerour, and F. J. Villarreal. 2000. Role of mechanical factors in modulating cardiac fibroblast function and extracellular matrix synthesis. *Cardiovascular Research* 46(2): 257–263.

Masoumi, N., N. Annabi, A. Assmann et al. 2014. Tri-layered elastomeric scaffolds for engineering heart valve leaflets. *Biomaterials* 35(27): 7774–7785.

Movasaghi, Z., S. Rehman, and I. U. Rehman. 2007. Raman spectroscopy of biological tissues. *Applied Spectroscopy Reviews* 42(5): 493–541.

Nguyen, T. T., C. Gobinet, J. Feru et al. 2012. Characterization of type I and IV collagens by Raman microspectroscopy: Identification of spectral markers of the dermo-epidermal junction. *Spectroscopy: An International Journal* 27(5–6): 7.

Noda, K., B. Dabovic, K. Takagi et al. 2013. Latent TGF-β binding protein 4 promotes elastic fiber assembly by interacting with fibulin-5. *Proceedings of the National Academy of Sciences of the United States of America* 110(8): 2852–2857.

Opitz, F., K. Schenke-Layland, T. U. Cohnert et al. 2004. Tissue engineering of aortic tissue: Dire consequence of suboptimal elastic fiber synthesis in vivo. *Cardiovascular Research* 63(4): 719–730.

Patel, A., B. Fine, M. Sandig, and K. Mequanint. 2006. Elastin biosynthesis: The missing link in tissue-engineered blood vessels. *Cardiovascular Research* 71(1): 40–49.

Pudlas, M., E. Brauchle, T. J. Klein, D. W. Hutmacher, and K. Schenke-Layland. 2013. Non-invasive identification of proteoglycans and chondrocyte differentiation state by Raman microspectroscopy. *Journal of Biophotonics* 6(2): 205–211.

Pudlas, M., D. A. C Berrio, M. Votteler et al. 2011. Non-contact discrimination of bone marrow mesenchymal stem cells and fibroblasts using Raman microspectroscopy. *Medical Laser Application* 26(3): 119–125.

Qiu, J., Y. Zheng, J. Hu et al. 2013. Biomechanical regulation of vascular smooth muscle cell functions: From in vitro to in vivo understanding. *Interface* 11(90).

Schenke-Layland, K., A. Nsair, B. Van Handel et al. 2011. Recapitulation of the embryonic cardiovascular progenitor cell niche. *Biomaterials* 32(11): 2748–2756.

Seliktar, D., R. M. Nerem, and Z. S. Galis. 2003. Mechanical strain-stimulated remodeling of tissue-engineered blood vessel constructs. *Tissue Eng* 9(4): 657–666.

Shi, Z. D. and J. M. Tarbell. 2011. Fluid flow mechanotransduction in vascular smooth muscle cells and fibroblasts. *Annals of Biomedical Engineering* 39(6): 1608–1619.

Sommer, N., M. Sattler, J. M. Weise et al. 2013. A tissue-engineered human dermal construct utilizing fibroblasts and transforming growth factor β1 to promote elastogenesis. *Biotechnology Journal* 8(3): 317–326.

Sumpio, B. E., A. J. Banes, W. G. Link, and G. Johnson, Jr. 1988. Enhanced collagen production by smooth muscle cells during repetitive mechanical stretching. *Archives of Surgery* 123(10): 1233–1236.

Tu, Yi., S. G. Wise, and A. S. Weiss. 2010. Stages in tropoelastin coalescence during synthetic elastin hydrogel formation. *Micron* 41(3): 268–272.

Venkataraman, L., C. A. Bashur, and A. Ramamurthi. 2014. Impact of cyclic stretch on induced elastogenesis within collagenous conduits. *Tissue Engineering Part A* 20(9–10): 1403–1415.

Votteler, M., D. A. Carvajal Berrio, A. Horke et al. 2013. Elastogenesis at the onset of human cardiac valve development. *Development* 140(11): 2345–2353.

Votteler, M., D. A. Carvajal Berrio, M Pudlas, H Walles, and K Schenke-Layland. 2012a. Non-contact, label-free monitoring of cells and extracellular matrix using Raman spectroscopy. *Journal of Visualized Experiments* 29(63): 3977.

Votteler, M., D. A. Carvajal Berrio, M. Pudlas et al. 2012b. Raman spectroscopy for the non-contact and non-destructive monitoring of collagen damage within tissues. *Journal of Biophotonics* 5(1): 47–56.

Wang, J. H., G. Yang, Z. Li, and W. Shen. 2004. Fibroblast responses to cyclic mechanical stretching depend on cell orientation to the stretching direction. *Journal of Biomechanics* 37(4): 573–576.

Waterhouse, A., S. G. Wise, M. K. Ng, and A. S. Weiss. 2011. Elastin as a non-thrombogenic biomaterial. *Tissue Engineering Part B Reviews* 17(2): 93–99.

Wernig, F., M. Mayr, and Q. Xu. 2003. Mechanical stretch-induced apoptosis in smooth muscle cells is mediated by β1-integrin signaling pathways. *Hypertension* 41(4): 903–911.

Wise, S. G., M. J. Byrom, A. Waterhouse et al. 2011. A multilayered synthetic human elastin/polycaprolactone hybrid vascular graft with tailored mechanical properties. *Acta Biomaterialia* 7(1): 295–303.

Wong, T., J. A. McGrath, and H. Navsaria. 2007. The role of fibroblasts in tissue engineering and regeneration. *The British journal of dermatology* 156(6): 1149–1155.

Yang, G., R. C. Crawford, and J. H. Wang. 2004. Proliferation and collagen production of human patellar tendon fibroblasts in response to cyclic uniaxial stretching in serum-free conditions. *Journal of Biomechanics* 37(10): 1543–1550.

Yeo, G. C., B. Aghaei-Ghareh-Bolagh, E. P. Brackenreg et al. 2015. Fabricated elastin. *Advanced Healthcare Materials* 4(16): 2530–2556.

Zampetaki, A., Z. Zhang, Y. Hu, and Q. Xu. 2005. Biomechanical stress induces IL-6 expression in smooth muscle cells via Ras/Rac1-p38 MAPK-NF-κB signaling pathways. *American Journal of Physiology* 288(6): H2946–H2954.

Zanetti, M., P. Braghetta, P. Sabatelli et al. 2004. EMILIN-1 deficiency induces elastogenesis and vascular cell defects. *Molecular and Cellular Biology* 24(2): 638–650.

Zhang, X., X. Wang, V. Keshav et al. 2009. Dynamic culture conditions to generate silk-based tissue-engineered vascular grafts. *Biomaterials* 30(19): 3213–3223.

Appendix III: Shen N, Riedl JA et al. 2018.

IOP Publishing Biomed. Mater. 13 (2018) 024101 https://doi.org/10.1088/1748-605X/aa9b3c

Biomedical Materials

PAPER

A flow bioreactor system compatible with real-time two-photon fluorescence lifetime imaging microscopy

Nian Shen[1,2,8], Julia A Riedl[1,2,3,8], Daniel A Carvajal Berrio[1], Zachary Davis[1,4], Michael G Monaghan[1,5,6], Shannon L Layland[1,2], Svenja Hinderer[1,2] and Katja Schenke-Layland[1,2,7,9]

[1] Department of Women's Health, Research Institute of Women's Health, University Hospital of the Eberhard Karls University, Tübingen, Germany
[2] Department of Cell and Tissue Engineering, Fraunhofer Institute for Interfacial Engineering and Biotechnology IGB, Stuttgart, Germany
[3] Medical Scientist Training Program (MD/PhD), University of Minnesota Medical School, Minneapolis, MN, United States of America
[4] Department of Material Science and Engineering, North Carolina State University, Raleigh, NC, United States of America
[5] Trinity Centre for Bioengineering, Trinity College Dublin, Dublin, Ireland
[6] Department of Mechanical & Manufacturing Engineering, Trinity College Dublin, Dublin, Ireland
[7] Department of Medicine/Cardiology, CVRL, David School of Medicine at UCLA, Los Angeles, CA, United States of America
[8] These authors contributed equally to this work.
[9] Author to whom any correspondence should be addressed.

E-mail: nian.shen@med.uni-tuebingen.de, brekk129@umn.edu, Daniel.Carvajal-Berrio@med.uni-tuebingen.de, zgdavis@ncsu.edu, MONAGHMI@tcd.ie, shannon.layland@igb.fraunhofer.de, svenja.hinderer@igb.fraunhofer.de and katja.schenke-layland@med.uni-tuebingen.de

Keywords: FLIM, HUVEC, multiphoton imaging, endothelial cells, 3D cell culture, 2P-FLIM

Supplementary material for this article is available online

OPEN ACCESS

RECEIVED
30 July 2017

REVISED
31 October 2017

ACCEPTED FOR PUBLICATION
17 November 2017

PUBLISHED
1 February 2018

Abstract

Bioreactors are essential cell and tissue culture tools that allow the introduction of biophysical signals into *in vitro* cultures. One major limitation is the need to interrupt experiments and sacrifice samples at certain time points for analyses. To address this issue, we designed a bioreactor that combines high-resolution contact-free imaging and continuous flow in a closed system that is compatible with various types of microscopes. The high throughput fluid flow bioreactor was combined with two-photon fluorescence lifetime imaging microscopy (2P-FLIM) and validated. The hydrodynamics of the bioreactor chamber were characterized using COMSOL. The simulation of shear stress indicated that the bioreactor system provides homogeneous and reproducible flow conditions. The designed bioreactor was used to investigate the effects of low shear stress on human umbilical vein endothelial cells (HUVECs). In a scratch assay, we observed decreased migration of HUVECs under shear stress conditions. Furthermore, metabolic activity shifts from glycolysis to oxidative phosphorylation-dependent mechanisms in HUVECs cultured under low shear stress conditions were detected using 2P-FLIM. Future applications for this bioreactor range from observing cell fate development in real-time to monitoring the environmental effects on cells or metabolic changes due to drug applications.

Introduction

Fluid shear stress, due to blood flow through vessels, plays a crucial role in angiogenesis [1], cell proliferation [2], migration [3], differentiation [2, 4], and metabolism [5]. Cells are sensitive to shear stress, which can ultimately alter cell function through activation of mechanosensitive molecules involved in cell signaling pathways [6]. Bioreactor systems are commonly closed systems that employ mechanical stimuli to cells and *in vitro*-generated cell-based three-dimensional (3D) tissues with the goal to mimic *in vivo* physiological conditions [7]. Depending on the type of cell or tissue, parameters such as temperature, oxygen concentration, mechanical and electrical stimulation [8] are the typically manipulated and monitored in bioreactor systems. One limitation of the majority of the currently existing bioreactor systems is the need to interrupt the culture at defined time points to gather information about the status of the sample using invasive methods. High-resolution optical techniques such as Raman microspectroscopy and near-infrared

IOP Publishing Biomed. Mater. 13 (2018) 024101 N Shen et al

two-photon fluorescence lifetime imaging microscopy (2P-FLIM) are widely used to detect cell phenotypic changes, metabolic activity, and protein expression of cells without the need for exogenous markers [9–11]. It would be highly advantageous to develop a bioreactor system that allows real-time high-resolution imaging of cells and tissues that are exposed to biomechanical stress *in vitro* without the need to stop the experiment or sacrifice the sample. However, to combine high-resolution imaging modalities with continuous flow bioreactor systems is challenging due to short working distances and constraints of optical transparency. Although some custom-built and commercially available devices have been developed to apply shear stress *in vitro*, few existing designs are optimized to allow for simultaneous high-resolution live-cell microscopy [4, 12, 13]. Microfluidic devices were designed for high-resolution live-cell microscopy. However, these devices also face technical challenges [14]. For example, bubbles in the microfluidic channels/chambers are difficult to remove and may damage cells, therefore hindering the control of these devices [14]. Furthermore, unlike bioreactor systems, microfluidic devices are designed to culture and analyze single cells or monolayers of cells, but they are not suitable for the culture of larger samples such as 3D tissues [14].

Here, we present a bioreactor that combines high-resolution contact-free imaging and continuous flow in a closed system that is compatible with various types of microscopes. 2P-FLIM has recently emerged in the field biology as a tool to study complex biological samples [15–17]. It is a non-invasive method that relies on the principle that intrinsic molecules within cells, such as amino acids, proteins, and lipids often emit a well-perceivable fluorescence after excitation with light in the ultraviolet or visible range [18]. This excitation is accomplished using near-infrared femtosecond multi-photon lasers. Therefore, no exogenous fluorescent dyes must be added to the culture for visualization and analysis. In addition to cellular and tissue autofluorescence, 2P-FLIM can detect pH level, cation (Ca^{2+}, Mg^{+}, K^{+}) concentration, oxygen concentration and fluorescence resonant energy transfer [19–23]. NAD(P)H (nicotinamide adenine dinucleotide (phosphate)) is a key enzyme involved in glycolysis and oxidative phosphorylation [11, 23, 24]. Changes of NAD(P)H and FAD (flavin adenine dinucleotide) are reflective of cellular metabolism [25] that can be non-invasively detected with 2P-FLIM. Shear stress has been shown to influence metabolic activity and migration of endothelial cells [26], therefore, we aimed to investigate the influence of shear stress on cell migration, cell metabolism and apoptosis of human umbilical vein endothelial cells (HUVECs) by implementing bright field imaging and 2P-FLIM in our bioreactor system.

Materials and methods

Cell culture

HUVECs were obtained from Lonza (CC-2517, Basal, Switzerland). Passages 3–6 were used for all experiments with the corresponding EBM-2 MV BulletKit medium (CC-3156 and CC-4147; Lonza).

For the bioreactor experiments, HUVECs were trypsinized (0.25% trypsin-EDTA) and re-seeded at a density of 3×10^4 cells cm^{-2} on circular 25 mm diameter coverslips (Nunc Thermanox, Thermo Fischer Scientific, Langselbold, Germany). The cell-seeded coverslips were cultured overnight in a six-well plate at 37 °C and 5% CO_2 to allow cell attachment prior transfer into the bioreactor system.

Imaging bioreactor system

A custom-built, autoclavable imaging bioreactor system was designed using Solidworks (Solidworks2010, Dassault Systemes SolidWorks Corporation, Ludwigsburg, Germany) (figure 1). A computational model was developed to assess the performance of the bioreactor system in silico. Meshing and calculations were performed in COMSOL 4.3a based on the bioreactor geometry and dimensions (COMSOL Multiphysics GmbH, Berlin, Germany). The medium was considered as an incompressive Newtonian fluid. Therefore, the equation used in the simulation was incompressive Navier–Stokes equations as follows (equations (1) and (2)):

$$\nabla \cdot \mathbf{v} = \mathbf{0} \tag{1}$$

$$\rho\left(\frac{\partial}{\partial t}\mathbf{u}\right) + \rho(\mathbf{u} \cdot \nabla)\mathbf{u} = \nabla \cdot (-p\mathbf{I} + \mu(\nabla\mathbf{u} + (\nabla\mathbf{u})^T)), \tag{2}$$

where $\mathbf{u}$ is the fluid velocity, ρ is the fluid density, $\mathbf{p}$ is the fluid pressure, μ is the fluid dynamic viscosity of the culture medium and $\mathbf{F}$ is the volume forces vector. The numerical values of the model parameters used in the simulations are displayed in table 1.

The bioreactor system consists of three parts: a transparent chamber top (made of polycarbonate), a flow chamber block and a bottom (both made of polyether-ether-ketone) (figure 1(a)). For all experiments, cell-seeded coverslips were placed between the flow chamber block and bottom. There are four fluidic chambers; each with a distinct inlet and outlet valve to enable laminar flow. Each fluidic chamber was connected to a closed tubing system (Ismatec, Wertheim-Mondfeld, Germany) containing a 30 ml medium reservoir (Schott AG, Mainz, Germany) and a filter with a 20 μm pore size (Whatman GmbH, Dassel, Germany). The cell medium was pumped from the reservoir through the system using a peristaltic pump with a CA8 pump head and cassette (Ismatec). All *in vitro* experiments were performed at 37 °C and 5% CO_2.

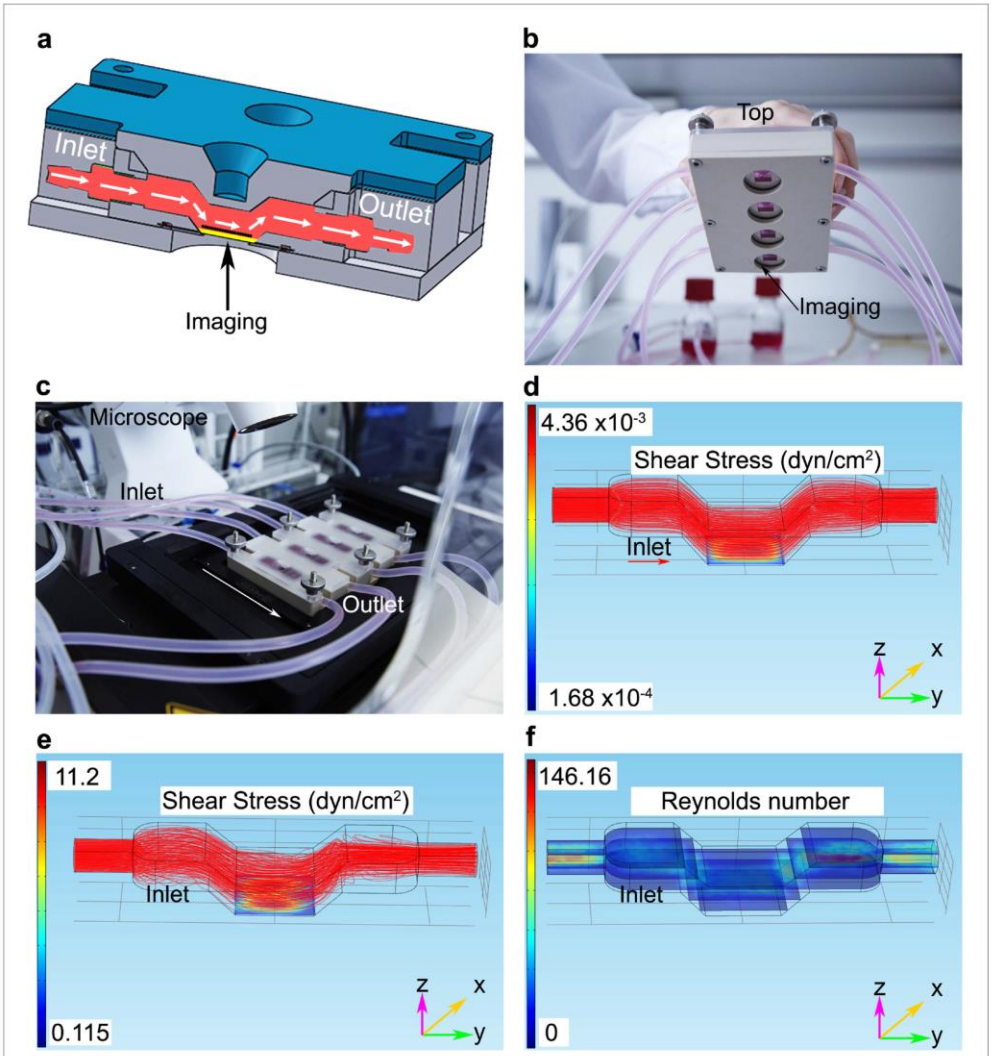

Figure 1. Overview and in silico characterization of the imaging bioreactor employed in this study. (a) SolidWorks computer-aided design drawing. Cross-section of bioreactor flow chamber with the white arrows indicating the flow of medium, the top component is blue and the yellow color depicts the cell-seeded area. (b) Bottom view of the bioreactor system shows the four distinct flow chambers. (c) Bioreactor in the experimental set up: fluorescence microscope with built-in incubator for live-cell imaging. (d) COMSOL in silico characterization of flow dynamics using a flow rate of 1.48 ml min^{-1}. Red stream lines show laminar flow through the chamber. The applied shear stress on the cell-seeded substrate is visualized via a color code.

Table 1. Numerical values of the model parameters used for the simulation.

Parameters (units)	Value	Reference
Inlet velocity	0	
Outlet pressure (Pa)	0	
Boundaries	No slip	
Fluid viscosity (Pa s)	8.1×10^{-4}	[51, 52]
Fluid density at 37 °C	10^3	[51, 52]
Temperature (K)	310.15	[51, 52]

Live-cell bright field microscopy

After 24 h of static cell culture, a p100 pipette tip (Eppendorf, Hamburg, Germany) was used to create a scratch and then coverslips were placed in the bioreactor system, with the scratch perpendicular to flow direction, medium was added, the closed system was connected to the medium pump and placed on the microscope stage for live-cell and 2P-FLIM data acquisition.

In this study, we utilized a Zeis AxioObserver Z1 (Carl Zeiss GmbH, Jena, Germany) with live-cell imaging compatibility and an attached, closed incubator to ensure 37 °C and 5% CO_2 during the entire experiment (figure 1(c)). A bright-field imaging channel and a 40× water immersion objective (N.A 1.1, Carl Zeiss GmbH) were used to acquire images every 5 min for

IOP Publishing Biomed. Mater. 13 (2018) 024101 N Shen et al

20 h after initial injury. The focus was set and fixed prior to the experiment.

Immunofluorescence and live/dead cell staining

After 24 h of culture within the bioreactor system, the cell-seeded coverslips were extracted from the bioreactor, fixed with 4% paraformaldehyde for 15 min, washed and then stained for the endothelial cell marker CD31 as described previously in detail [24]. Cell nuclei were visualized using 4′, 6-Diamidin-2-phenylindol (DAPI). Mouse IgG1 PECAM 1 (CD31; sc-71872, 1:100; Santa Cruz, Heidelberg, Germany) served as the primary antibody, and anti-mouse-IgG1-Alexa Fluor 594 (A-11005, 1:250; Life Technologies, Carlsbad, USA) was used as the secondary antibody. A confocal microscope LSM710 (Carl Zeiss GmbH) was used to obtain the images, which were processed using Photoshop CS3 (Adobe Systems, San Jose, USA).

To further characterize the bioreactor system, cell viability following a 24 h dynamic culture was assessed using a live/dead staining protocol. Fluorescein diacetate (FDA; Sigma-Aldrich, Darmstadt, Germany) at a concentration of 1 μg ml^{-1} and propidium iodide (PI; Sigma-Aldrich) at a concentration of 1 μg ml^{-1} were used. Dilutions were prepared with cell culture medium without fetal calf serum. For staining, the cells were washed with PBS and incubated for 15 min in the dark at 37 °C with the dye solution. The dye was then removed, the cells were washed with PBS and images were immediately acquired.

Two-photon fluorescence lifetime imaging microscopy (2P-FLIM)

2P-FLIM measurements were performed on a custom-made multiphoton laser system (JenLab GmbH, Jena, Germany) that has been previously described in detail [11, 25]. Two-photon excitation was generated using a Ti:Sapphire femtosecond laser (MaiTai XF1 Spectra Physics, United States, Santa Clara). The following settings were maintained for all 2P-FLIM experiments: multiphoton images were collected in the region of interest with a total acquisition time of 23 s, a laser power of 25 mW and a wavelength of 710 nm. Afterwards, the microscope was switched to 2P-FLIM mode for the acquisition of the decay data. All recording settings were adjusted using the software SPCM (Becker & Hickl GmbH, Berlin, Germany). Each 2P-FLIM measurement had a total recording time of 180 s and was controlled through the SPCM software (Becker & Hickl GmbH). Instrumental response function (IRF) was considered to acquire accurate results [26, 27]. The measurement of IRF was performed as previously described [28]. In detail, amorphous urea (Sigma-Aldrich) was dissolved in distilled water and added to a glass bottom dish (ibidi GmbH, Martinsried, Germany). After resting overnight, the water was evaporated, and the saturated concentration of urea formed crystals on the glass surface. Urea crystals were then measured to acquire the time-resolved scattering signal coming from the crystals. The excitation wavelength was 920 nm and acquisition time was 180 s with a laser power of 5 mW.

2P-FLIM data analysis

It is known that fluorescence signals originating from NAD(P)H contain contributions from free and protein-bound NAD(P)H [29]. Biexponential decay fitting was used to calculate the short and long lifetime components (τ_1 and τ_2, respectively), which mostly correspond to free and protein-bound NAD(P)H [30]. The relative contributions of the lifetime components (α_1 and α_2, where $\alpha_1 + \alpha_2 = 100\%$) were also calculated. The IRF was recorded from urea crystals, and the instrumental delays were taken into account in the lifetime calculations as previously described [11]. At the end of every fitting, χ^2, a parameter expressing the quality and accuracy of the biexponential decay fitting, was calculated. The fitting parameters were reevaluated until the average χ^2 per image was lower than 1.1. Every pixel was independently calculated to enable false color-coding based on the values of the different parameters (τ, α, and χ^2). Afterwards, every decay map pixel (2P-FLIM image) was exported as a text file and analyzed using ImageJ (freely available from www.nih.org). All data analyses were performed with the software SPCM (Becker & Hickl GmbH) with a binning factor of 6 and a threshold of approximately 30% of the maximum signal.

Statistical analysis

Normal data distribution was assessed using a Shapiro–Wilk test. For statistical analysis, the commercially available program GraphPad Prism 6 was used (GraphPad Software, Inc., La Jolla, CA). Students t-test was performed, and $p < 0.05$ was considered statistically significant.

Results

The imaging bioreactor system was designed and fabricated to allow cell and tissue cultures to be exposed to defined fluid shear stress while enabling high-resolution imaging (figure 1(a)). It has the same dimension as a typical cell culture plate (127 mm × 85 mm × 21 mm) making it compatible with various existing microscope systems. The bioreactor has four distinct flow chambers with no communication or connection between the chambers (figure 1(b)), enabling the execution of four independent experiments simultaneously. The transparent top component allows bright field light penetration and is suitable for inverted light microscopes. Windows were designed in the bottom component to ensure contact between the imaging objective and the cell-seeded area within the bioreactor system to allow for high-resolution imaging (figure 1(c)). In our proof-of-concept

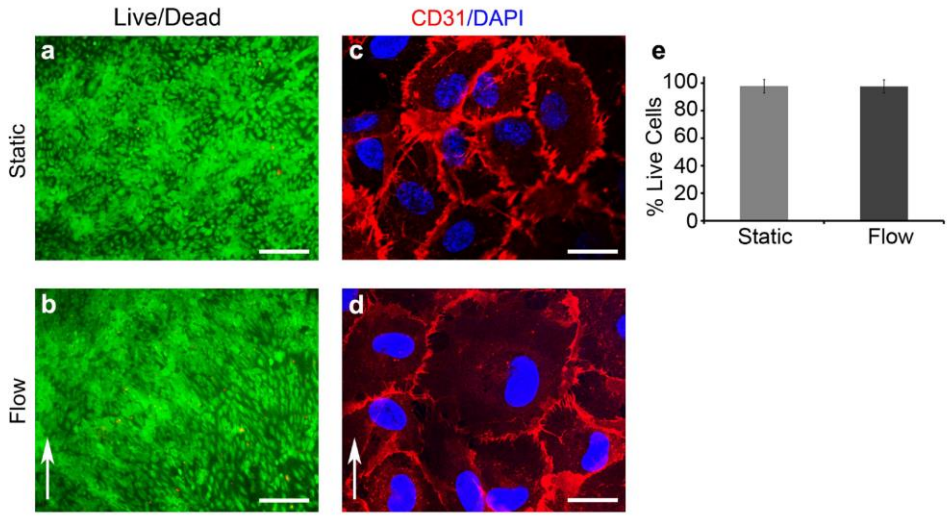

Figure 2. Fluorescence staining results 24 h after scratch assay under either static (a), (c) or dynamic (b), (d) conditions. (a), (b) Live/dead assay: living cells are stained in green and dead cells are visualized in red. Scale bars equal 100 μm. (c), (d) CD31 immunofluorescence staining (red) and DAPI (blue). Scale bars equal 20 μm. (e) Quantification of the live/dead assay from $n = 3$ images of both static and flow conditions. Error bars represent the standard deviation. There was no statistically significant difference between the two conditions.

experiment, cell-seeded coverslips were placed between the chamber block and bottom, with an O-ring seal. The coverslips are removable from the bioreactor system for end-point biological analysis. To characterize the dynamics of the flow chamber, simulations were performed using a computational simulation COMSOL. We simulated steady/state flow patterns within the fluidic chamber under the assumption of a fully-developed flow. As shown in figure 1(d), a constant shear stress between 1.69×10^{-4} and 4.36×10^{-3} dyn cm^{-2} was applied over the entire cell-seeded coverslip with a flow rate of 1.48 ml min^{-1}. The red streamlines confirmed a laminar flow of medium through the chamber. We identified 47 ml s^{-1} as the maximum flow rate to ensure laminar flow to the cells (figure 1(e)). With this flow rate, cell-seeded coverslips were subjected to a shear stress up to 11.2 dyn cm^{-2}. Here, the Reynolds number was lower than 2300, confirming laminar flow conditions in the bioreactor (figure 1(f)).

To assess the biocompatibility of the bioreactor system, HUVECs were dynamically cultured for 24 h at a flow rate of 1.48 ml min^{-1}. Cell viability was detected with a live/dead assay. As shown in figures 2(a), (b) and figure S1 is available online at stacks.iop.org/BMM/13/024101/mmedia, HUVECs cultured under static or flow conditions after 24 h retained viability (static: $97.4 \pm 0.01\%$ and bioreactor: $96.2 \pm 0.015\%$). No significant difference in the number of viable cells was detected between static and flow conditions (figure 2(e), $p > 0.05$). HUVECs in both conditions were CD31-positive, indicating that the phenotype of the cells was maintained (figures 2(c), (d)).

To demonstrate functionality of the bioreactor, HUVECs were subjected to a wound healing assay (scratch assay) similar to previous studies [31] and monitored in real-time (figure 3(a)). Interestingly, HUVECs under static conditions proliferated faster (a confluent monolayer was seen within 14 h) when compared with the cells that were subjected to flow (confluence was reached after 18 h) (figure 3(b)). We observed that similar to static cultures, HUVECs cultured with exposure to a flow rate of 1.48 ml min^{-1} showed a round morphology and did not align (figure S2).

We performed 2P-FLIM to analyze the cells under static and flow conditions in real-time in the bioreactor. The fluorescence decay curves for NAD(P)H were the best fit to a double exponential decay model, indicating the presence of two distinctly different lifetimes for the free and protein-bound forms of this coenzyme. The lifetimes of the free NAD(P)H (τ_1), and protein-bound NAD(P)H (τ_2), and the relative amplitude of free NAD(P)H (α_1) of HUVECs cultured under different conditions are displayed as false color-coded 2P-FLIM images in figure 4. Based on these images, histograms of α_1 of HUVECs cultured under different conditions were calculated (figure 5(a)). As indicated in figures 5(a), (b), α_1 and τ_1 of the 24 h laminar-sheared HUVECs were decreased when compared with the initial state (flow condition, 0 h). In contrast, α_1 in HUVECs cultured under static conditions showed similar lifetime distributions after 24 h of culture when compared to the initial state. An increased τ_2 was detected in the 24 h laminar-sheared

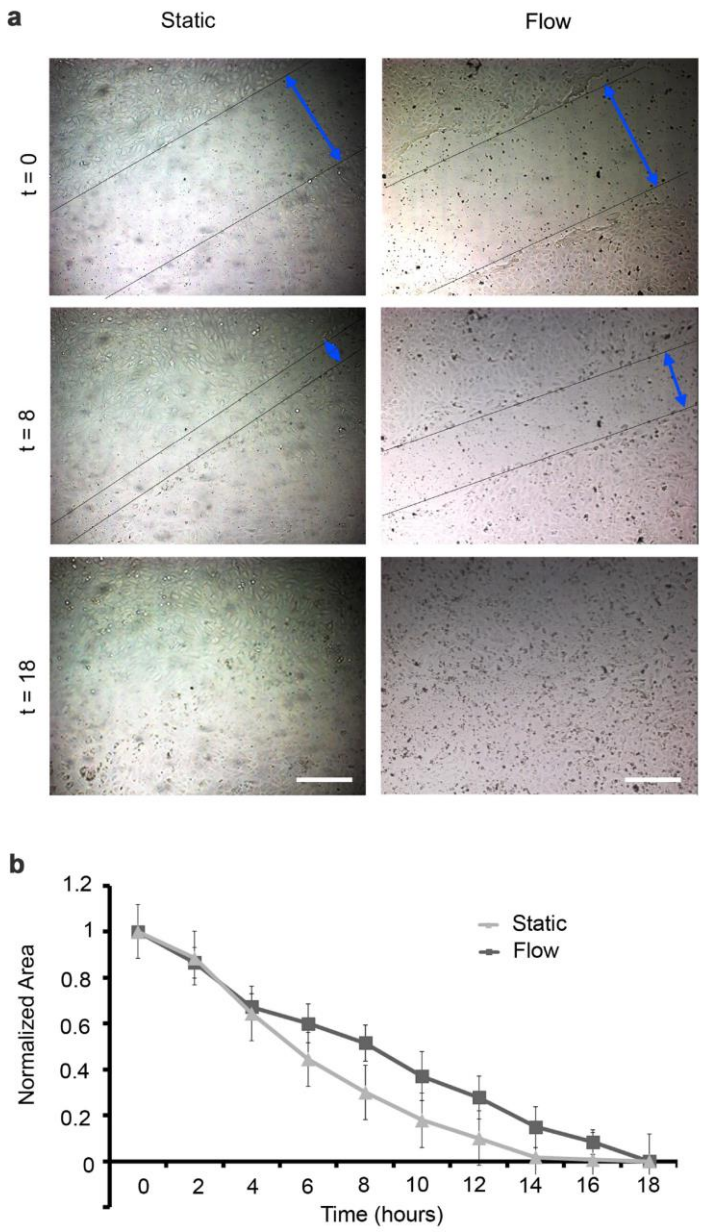

Figure 3. (a) Bright field images of HUVECs in the bioreactor during live-cell imaging. The black lines trace out the scratch area. The blue arrows show the scratch channels. Scale bars equal 100 μm. (b) Quantification of the reduction of scratch area over time for both static and flow conditions (each $n = 3$). Error bars represent the standard deviation.

HUVECs when compared to the cells prior exposure to defined shear (figure 5(c)).

Discussion

Bioreactor systems are widely used to mimic physiological conditions in cell and tissue cultures, and to specifically impact cellular behavior such as cell migration, proliferation, and phenotype maintenance [32]. However, many bioreactors do not permit *in situ* imaging and analyses [33, 34]. As a result, the sample must be removed from the bioreactor system and be prepared for further assessment. Thus, it is not possible to continuously monitor the culture and obtain data at several time points. Devices exist to support continuous low-resolution visualization of cells during flow, or high-resolution visualization of cells while stretching the

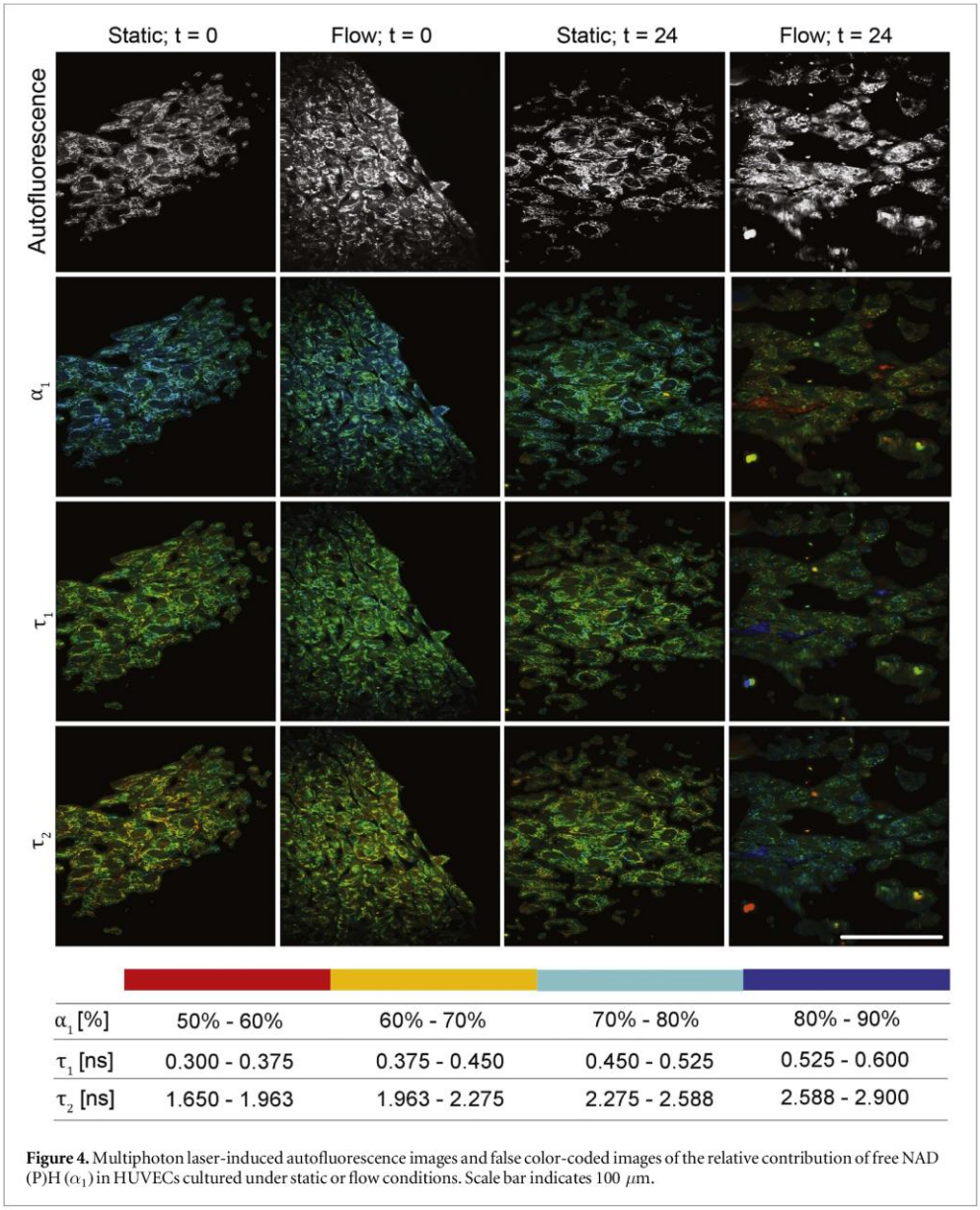

Figure 4. Multiphoton laser-induced autofluorescence images and false color-coded images of the relative contribution of free NAD (P)H (α_1) in HUVECs cultured under static or flow conditions. Scale bar indicates 100 μm.

substrate [35–39]. Nevertheless, high-resolution imaging of intracellular structural dynamics during shear stress applications is not readily feasible.

Here, we present a high throughput bioreactor system that is designed for real-time high-resolution imaging of cells and tissues that are exposed to fluid shear stress. To our knowledge, this is the first demonstration of combining a flow bioreactor system with 2P-FLIM. The windows at the bottom of the bioreactor allowed easy assembly onto the stage of a standard inverted light microscope system without interferences with the optical setup. The newly designed bioreactor system combines four independent flow chambers that allow the assessment of distinct culture conditions simultaneously and thereby largely improves the culture efficiency. The simulation of shear stress indicated that the bioreactor provides homogeneous and reproducible laminar flow conditions with flow rates ranging from 1.48 ml min^{-1} to 47 ml s^{-1}. The bioreactor system can be used to mimic both low and high shear stresses up to approximately 11.2 dyn cm^{-2}. The system was tested using HUVECs, which are directly exposed to blood flow shear stresses *in vivo*. Cytotoxicity tests demonstrated that HUVECs retained a high viability after they were exposed to 1.48 ml min^{-1} flow within the bioreactor system for 24 h. The HUVECs showed a round morphology and no alignment occurred after the dynamic culture. This

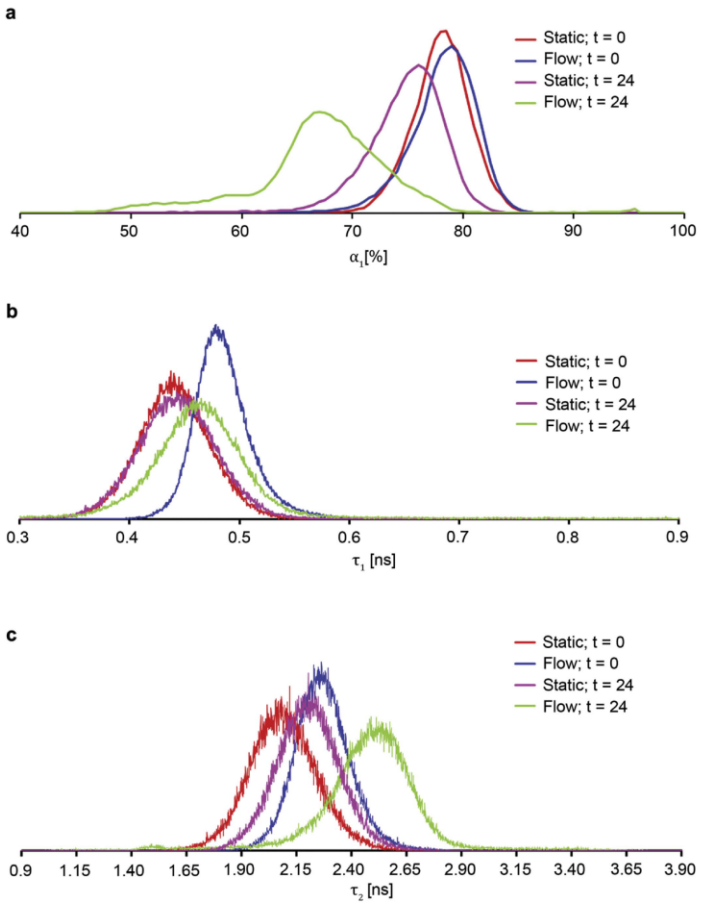

Figure 5. Histograms of (a) the relative contribution of free NAD(P)H (α_1), fluorescence lifetimes of the (b) free (τ_1) and (c) protein-bound (τ_2) NAD(P)H in HUVECs cultured under static or flow conditions.

is in accordance with a previous study, in which Chiu *et al* observed similar characteristics of HUVECs after exposure to a defined shear stress of approximately 0.5 dyn cm^{-2} [40]. In this study, HUVECs were round in shape with random actin filaments located mainly at the periphery of the cells [40]. In contrast, when exposing HUVECs to a relatively high shear stress (20 dyn cm^{-2}), the cells showed an elongated morphology and alignment with the direction of flow [40].

Here, the migration behavior of HUVECs was assessed under static and continuous flow conditions employing a scratch assay in real-time within the bioreactor system. The influence of high and disturbed shear stress on HUVEC migration has been controversially discussed as endothelial migration responses vary depending on the duration and type of applied shear stress [1, 41, 42]. For example, when HUVECs were preconditioned with a relatively high stress of 15 dyn cm^{-2} and then scratched, the migration was inhibited when compared with the static controls [1]. In contrast, when HUVECs were scratched without preconditioning and then cultured with approximately the same conditions (17 dyn cm^{-2}), the migration was increased compared with the static controls [40, 41]. In our study, we observed a low shear stress-induced reduction in migration of HUVECs when compared with the static conditions.

2P-FLIM was utilized to investigate the metabolic activity of HUVECs cultured under low shear stress conditions with the aim to show the suitability of the bioreactor for real-time high-resolution imaging. Kim *et al* have shown that shear stress can alter metabolism in endothelial cells from glycolysis to oxidative phosphorylation-dependent mechanisms [43]. Our data is consistent with these findings as we detected decreased α_1 in 24 h laminar-sheared HUVECs when compared with the static controls or with cells before expose to shear ($t = 0$). This indicates a metabolic switch from glycolysis to oxidative phosphorylation [44]. One possible explanation for this metabolic switch is that laminar shear stress induces apoptosis of endothelial cells by reducing glucose uptake (glycolysis) [45]. A relation between metabolic phenotypes and fluorescence lifetimes of NAD(P)H has been previously reported

[44, 46]. We also observed an increased τ_2 that may correlate to the elevated level of oxidative phosphorylation. Others have suggested that τ_1 is associated with the cytosolic acidification in cells [47]. Interestingly, a previous study has shown that laminar shear stress induces intracellular acidification in endothelial cells [48]. The pH value changes may act as a signaling mechanism for flow-induced changes in endothelial cell metabolism [48]. Therefore, it is possible that the metabolic shifts in laminar-sheared HUVECs are regulated via pH value changes.

In our study, we showed that our newly designed bioreactor system can control shear stress stimulation parameters while allowing visualization and quantification of cell migration and cell–cell interaction under shear stress-stimulated conditions. As this bioreactor system has been designed to also house 3D substrates, such as cell-populated electrospun scaffolds or hydrogels, a future application of this bioreactor system is to study cell-biomaterial interactions. Recently, it was shown that the combination of electrospun scaffolds with shear stress resulted in the increased maturation of induced-pluripotent stem cells-derived smooth muscle cells [49]. With the here presented next generation bioreactor system, simultaneous real-time monitoring and contact-free cell state analyses are now additionally possible. Moreover, due to the combination of bioreactor technology and imaging, the system can also be used in the future for direct cell manipulation such as optoporation and optical reprogramming with the ability to quantify expression, subcellular location and trafficking of receptors in living cells as seen in previous studies [50, 51]. Other potential applications of this bioreactor system have broad implications especially with the recent advances in gene editing. For example, fluorescence-reporter genes could be monitored *in vitro* using this bioreactor system. This real-time monitoring would help uncover mechanisms of disease in order to improve treatments and gain mechanistic knowledge. The ability to modulate the physical parameters such as shear stress and oxygen content could play an important role in cardiovascular tissue engineering and coagulation studies. Real-time monitoring of cells could give insight into the progression and mechanism of disease, which is vital for the advancement of treatment and knowledge in the field of tissue engineering and biomaterials design.

Conclusion

The newly designed flow bioreactor system presented in this study enables the exposure of cells and 3D tissues to shear stress while allowing simultaneous real-time contact-free analyses. We demonstrated that the system is capable of providing reproducible laminar flow in a wide flow range. It is biocompatible, easy-to-use and compatible with a wide range of microscope systems. To prove the functionality of the bioreactor system, we cultured HUVECs under low shear stress conditions for 24 h. Future studies will focus on a systematic study of a long-term culture of HUVECs under various types and magnitudes of shear stresses. Future possibilities for this bioreactor range from observing *in vitro* cell development, including but not limited to direct cell reprogramming or stem cell differentiation, and real-time monitoring of cellular (micro)environments, cell-biomaterial interactions or cellular metabolic changes due to drug applications.

Acknowledgments

The authors thank Pirmin Lakner, Katarina Klett and Simone Liebscher (University Women's Hospital Tübingen) for their support with imaging and cell cultures. This work was funded by the Fulbright US Student Program (JAR), RISE DAAD (ZD), the Ministry of Science, Research and the Arts of Baden-Württemberg (33-729.55-3/214 and SI-BW 01222-91 to KS-L), and the Deutsche Forschungsgemeinschaft (INST 2388/30-1, INST 2388/34-1, SCHE 701/7-1, SCHE 701/10-1 to KS-L).

Disclosure statement

No competing financial interests exist.

ORCID iDs

Katja Schenke-Layland https://orcid.org/0000-0001-8066-5157

References

[1] Tressel S L *et al* 2007 Laminar shear inhibits tubule formation and migration of endothelial cells by an angiopoietin-2-dependent mechanism *Arterioscler. Thromb. Vasc. Biol.* **27** 2150
[2] Wang Y-K and Chen C S 2013 Cell adhesion and mechanical stimulation in the regulation of mesenchymal stem cell differentiation *Int. J. Mol. Cell Med.* **17** 823
[3] Brafman D A 2013 Constructing stem cell microenvironments using bioengineering approaches *Physiol. Genomics* **45** 1123
[4] Kshitiz *et al* 2012 Control of stem cell fate and function by engineering physical microenvironments *Integr. Biol.* **4** 1008
[5] Mammoto T and Ingber D E 2010 Mechanical control of tissue and organ development *Development* **137** 1407
[6] Kaazempur Mofrad M R *et al* 2005 Exploring the molecular basis for mechanosensation, signal transduction, and cytoskeletal remodeling *Acta Biomater.* **1** 281
[7] Grayson W L *et al* 2009 Biomimetic approach to tissue engineering *Semin. Cell Dev. Biol.* **20** 665
[8] Minteer D M, Gerlach J C and Marra K G 2014 Bioreactors addressing diabetes mellitus *J. Diabetes Sci. Technol.* **8** 1227
[9] Mousoulis C *et al* 2013 Single cell spectroscopy: noninvasive measures of small-scale structure and function *Methods* **64** 119
[10] Haagensen J A, Regenberg B and Sternberg C 2011 Advanced microscopy of microbial cells *Adv. Biochem. Eng. Biotechnol.* **124** 21–54

[11] Lakner P H *et al* 2017 Applying phasor approach analysis of multiphoton FLIM measurements to probe the metabolic activity of three-dimensional *in vitro* cell culture models *Sci. Rep.* **7** 42730

[12] Hinderer S *et al* 2015 *In vitro* elastogenesis: instructing human vascular smooth muscle cells to generate an elastic fiber-containing extracellular matrix scaffold *Biomed. Mater.* **10** 034102

[13] Wang C *et al* 2013 Endothelial cell sensing of flow direction *Arterioscler. Thromb. Vasc. Biol.* **33** 2130

[14] Bhatia S N and Ingber D E 2014 Microfluidic organs-on-chips *Nat. Biotechnol.* **32** 760

[15] Niehorster T *et al* 2016 Multi-target spectrally resolved fluorescence lifetime imaging microscopy *Nat. Methods* **13** 257

[16] Sun Y *et al* 2012 Monitoring protein interactions in living cells with fluorescence lifetime imaging microscopy *Methods Enzymol.* **504** 371

[17] Cahalan M D *et al* 2002 Two-photon tissue imaging: seeing the immune system in a fresh light *Nat. Rev. Immunol.* **2** 872

[18] Cubeddu R *et al* 2002 Time-resolved fluorescence imaging in biology and medicine *J. Phys. D: Appl. Phys.* **35** R61

[19] Sanders R *et al* 1995 Quantitative pH imaging in cells using confocal fluorescence lifetime imaging microscopy *Anal. Biochem.* **227** 302

[20] Szmacinski H, Gryczynski I and Lakowicz J R 1996 Three-photon induced fluorescence of the calcium probe Indo-1 *Biophys. J.* **70** 547

[21] Szmacinski H and Lakowicz J R 1997 Sodium green as a potential probe for intracellular sodium imaging based on fluorescence lifetime *Anal. Biochem.* **250** 131

[22] Gerritsen H C *et al* 1997 Fluorescence lifetime imaging of oxygen in living cells *J. Fluorescence* **7** 11

[23] Murata S, Herman P and Lakowicz J R 2001 Texture analysis of fluorescence lifetime images of nuclear DNA with effect of fluorescence resonance energy transfer *Cytometry* **43** 94

[24] Hinderer S *et al* 2014 Engineering of a bio-functionalized hybrid off-the-shelf heart valve *Biomaterials* **35** 2130

[25] Monaghan M G *et al* 2016 Enabling multiphoton and second harmonic generation imaging in paraffin-embedded and histologically stained sections *Tissue Eng.* C **22** 517

[26] Liu M *et al* 2014 Instrument response standard in time-resolved fluorescence spectroscopy at visible wavelength: quenched fluorescein sodium *Appl. Spectrosc.* **68** 577

[27] Luchowski R *et al* 2009 Instrument response standard in time-resolved fluorescence *Rev. Sci. Instrum.* **80** 033109

[28] Sun Y, Day R N and Periasamy A 2011 Investigating protein–protein interactions in living cells using fluorescence lifetime imaging microscopy *Nat. Protocols* **6** 1324

[29] Georgakoudi I and Quinn K P 2012 Optical imaging using endogenous contrast to assess metabolic state *Annu. Rev. Biomed. Eng.* **14** 351

[30] Scott T G *et al* 1970 Synthetic spectroscopic models related to coenzymes and base pairs: V. Emission properties of NADH. Studies of fluorescence lifetimes and quantum efficiencies of NADH, AcPyADH, [reduced acetylpyridineadenine dinucleotide] and simplified synthetic models *J. Am. Chem. Soc.* **92** 687

[31] Jonkman J E *et al* 2014 An introduction to the wound healing assay using live-cell microscopy *Cell Adhes. Migr.* **8** 440

[32] Rangarajan S, Madden L and Bursac N 2014 Use of flow, electrical, and mechanical stimulation to promote engineering of striated muscles *Ann. Biomed. Eng.* **42** 1391

[33] Zhao F and Ma T 2005 Perfusion bioreactor system for human mesenchymal stem cell tissue engineering: dynamic cell seeding and construct development *Biotechnol. Bioeng.* **91** 482

[34] Price A P *et al* 2010 Development of a decellularized lung bioreactor system for bioengineering the lung: the matrix reloaded *Tissue Eng.* A **16** 2581

[35] Kensah G *et al* 2011 A novel miniaturized multimodal bioreactor for continuous *in situ* assessment of bioartificial cardiac tissue during stimulation and maturation *Tissue Eng.* C **17** 463

[36] Bachmann B J *et al* 2016 A novel bioreactor system for the assessment of endothelialization on deformable surfaces *Sci. Rep.* **6** 38861

[37] Wang D *et al* 2010 A stretching device for imaging real-time molecular dynamics of live cells adhering to elastic membranes on inverted microscopes during the entire process of the stretch *Integr. Biol.* **2** 288

[38] Sim J Y *et al* 2012 Uniaxial cell stretcher enables high resolution live cell imaging *2012 IEEE 25th Int. Conf. on Micro Electro Mechanical Systems (MEMS)*

[39] Huang L, Mathieu P S and Helmke B P 2010 A stretching device for high-resolution live-cell imaging *Ann. Biomed. Eng.* **38** 1728

[40] Chiu J-J and Chien S 2011 Effects of disturbed flow on vascular endothelium: pathophysiological basis and clinical perspectives *Physiol. Rev.* **91** 327

[41] Hsu P-P *et al* 2001 Effects of flow patterns on endothelial cell migration into a zone of mechanical denudation *Biochem. Biophys. Res. Commun.* **285** 751

[42] Tardy Y *et al* 1997 Shear stress gradients remodel endothelial monolayers *in vitro* via a cell proliferation-migration-loss cycle *Arterioscler. Thromb. Vasc. Biol.* **17** 3102

[43] Kim B *et al* 2014 Exercise-mediated wall shear stress increases mitochondrial biogenesis in vascular endothelium *PLoS One* **9** e111409

[44] Meleshina A V *et al* 2016 Probing metabolic states of differentiating stem cells using two-photon FLIM *Sci. Rep.* **6** 21853

[45] Doddaballapur A *et al* 2015 Laminar shear stress inhibits endothelial cell metabolism via KLF2-mediated repression of PFKFB3 *Arterioscler. Thromb. Vasc. Biol.* **35** 137

[46] Blacker T S *et al* 2014 Separating NADH and NADPH fluorescence in live cells and tissues using FLIM *Nat. Commun.* **5** 3936

[47] Damalakiene L *et al* 2016 Fluorescence-lifetime imaging microscopy for visualization of quantum dots' endocytic pathway *Int. J. Mol. Cell Med.* **17** 473

[48] Ziegelstein R C, Cheng L and Capogrossi M C 1992 Flow-dependent cytosolic acidification of vascular endothelial cells *Science* **258** 656

[49] Eoh J H *et al* 2017 Enhanced elastin synthesis and maturation in human vascular smooth muscle tissue derived from induced-pluripotent stem cells *Acta Biomater.* **52** 49

[50] Perrio C, Nicole O and Buisson A 2017 GluN2B subunit labeling with fluorescent probes and high-resolution live imaging *Methods Mol. Biol.* **1677** 171

[51] Ribas J *et al* 2016 Cardiovascular organ-on-a-chip platforms for drug discovery and development *Appl. In Vitro Toxicol.* **2** 82

[52] Nava M M, Raimondi M T and Pietrabissa R 2013 A multiphysics 3D model of tissue growth under interstitial perfusion in a tissue-engineering bioreactor *Biomech. Model Mechanobiol.* **12** 1169